MICROCOPY RESOLUTION TEST CHART

NATIONAL BUREAU OF STANDARDS 1963 A

OFFICE OF NAVAL RESEARCH

Contract N00014-82-K-0576

TECHNICAL REPORT No. 30

BONDING AND COUPLING OF C_1 FRAGMENTS

ON METAL SURFACES

by

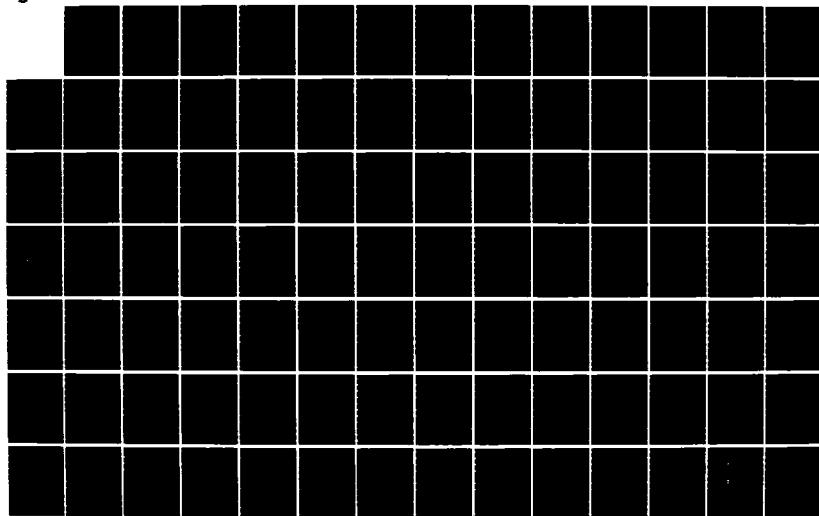Chong Zheng, Yitzhak Apeloig, and

Roald Hoffmann

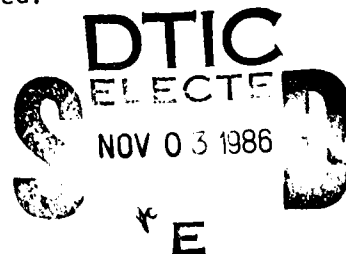Materials Science Center

Cornell University

Ithaca, New York 14853

October, 1986

DTIC
ELECTE
NOV 0 3 1986
E

86 11 3 011

SECURITY CLASSIFICATION OF THIS PAGE (When Data Entered)

REPORT DOCUMENTATION PAGE	READ INSTRUCTIONS BEFORE COMPLETING FORM

1. REPORT NUMBER 30	2. GOVT ACCESSION NO. AD-A173987	3. RECIPIENT'S CATALOG NUMBER

4. TITLE (and Subtitle)	5. TYPE OF REPORT & PERIOD COVERED
Bonding and Coupling of C1 Fragments on Metal Surfaces	Technical
	6. PERFORMING ORG. REPORT NUMBER

7. AUTHOR(s)	8. CONTRACT OR GRANT NUMBER(s)
Chong Zheng, Yitzhak Apeloig, and Roald Hoffmann	N00014-82-K-0576

9. PERFORMING ORGANIZATION NAME AND ADDRESS	10. PROGRAM ELEMENT, PROJECT, TASK AREA & WORK UNIT NUMBERS
Laboratoy of Atomic and Solid State Physics Cornell University Ithaca, NY 14850	

11. CONTROLLING OFFICE NAME AND ADDRESS	12. REPORT DATE
Office of Naval Research 800 Quincy St. Alrington, VA	October, 1986
	13. NUMBER OF PAGES 80

14. MONITORING AGENCY NAME & ADDRESS(if different from Controlling Office)	15. SECURITY CLASS. (of this report)
	unclassified
	15a. DECLASSIFICATION/DOWNGRADING SCHEDULE

16. DISTRIBUTION STATEMENT (of this Report)

Thsi document has been approved for public release and sale, its distribution is unlimited.

17. DISTRIBUTION STATEMENT (of the abstract entered in Block 20, if different from Report)

18. SUPPLEMENTARY NOTES

19. KEY WORDS (Continue on reverse side if necessary and identify by block number)

20. ABSTRACT (Continue on reverse side if necessary and identify by block number)

The bonding and reactivity of CH_3, CH_2, and CH fragments to Ti (0001), Cr(110) and Co(0001) metal surfaces is examined with extended Huckel band calculations on two dimensional slabs of metal and adsorbate. A local chemical viewpoint is sought through fragment analyses, decompositions of the density of states and overlap population studies. All fragments tend to restore their missing C-H bonds when bound to these surfaces - CH_3 prefers the on-top, CH_2 the bridging and CH the capping geometry. CH_3 anchors more strongly to the on-top site of a metal surface of high d band filling since the antibonding feature at the top of the d band that (OVER)

DD FORM 1473 EDITION OF 1 NOV 53 IS OBSOLETE
S/N 0102-014-6601

SECURITY CLASSIFICATION OF THIS PAGE (When Data Entered)

results from σ-bonding destabilizes sites of higher coordination. Similar conclusions holds for other fragments. Thus, the mobility of theses fragments is reduced on metal surfaces of higher d band filling. The mobility patterns of CH_3, CH_2, CH are examined. In general, on the way to products there are barriers to migration on the surface, a proximity or crowding effect which makes it costly for two fragments to approach on the surfaces, and a barrier, small or large, to their reaction with each other. When two C_1 fragments couple, the C-C σ^* orbital rises from below the Fermi level. It is initally filled, then empties as the reaction proceeds. Hence the lower the Fermi level (for metals at the right side of the transition series), the smaller the reaction barrier. The decrease of the mobility and the lower coupling barrier as the metal is changed from the left ot the right side of the in the Periodic Table may be two of many reasons why metals in the middle of the transition series have higher reactivity in Fischer-Tropsch catalysis.

BONDING AND COUPLING OF C_1 FRAGMENTS ON METAL SURFACES.

Chong Zheng[a†], Yitzhak Apeloig[b], and Roald Hoffmann*[a]

Contribution for [a]the Department of Chemistry and Materials Science Center, Cornell University, Ithaca, NY 14853; [b]the Department of Chemistry, Technion-Israel Institute of Technology, Haifa, 30012 Israel.

Abstract: The bonding and reactivity of CH_3, CH_2 and CH fragments to Ti (0001), Cr(110) and Co(0001) metal surfaces is examined with extended Hückel band calculations on two dimensional slabs of metal and adsorbate. A local chemical viewpoint is sought through fragment analyses, decompositions of the density of states and overlap population studies. All fragments tend to restore their missing C-H bonds when bound to these surfaces - CH_3 prefers the on-top, CH_2 the bridging and CH the capping geometry. CH_3 anchors more strongly to the on-top site of a metal surface of high d band filling since the antibonding feature at the top of the d band that results from σ-bonding destabilizes sites of higher coordination. Similar conclusions holds for other fragments. Thus, the mobility of these fragments is reduced on metal surfaces of higher d band filling. The mobility patterns of CH_3, CH_2, CH are examined. In general, on the way to products there are barriers to migration on the surface, a proximity or crowding effect which makes it costly for two fragments to approach on the surface, and a barrier, small or large, to their reaction with each other. When two C_1 fragments couple, the C-C σ^* orbital rises from below the Fermi level. It is initially filled, then empties as the reaction proceeds. Hence the lower the Fermi level (for metals at the right side of the transition series), the smaller the reaction barrier. The decrease of the mobility and the lower coupling barrier as the metal is changed from the left to the right side in the Periodic Table may be two of many reasons why metals in the middle of the transition series have higher reactivity in Fischer-Tropsch catalysis.

---

† Present address: Department of Chemistry, Stanford University, Stanford, CA 94305

The Fischer-Tropsch (FT) synthesis, which can be defined as the reductive oligomerization of carbon monoxide over a heterogeneous catalyst (eq. 1), was described nearly 60 years ago.[1,2] Because of the great technological importance of this reaction much effort, especially during the last two decades, has been devoted to the elucidation of its mechanism.[1-3]. Although the subject still continues to be

$$n\,CO + m\,H_2 \xrightarrow{\text{Catalyst}} C_x H_y O_z \qquad (1)$$
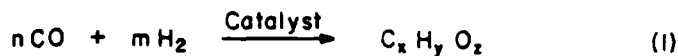
strongly debated[4] the accumulated evidence suggests that under conditions which lead to oxygen-free products (i.e., $z = 0$ in eq. 1 the FT reaction proceeds via the "carbide/methylene" mechanism[1-3] which is drawn schematically in Scheme 1. Under these conditions, the major products are α-olefins and hydrocarbons, and the oxygen ends up primarily as water, along with some oxygenated products.
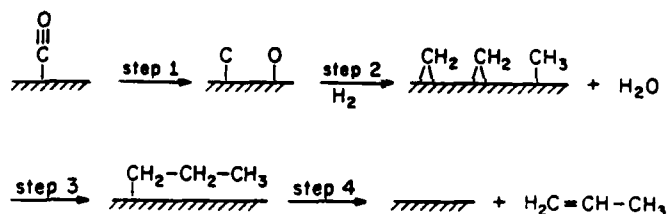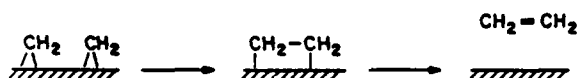

Scheme 1

The carbide/carbene mechanism was first suggested by Fisher and Tropsch themselves as early as 1926,[2] and it was re-introduced with additional details by Craxford and Rideal.[3] According to this mechanism carbon monoxide is first adsorbed and then dissociates on the metal surface to give "surface carbides" (step 1, Scheme 1), which are then hydrogenated to give surface-bonded methylene and methyl fragments (step 2). The oligomerization of these metal-bonded fragments (step 3) is followed by a termination step such as a β-elimination (step 4), which followed by desorption yields the final products.[1]

The most extensive and convincing support for the carbide/methylene mechanism comes from the elegant studies by the research groups of Biloen[5] and Petit[6]. Biloen

and Sachtler found that Ni, Co and Ru-based catalysts which are pre-doped with ^{13}C labeled carbon yield upon treatment with [13]CO/H$_2$ mixtures under FT conditions a product mixture consisting mainly of [13]CH$_4$ and of hydrocarbons containing _several_ ^{13}C-atoms in the _same_ molecule[5]. These results indicate that the carbidic species, once formed, can react with hydrogen to give CH$_x$ intermediates (x = 1-3) which polymerize to produce hydrocarbons, in agreement with steps 2 and 3 in Scheme 1. The feasibility of the first step in the mechanism, in which the carbidic surface is formed, has been demonstrated convincingly by other investigators.[7] Thus, a rapid dissociative chemisorption of carbon monoxide has been shown to occur on various clean metal surfaces, including typical FT catalysts such as iron.[7] More importantly, the formation of a "carbidic layer" under real FT conditions is well known.[8]

The beautiful studies of Petit and Brady on the induced decomposition of gaseous diazomethane (CH$_2$N$_2$) on typical FT catalysts provides additional strong and independent evidence for the operation of the carbide/carbene mechanism.[6] Decomposition of CH$_2$N$_2$ on Ni-, Pd-, Fe-, Co-, Ru-, and Cu- surfaces, at atmospheric pressure and in the temperature range of 25-250 °C, produces only ethylene and dinitrogen.[6] This indicates that in the absence of hydrogen the absorbed CH$_2$ fragments dimerize to ethylene (Scheme 2), but polymerization to higher hydrocarbons

Scheme 2

does not occur. However, reaction of a mixture of H$_2$ and CH$_2$N$_2$ over Co-, Fe-, and Ru-surfaces, all typical FT catalysts, produces a variety of hydrocarbons with isomer and molecular weight distribution typical of a "real" FT reaction.[6] Furthermore, decomposition of CH$_2$N$_2$ on surfaces which are not capable of dissociative chemisorption of H$_2$, such as Cu, yields only ethylene, even in the presence of H$_2$.[6] Wang and Ekerdt in a more recent study showed that pyridine can be

used to scavenge C_1-C_3 alkyl species from the surface of an iron catalyst during FT synthesis.[9] These findings are also consistent with the carbide/carbene mechanism in which alkyl fragments are the immediate precursors to the FT products. In another important recent paper, Ekstrom and Lapszewicz showed that high molecular weight hydrocarbons can be formed by the reaction of carbides with hydrogen in the presence of water[10]. Furthermore, Winograd et al have recently reported direct observation of CH, CH_2 and CH_3 intermediates on a Ni(111) methanation catalyst.[12]

Additional support, although indirect, for the chemical feasibility of the various steps of the carbide/methylene mechanism stems from the study of appropriate model organometallic complexes. Substantial experimental effort has been devoted in the last decade to the study of such model complexes[1a]. Relevant systems and molecular reactions will be mentioned briefly along the paper, and reviews (in addition to ref. 1a) are gathered in reference 11.

Despite the extensive study of the FT synthesis many of the mechanistic details remain poorly understood. In particular, there is virtually no knowledge of the electronic and geometrical factors that control the polymerization process (step 3, Scheme 1) and very little is known of the nature of the bonding of the organic fragments to the surface. Representative questions that remain unanswered are: What are the most effective binding sites on the metal surface for the adsorbed fragments and are these sites the same for all radicals? What is the favored orientation for the coupling of two methylenes to produce ethylene (Scheme 2)? Are the binding sites and the dimerization mechanism the same for different metals? What is the relative mobility of CH_2 and CH_3 fragments on the metal surface, and how does this mobility change as the metal is varied? At present these and similar questions are difficult to answer experimentally, although encouraging advances have been made recently.[13] We will address these and other interesting mechanistic questions regarding the FT synthesis in this paper.

A full theoretical treatment of the FT reaction is a vast project and we have to impose some limitations on the scope of problems that will be tackled. In this

study we concentrate on three major issues: (1) The mode of binding of the postulated reaction intermediates -- methyl, methylene and methyne -- to the metal surface. (2) The mobility of these radicals on the metal surface. (3) The electronic and geometrical requirements for the surface induced coupling of the organic radicals.

We use in our work tight binding extended Hückel calculations,[14] with details given in Appendix I. The analysis of the surface calculations is based on the methodology and the tools that we have described in detail in our recent study of C-H and H-H activation on surfaces.[15] The extended Hückel method, whether applied to discrete molecules or extended systems, has well-known limitations. It does not do well at predicting distances, and this will impose severe limitations in the analses of mobility and coupling. But the method does seem to capture the essence of bonding. It is also transparent and useful in constructing explanations, and it is for this reason that we use it.

While many of the problems we will attack have not been investigated theoretically before, some have. The relevant studies of Baetzold, Muetterties and Shustorovich,[16,17] of Minot, Van Hove and Somorjai,[18] of Anderson,[18b-d] as well as other related theoretical work will be discussed in the paper. We also note that the first step of the FT reaction, the chemisorption of CO on various metal surfaces, has been studied extensively by many theoreticians.[17,18b-d,19]

This will be a long paper. It could easily have been chopped up into three papers, one on fragment bonding, a second on migration, a third on fragment coupling. We think nothing would be gained by this, and continuity lost. We ask the reader to bear with us as we analyze in detail, an important reaction at the border of chemistry, physics and catalysis.

GENERAL CONSIDERATIONS

The FT synthesis occurs on Fe and Co catalysts and to some extent also on Ni surfaces.[1] A major goal of any mechanistic study of the FT synthesis is to try to define and understand the factors that determine the catalytic reactivity of the metal surface. In this respect two key parameters are the identity of the metal and the lattice form in which it crystallizes.[13,20] For each metal, one can choose surfaces with different indices, and generally each surface is expected to exhibit a different reactivity. We are going to use a fixed surface throughout the paper, to model what must be only one aspect of reality. The surface we chose is the (0001) surface of a hexagonal metal. With the high symmetry of this surface the computational times can be greatly reduced. For example, when a methyl group is adsorbed on this surface in an "on-top" or "three-fold" geometry, the hexagonal symmetry is still retained and the computational advantage of this over other surfaces of FT catalysts (e.g. Fe (110)) is obvious. The results can also be compared with our previous studies on other hexagonal surfaces.[15,21]

To extract the basic electronic effects that determine the reactivity of the metal, we are going to compare three metal surfaces: Ti (0001), Cr (110) and Co (0001). They are shown in 1, 2 and 3, respectively. Although the Cr (110) surface is not hexagonal, it can be viewed as a distortion therefrom.

Ti (0001)·   Cr (110)   Co (0001)

2.49 Å

—|2.93Å|—   —|2.88 Å|—   —|2.51 Å|—

1   2   3
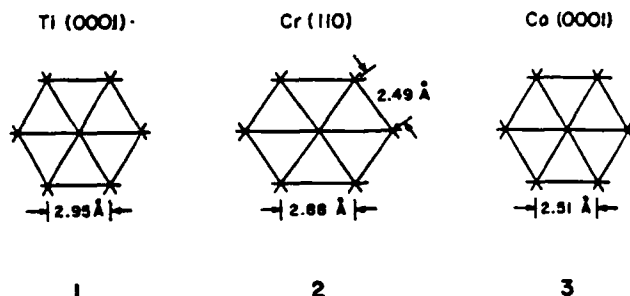
Ley us begin with the hcp lattice of cobalt and employ the experimental Co-Co distance of 2.51 Å. The next choice to be made is that of the thickness of the slab of the metal to be used in the calculations, of necessity a compromise between computational economy and reasonable accuracy. Our previous studies[14c,15a,19a,21] as well as exploratory calculations on the the cobalt slab lead to the conclusion

that a reasonable choice is a 3-layer slab. We use here a slab of three layers
because the changes in the important surface properties (e.g., the Fermi level,
charge distribution, overlap population *etc.*) are small on going to a 4-layer slab.
The 3-layer slab model for the hcp Co surface is shown in a side view in 4. We
choose the z axis to be perpendicular to the surface. A top view is in 5, where
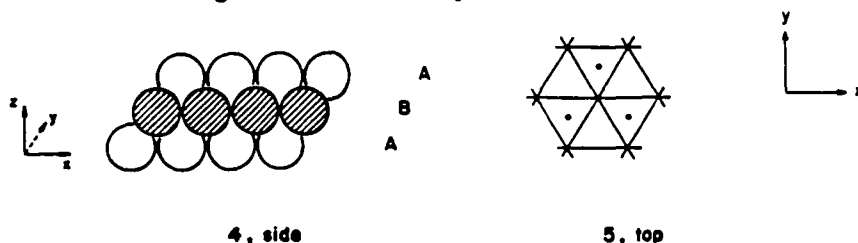the dots in the triangular hollows represent the Co atoms in the next layer below.

4, side   5, top

Figure 1 shows the density of states (DOS) curve of the slab. A DOS curve is
the solid state analogue of an energy level diagram and it gives the number of
levels in a particular energy interval. The metal bands (or orbitals) are filled up
to the Fermi level -- the solid state equivalent of the molecular HOMO. The dashed
lines in Figure 1 refer to the total DOS curve. The darkened areas indicate the
contribution of the s (Figure 1a) and the p states (Figure 1b) to the total DOS.
The darkened areas are examples of projected or local DOS curves which single

Figure 1 here

out the contribution of a certain atom or a group of atomic or fragment orbitals to
the overall DOS plot. The states that are not s or p are d states. The dotted
lines are integration curves, from 0 to 100%, which additively count the relative
number of states occupied as one sweeps up the energy scale. It is clear from
Figure 1 that a substantial number of s and some p states penetrate into the d band.
On the average any Co atom has its s band approximately one third filled.

In __any__ reactivity problem, molecular or solid state, the energy and bonding
capabilities of the frontier orbitals, the lower unoccupied and higher occupied
orbitals of the system will play a crucial role. In the case of a metal surface
these are the orbitals near the Fermi level. It is important to know how the
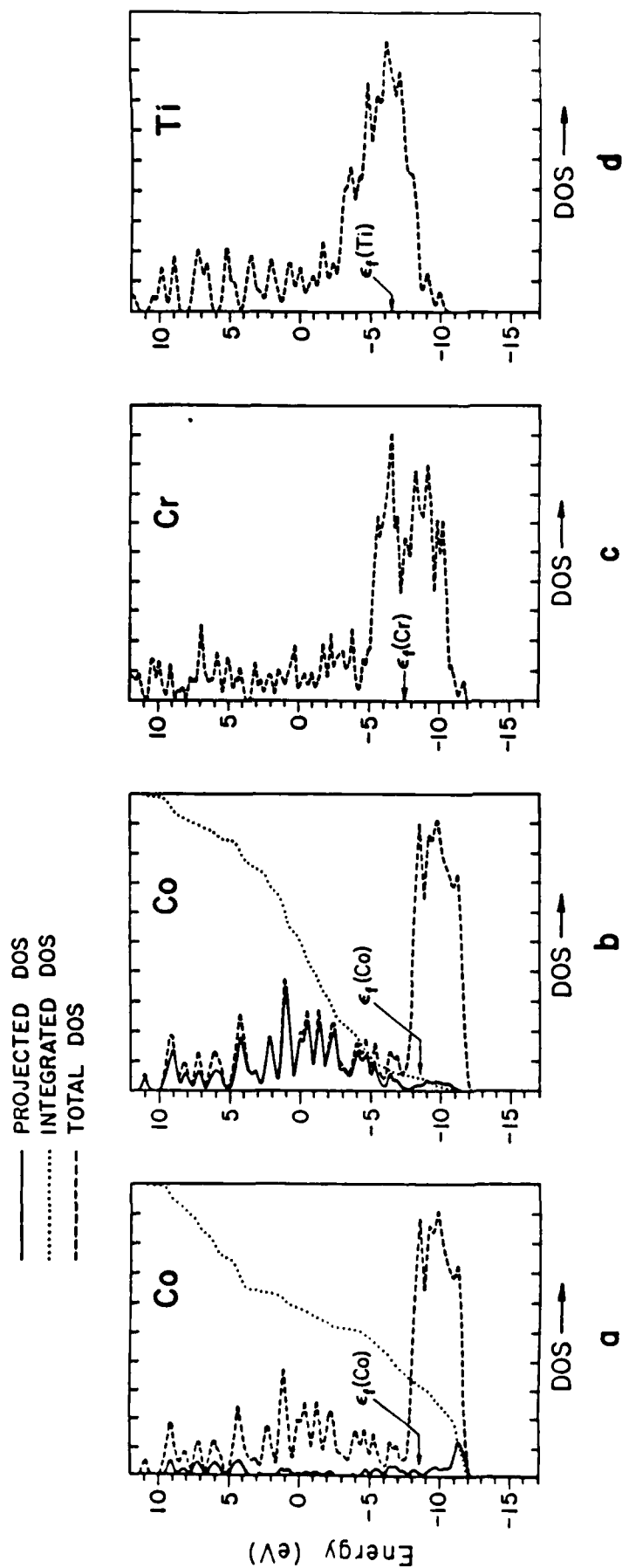essential features of these frontier orbitals of the surface change as the metal is

Figure 1: Total DOS (dashed lines) of the Co(0001), Cr(110) and Ti(0001) three-layer slabs. The solid lines show the contribution from s and p states in a and b respectively for the Co case. ϵ_f indicates the Fermi level. Cr and Ti total state densities are shown in c and d. The d band center of gravity and the Fermi level shifts to higher energy on going from Co to Ti.
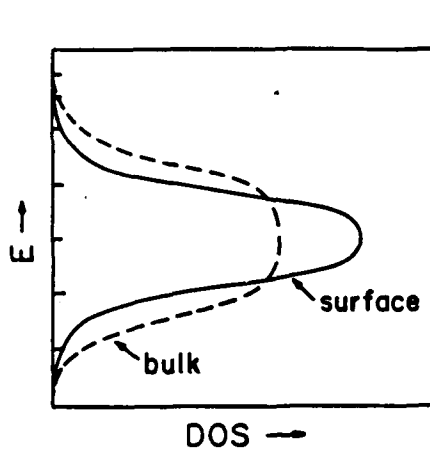
a
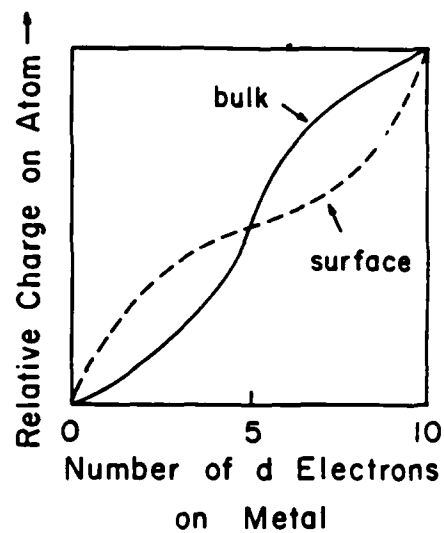
b

Figure 2: A schematic picture showing the relative charge on surface and bulk atoms
(b) caused by different effective band width for each kind of atoms (a).

varied. As the number of the d electrons increases from Ti to Co, the nuclear charge is less effectively "screened" and d electrons are more strongly bound by the bigger Coulomb interaction. There are therefore two factors competing in the determination of the Fermi level: the filling of the d band, which tends to raise the Fermi level, and the Coulomb interaction that pulls down the Fermi level with increasing d electron count. It turns out that the Coulomb interaction wins out, and the Fermi level descends slowly along the right side of the transition series (the relevant work functions are Ti: 4.33, Cr: 4.5, Co: 5.0 eV[20d]). Another consequence of the increasing Coulomb attraction is the decreasing d band width along the transition series, due to the "tighter" wave functions of the d electrons. The calculations confirm these general considerations. The extended Hückel method, as usaual, gives a much too high magnitude of the ionization potential or Fermi level. It does so for molecule as well as for extended structures.

In analogy to our previous studies[15,21], we find that the charge distribution among the slab layers changes as a function of the number of electrons per metal atom. Basically, this results from the fact that an inner atom has more neighbors than a surface one. The band dispersion is a function of inter-unit-cell interaction, so that the more interactions (neighbors) one has, the wider the resulting band. Thus the states of the "surface atoms" (layer A in 4) form narrower bands than the bulk-like atoms (layer B in 4). The wider bulk bands are filled first and thus the bulk atoms become negative relative to the surface. At some point along the transition series the two layers will have equal charges and past this point the surface layer will become negative. This argument is presented schematically in Figure 2. The conclusions from these qualitative arguments are that at the right side of the transition series surfaces are expected to be negative relative to the bulk (or to the isolated atom), while at the left side of the transition series surface are expected to be positive.

Figure 2 here

The calculations fully support these conclusions. For Co we find that each of the surface atoms carries a negative charge of 0.305 electrons (note that because of the ABA arrangement the charge on each bulk metal is twice as large and of opposite sign to charge on a surface atom). For Cr we get a negative charge of -0.288 at a surface atom. For Ti the polarization is small and both surface and bulk layers are nearly neutral (each surface Ti atom carries a charge of -0.025 electrons). To put these charge distributions in a chemical context we might say that the surface layers of the Co and Cr slabs can be described as being nucleophilic and Ti neutral. Better calculations will temper the indubitably exaggerated density shifts between surface and bulk, but the trend should remain.

Another important difference between the surface and the bulk atoms, shown in Table 1, is in the electron distribution between the atomic metal orbitals. Let us examine first the surface. The data in Table 1 reveal in the Co case, a significant electron flow from the "in-plane" orbitals ($d_{x^2-y^2}$, d_{xy}) into orbitals which are perpendicular to the surface (d_{z^2}, d_{xz}, d_{yz}) in the Co case. But as the d electron filling decreases the situation is reversed: for Ti there is an electron flow from d_{z^2}, d_{xz} and d_{yz} to $d_{x^2-y^2}$ and d_{xy}. This is again due to the fact the "in-plane" orbitals on the surface overlap better with their neighbors, resulting a wider band. At low electron counts these orbitals are filled first, but as the filling increases the narrower bands, which are at intermediate energy, are filled more.

Table 1 here

For the bulk orbitals, the perpendicular orbitals (d_{z^2}, d_{xz}, d_{yz}) overlap not only with orbitals in the same plane (B in $\underline{4}$) but also the layers sandwiching them (A layers in $\underline{4}$), thus the band widths are bigger than those of $d_{x^2-y^2}$ and d_{xy}. For the same reason that we have adduced above the charge flows from d_{z^2}, d_{xz} and d_{yz} to $d_{x^2-y^2}$ and d_{xy} at high electron counts, but is reversed for low electron fillings.

We are now in a position to bring to the surface a layer of organic molecules.

TABLE 1. Electron Distribution Among the Metal Atomic Orbitals of Co(0001), Cr(110), and Ti(0001) Slabs. Coordinate Axes are given in 1.

Orbital	Co d^9		Cr d^6		Ti d^4	
	"surface"	"bulk"	"surface"	"bulk"	"surface"	"bulk"
$d_{x^2-y^2}$ or d_{xy}	1.569	1.541	1.034	0.896	0.632	0.566
d_{z^2}	1.731	1.510	1.041	0.947	0.566	0.570
d_{xz} or d_{yz}	1.764	1.445	1.046	0.856	0.588	0.612
s	0.651	0.616	0.752	0.666	0.798	0.730
p	0.258	0.293	0.334	0.305	0.221	0.295
Total	9.305	8.390	6.288	5.424	4.025	3.951

GENERAL CONSIDERATIONS FOR ADSORPTION OF METHYL, METHYLENE AND METHYNE RADICALS ON
METAL SURFACES

In order to study the adsorption of CH_3 (x — 1-3) radicals on the metal surface
we have to simplify the calculations further by covering only one side of the 3-
layer slab. For justification we rely on our previous study which showed that very
similar results are obtained for a coverage of a 4-layer Ni slab with H_2 on one side
or on both sides.[15]

The one-side coverage makes the two identical A layers in 4 different in the
covered metal slab, as shown schematically in 6. The top layer A' can be
described as the "adsorbing" layer, the inner layer B' is "bulk-like" and the bottom
layer C' is similar in character to the surface layer A in the bare metal (except
for a small perturbation by the remote adsorbent).

CH_x

A'

B'

C'
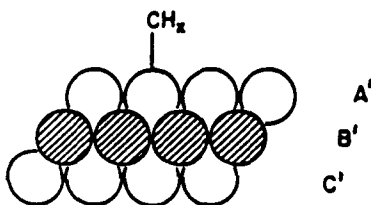
6

We have studied the adsorption of three organic radicals, CH_3, CH_2 and CH, all
believed to be intermediates in the FT synthesis.[1] Regardless of the geometry that
is chosen, a 1:1 coverage of the metal surface by CH_3 or CH_2 is chemically
unrealistic due to the very short distances and the resulting excessive steric
repulsions between the hydrocarbons. We have chosen a one-third coverage, which
ensures minimal interactions between neighboring fragments but which still allows
the use in the calculation of a convenient unit cell which is only three times
larger than in the bare metal. The details concerning the unit cell which was used,
the Brillouin Zone, the special k points, etc. are given in Appendix I. For each of
the organic radicals we have considered three possible adsorption sites: a mono-
coordinated "on-top" site 7, a site "bridging" two metal atoms 8, and "triply-
bridging", "capping" or "hollow" site 9.

7   8   9
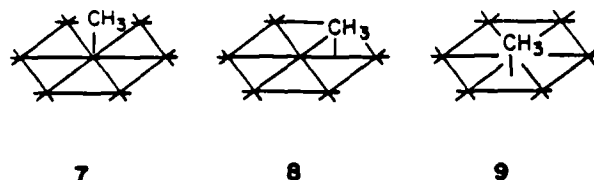
As in our previous studies[15,19,21] we use the language and formalism of simple perturbation theory. Within this framework the interaction of two levels, ΔE, is given by equation 2. The magnitude of the matrix element H_{ij} in the numerator is

$$\Delta E = \frac{|H_{ij}|^2}{E_j^* - E_i^*} \qquad (2)$$

related to the overlap of the relevant orbitals, and the denominator tells us that the interaction is greater the more two orbitals come into resonance.

The consequence of orbital interactions between the metal bands and the orbitals of the organic fragment can be traced down and analyzed by examining the DOS curves. Contributions or projections of specific orbitals are particularly helpful. In general, a strong shift in the position of a particular fragment orbital as it approaches the metal surface indicates strong interaction, either bonding or antibonding. A small shift, on the other hand, indicates little interaction.

Another important tool for the analysis is the COOP (for Crystal Orbital Overlap Population) curve, which gives the relative number of levels in a given energy interval weighted by the contribution that these levels make to the overlap population of a specified bond. In other words a COOP curve allows us to determine if a collection of energy levels contributes to bonding or antibonding between two atoms or fragments. We find that both the DOS and the COOP curves, but in particular their combination, are very effective in analyzing the bonding properties of metal surfaces. The use of these tools will be demonstrated throughout the paper. The interested reader is referred to our previous studies[14c,15a,19,21] for a more complete discussion.

We proceed now to analyze in some detail the bonding between each of the organic radicals and the metal surface.

ADSORBED METHYL

The orbitals of the methyl fragment are well known and they are shown in Figure 3. We arbitrarily choose to define the methyl fragment as a radical so that at infinite separation both the metal and the radical are neutral. The HOMO of the methyl radical is n-CH_3, a nonbonding type orbital at -11.75 eV. This orbital, which we will call n, is singly occupied. Lower in energy, at -15.56 eV, are the two degenerate π-CH_3 orbitals and still lower is the σ-CH_3 orbital. The LUMO consists of the two degenerate π^*-CH_3 orbitals at 4.99 eV.

Figure 3 here

There are many interaction modes between the methyl radical and the metal slab, but the perturbation expression helps one sort these out. In the schematic diagram 10 we have assigned number ①, ② and ③ to the interactions of n, π^*-CH_3 and π-CH_3 with the unfilled band states of the surface slab, and ①', ②', ③' to the interaction with filled metal states. Whether these are overall stabilizing or destabilizing is a function of the orbital filling. The magnitude of the interactions obviously depends critically on both the separation in energy between the interacting orbitals and the effectiveness of the overlap in question. 10 also contains a qualitative summary of our expectations, including the anticipated direction of charge transfer that is a consequence of each interaction.
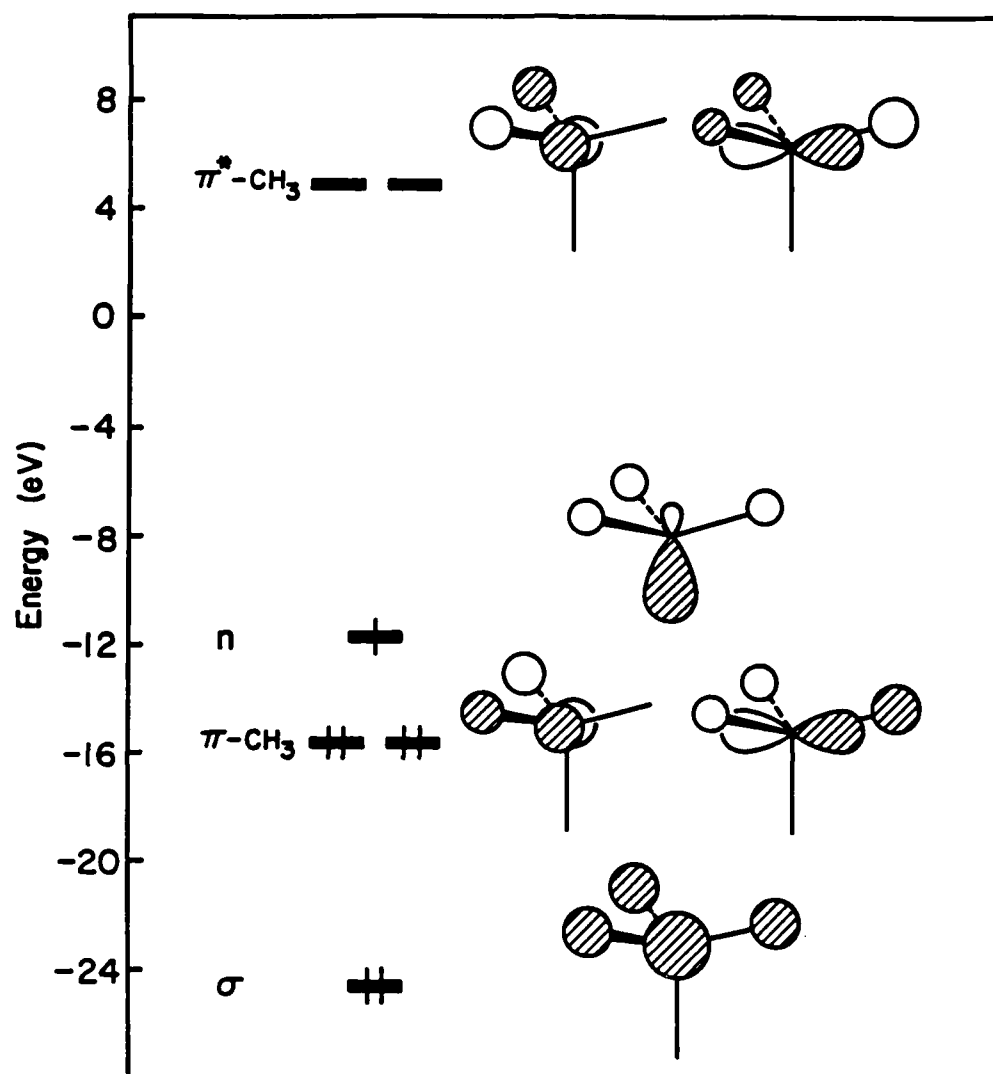

10
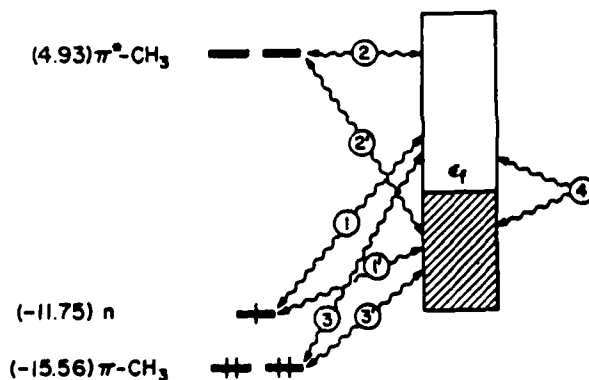
Figure 3: Molecular orbitals of a CH₃ group.

Interaction	# Electrons	Stabilizing?	Effective	Charge Transfer
①	1	yes	yes	to M
①'	3	yes	yes	to CH_3
②	0	no	no	none
②'	2	yes	no	to CH_3
③	2	yes	no	to M
③'	4	no	no	none

A word of explanation is needed on these expectations. Normally the focus would be on two-electron bonding interactions, for these are both stabilizing and effective in charge transfer. But in the case at hand none of the interactions of this type, ②' or ③ is very good, because the orbitals in question are far from resonance. Instead interactions ① and ①' of the methyl radical orbital become most important. And interaction ①', typical of energetically ambiguous and difficult to analyze 3-electron interactions, will be crucial.

In addition to these interactions, all of which have molecular equivalents, we have interaction ④ characteristic of surfaces. ④ represents schematically the metal slab's ability to shift electron density between the bulk and surface layers, or on the surface to shift density between those metal atoms involved in bonding and those left alone. This occurs in response to the electronic demands imposed by interactions with the organic adsorbate.

We can trace the validity of the perturbation theory based characterization of the primary interactions by examining the consequences or symptoms of interaction in the DOS curves of Figure 4a. This is for methyl on Co(0001) in the on-top geometry. Projections of the methyl orbitals are darkened and the position of these orbitals in the isolated organic fragments are indicated by the arrows.
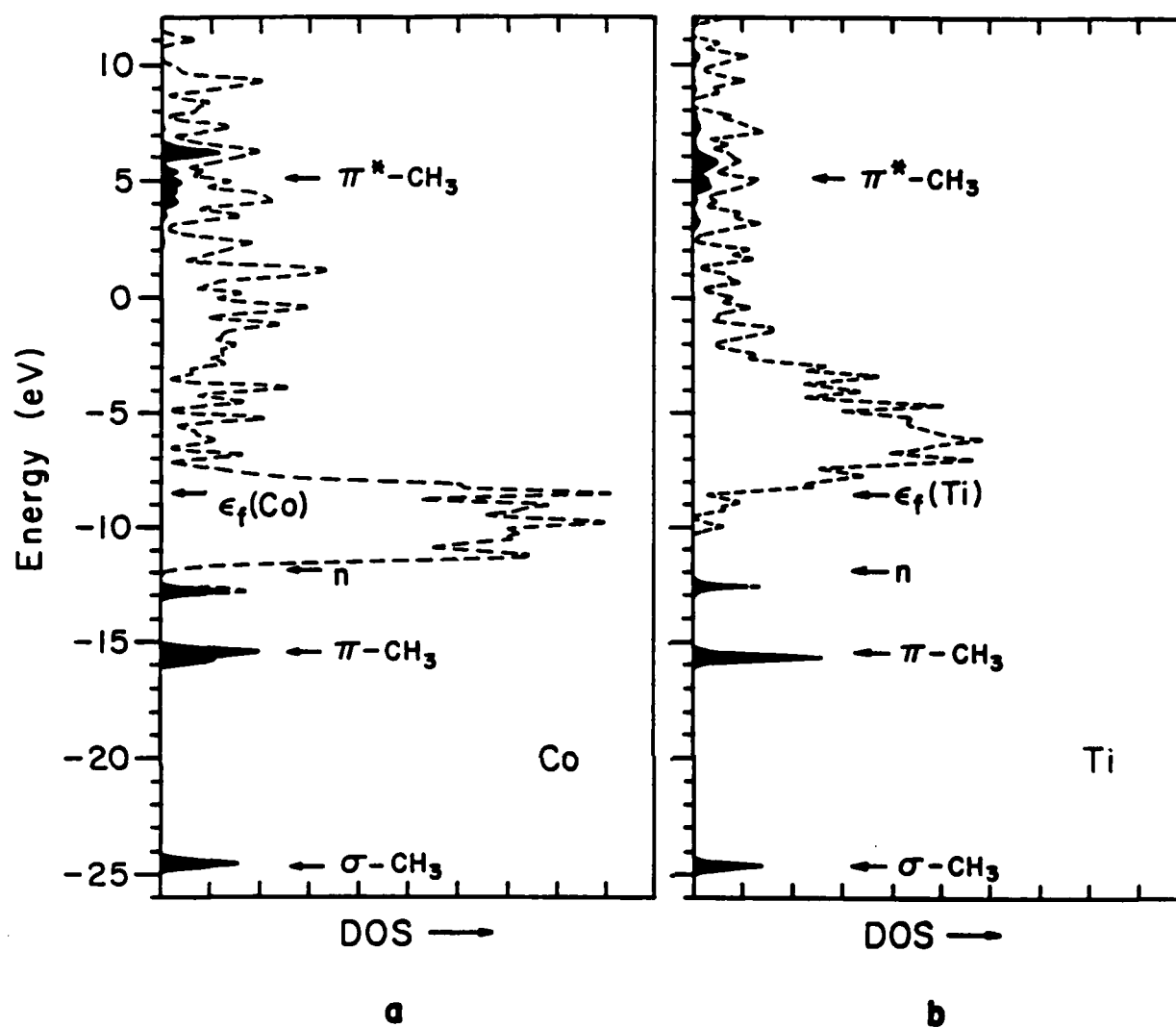
Figure 4 here

Figure 4: Total DOS (dashed line) and the CH_3 contribution (darkened area) when a CH_3 group is chemisorbed in an on-top geometry on Co(0001) (a) and Ti(0001) (b) surfaces. The arrows indicate the CH_3 MO levels before the adsorption occurs.

As expected, the σ-CH$_3$ and the π-CH$_3$ bands of the adsorbed CH$_3$ are essentially at the same energy as in the isolated radical and their bands are narrow -- a clear indication of their weak interaction with the surface. In contrast, the energies of the n and the π^*-CH$_3$ orbitals change significantly upon interaction with the metal. The n band is pulled down to a lower energy (by $\sim$ 1 eV), while the π^*-CH$_3$ band is pushed up in energy approximately to the same degree. The large shifts of these orbitals relative to the orbitals of the isolated radical are clear indications of their strong interaction with the surface. The interaction, of course, depends on the M-C distance. The DOS in Figure 4 are calculated for a typical M-C distance of 2.1 Å (for the choice of the M-C distance see Appendix I).

Figure 4b is the DOS curve for the Ti case. Since the center of gravity of the d band and the Fermi level are higher in energy, we should expect a weaker interaction between the metal and the CH$_3$. n in Figure 4b is pushed down less than in Figure 4a. However, the main feature remains the same. The Cr case is intermediate between the Co and Ti, and we omit it.

CH$_3$ IN THE ON-TOP GEOMETRY

We will analyze this specific case in more detail than the others so as to demonstrate how the DOS and COOP curves may be used to understand the bonding. The other geometries can be then analyzed in less detail. We concentrate on the Co surface. The DOS curve of geometry 7 (Figure 4), was already discussed above. We have concluded that among the methyl orbitals only the n and π^*-CH$_3$ orbitals contribute to metal-carbon bonding (i.e., interactions ①, ① and ② in 10). We proceed now to examine these interactions in more detail.

We shall begin with interaction between the n-CH$_3$ orbital and the metal bands. If we were in a discrete mono-nuclear complex then we could simply say that the σ nature of the CH$_3$ n orbital allows interaction with d$_z$2, 11, but prohibits them with, say, d$_{xz}$, 12. Life is not so simple in the solid. Each metal orbital

spreads out into a band. Local interactions are dominant, but symmetry limitations on interaction are not so strong. We often have to replace statements such as "does (or does not) interact with a given level" by "interacts more (or less) with such and such part of a band."
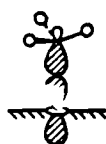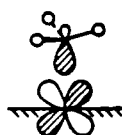

11   **12**

Let us illustrate this point qualitatively with the interaction of n. In the metal there is not one d_{z^2} and d_{xz}. orbital but many. 13 illustrates schematically some representative orbitals in the d_{z^2} and d_{xz} bands. The orbitals at the bottom of a band are metal-metal bonding, those in the middle non-bonding, those at the top antibonding. Things are more complicated in three (or two) dimensions, but these one-dimensional representations are indicative of what transpires.

d_{z^2} d_{xz}
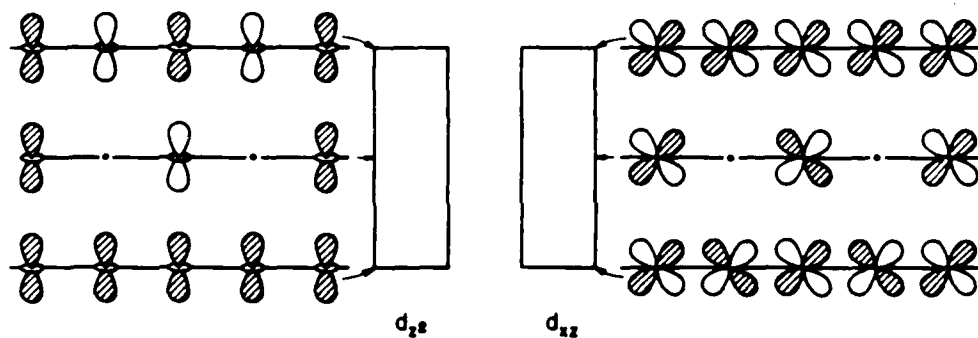
13

What we can say now is that n interacts with the entire d_{z^2} band, but perhaps more strongly with the bottom of the band than with the top, judging by the overlap differences between 14 and 15. For interaction with the d_{xz} band, the overlap is strictly zero only at the zone center and edge (the most antibonding and bonding combinations, respectively). It is never very efficient, but as 16 shows, one can have an overlap between the middle of the d_{xz} band and n. Still, the overlap in 16, depending as it does on non-nearest neighbor interaction, is not

very good for on-top adsorption. So in analogy to discrete complexes we can focus
our attention on locally strong σ interactions. In addition to d_{z^2}, s and p_z have
the proper local symmetry to interact. They will do so, but the mixing with p_z is
not great since it is very high in energy relative to n.

14   15
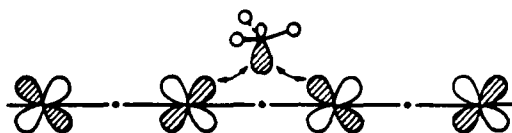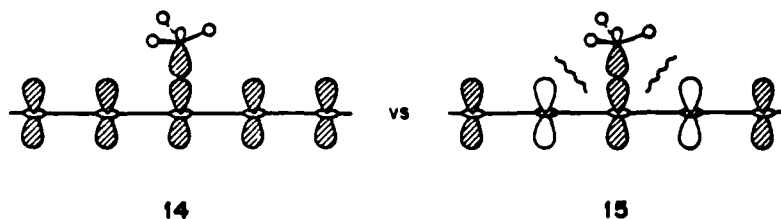
16

The interactions between n of substrate and the surface are shown schematically
in 17. We have drawn the s and d_{z^2} contribution (and omitted p_z), but really
one has a linear combination of these, i.e. hybridization of the surface orbitals,
in a chemically intuitive way, so as to produce hybrids reaching out for better
interaction with n.
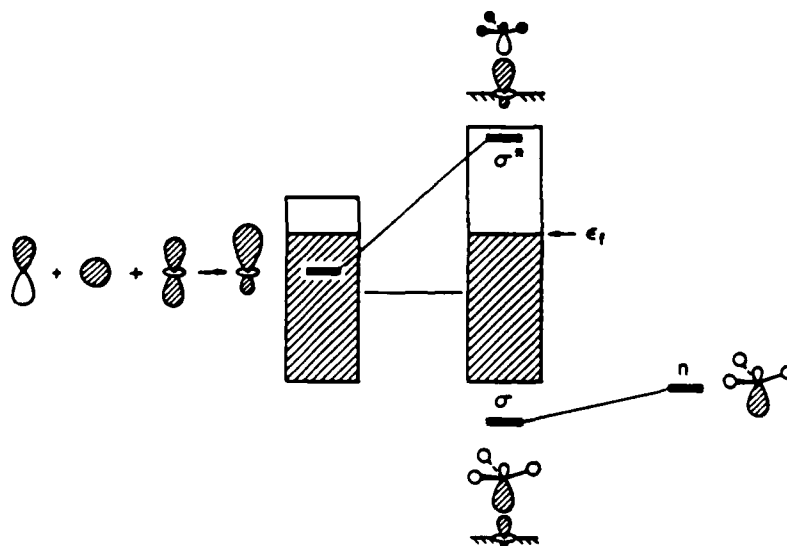
17

Interaction diagram $\underline{17}$ is highly schematic. Let's see the actual manifestations of the bonding in the DOS. We already saw the n peak move down in energy in the DOS decomposition of Figure 4. Now let us examine the detailed contribution of n, s and d_z2 to the DOS. This is shown in Figure 4, along with the COOP curve of Figure 6.

Figures 5 and 6 here

The peak in the DOS of the composite system at -13 eV is mainly the methyl lone pair, n. It is stabilized by interaction with surface d_z2 and s. This is attested to by the contribution of these orbitals -- 10% of the total s states and 9% of the d_z2 states lie in this band (see projections in Figure 5) and their predominant metal-carbon bonding character (see COOP curve in Figure 6).

The antibonding component of the metal-methyl interaction is also clearly seen. The metal d_z2 band, formerly confined to the region of -12 to -8 eV, is now broader, -13 to +2 eV. Much of the density in it is pushed up above the Fermi level. The COOP curve shows a broad region of M-C antibonding from -11 to -4 eV. Here are disposed, highly delocalized, the n-d_z2 antibonding combinations. The still higher energy M-C antibonding region arises from out-of-phase mixing of metal s and p_z with methyl lone pair.

Some further insight into the special interaction of surface d_z2 may be obtained by looking at the contribution to the DOS of the surface Co atom not involved in bonding to a methyl group, Co2, and comparing it with the bonded Co1. This is done in Figure 7. Note how the Co2 d_z2 DOS remains compact, relatively undispersed, while that of Co1 d_z2 becomes quite spread out. Bonding implies dispersion.
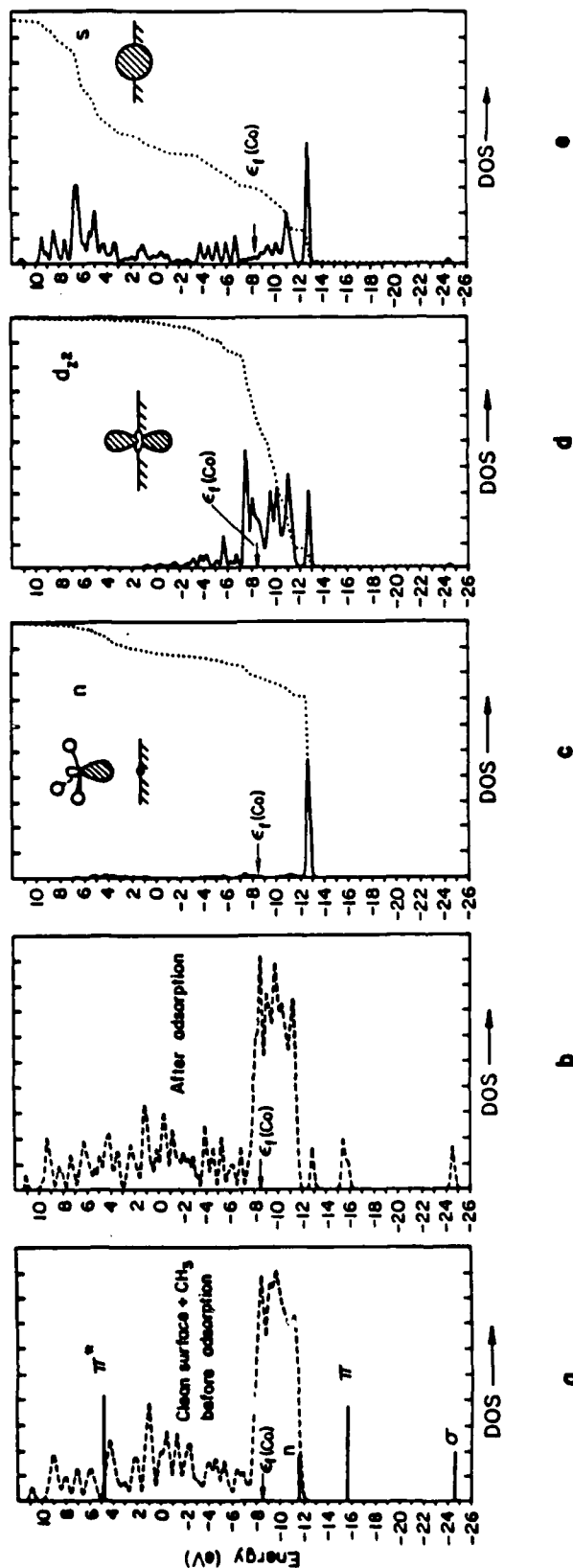
Figure 7 here

Figure 5: DOS of the chemisorbed Co(0001) (CH₃ on-top). a. DOS before the adsorption, the dashed line indicates the metal DOS, the horizontal lines show the free CH₃ MO levels. b. Total DOS after the chemisorption occurs. c. n-CH₃ (magnified) states in the chemisorbed system. d and e show the d_{z^2} and s states (magnified) of the metal atom below the CH₃ group.
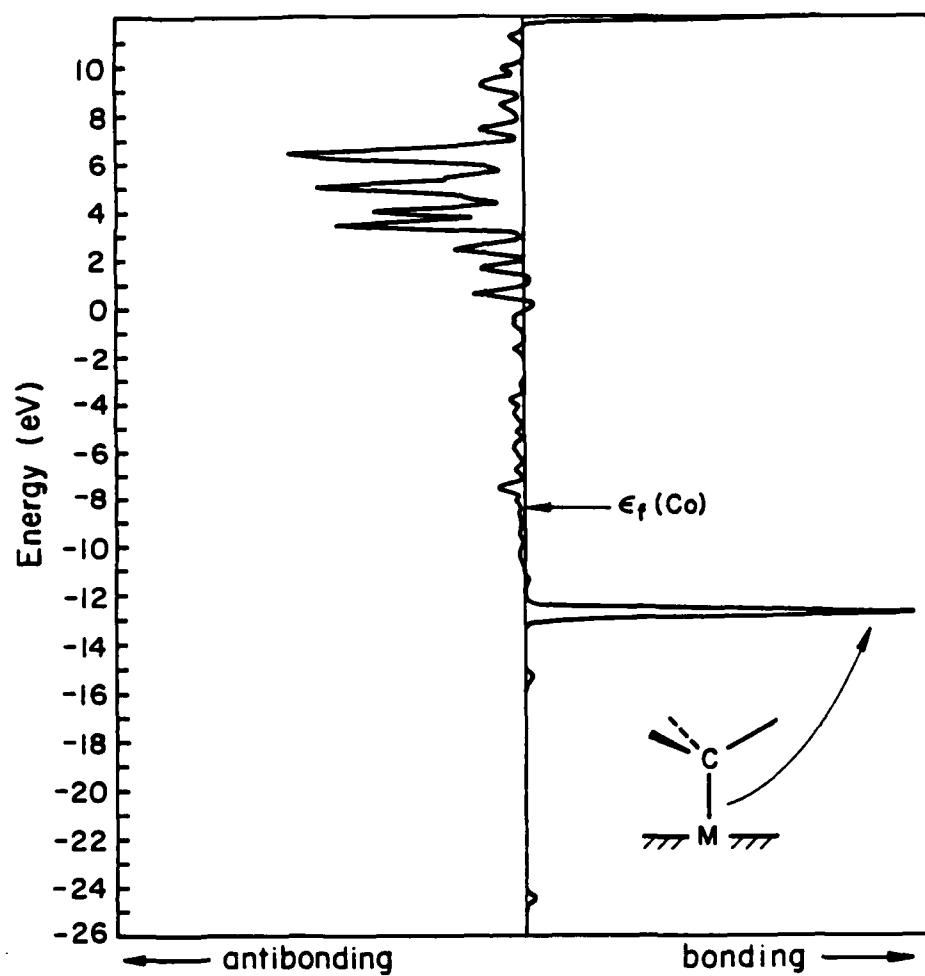
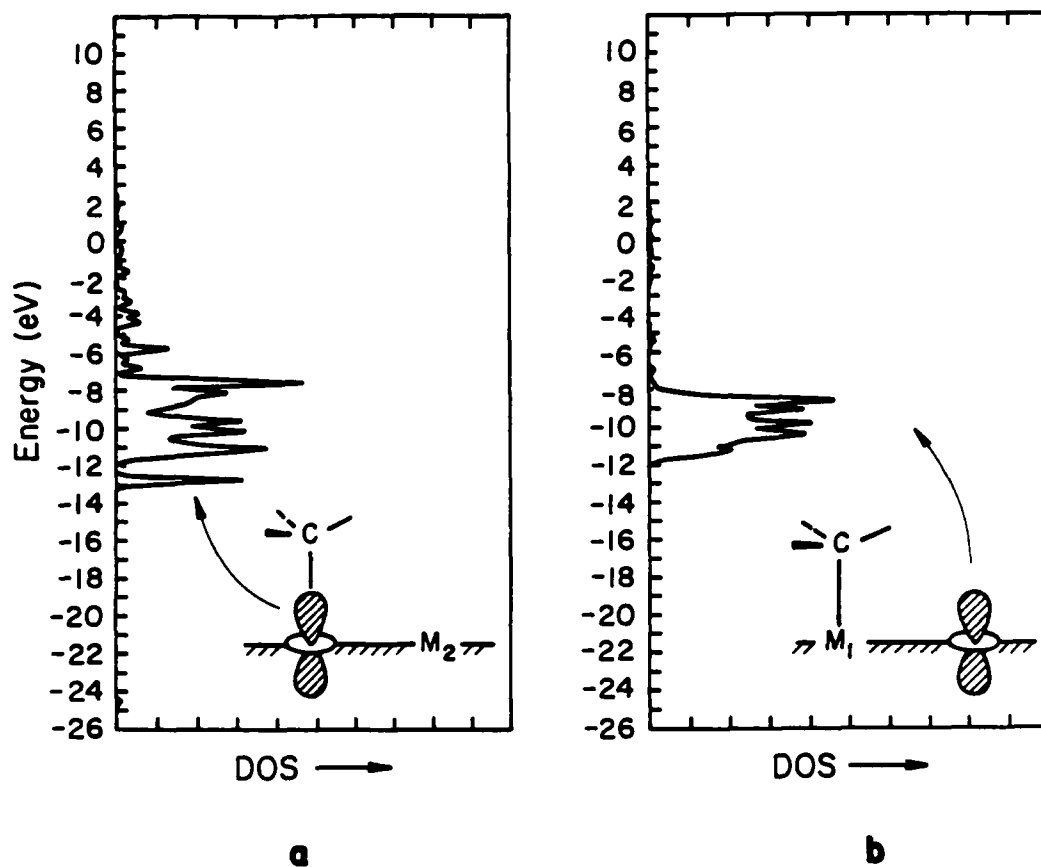Figure 6: COOP curve of the M-C bond of a CH$_3$ group on Co(0001) in the on-top geometry.

Figure 7: A comparison of the d_z2 states. a corresponds to the metal below the CH_3 group and b the adjacent metal atom (the one not capped by a CH_3).

We have now seen how the qualitative model of localized interactions and a perturbation theory based language for discussing these interactions are beautifully supported by the DOS and COOP curves. The molecule is bound to the surface primarily by the $n+d_z2,s$ interaction. Many M-C antibonding combinations are pushed above the Fermi level. The n band is nearly totally populated, with 1.6 electrons per methyl group. Note that this brings the CH_3 group closer to CH_3^-, but then the formalism of the methyl choice was just that, a formalism.

Another interaction that might have led to further charge transfer to CH_3 is ② between various metal orbitals, mainly d_{xz}, d_{yz} and methyl π^*-CH_3. The calculations show clear signs of that interaction, but it is not very effective, for the separation in energy between the interacting orbitals is large.

We have discussed so far the M-C bonding, which is obviously the major chemical event that occurs when methyl is attached to a metal surface. However, there are additional bonding interactions between the metal and the organic fragment as well as changes within the metal slab and within the organic fragment. Let us discuss now briefly these "secondary" changes which follow adsorption.

Looking first at the hydrogen-metal interactions, we find that these are extremely small and slightly M-H antibonding. This holds for both the M1-H and (M1 is the metal atom directly bonded to carbon, etc.) and the M2-H interactions. Thus, for Co, the corresponding overlap populations are -0.022 and -0.002 respectively. A detailed examination of the COOP curve for M-H bonding shows an antibonding contribution in the band at -12.6 eV, which is mainly the bonding $n+d_z2,s$ combination. The small M-H antibonding effect is set by the phase relationship defined in 18.

bonding ( ) antibonding
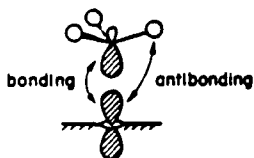
Our conclusion that the M-H interactions are weak and unimportant contrasts with those of Muetterties' group.[22] They have performed extended Hückel cluster type calculations[22a] and have reached the conclusion that multicenter metal-hydrogen-carbon interactions play a decisive role in the chemisorption of hydrocarbons on clean metal surfaces. They emphasized that the most stable geometries are those that achieve maximum multicenter bonding of this type. In light of this discrepancy we looked further into this problem. We changed the M-C-H angle from 109.5° to 95°, so that Co1-H distance decreases from 2.67Å in $\underline{6}$ to 2.45Å.

Still we find no indication of metal-hydrogen bonding. On the contrary, as the hydrogens approach the metal surface the antibonding interactions increase. Thus our calculations predict repulsion, not attraction, between the surface and the β-hydrogens. It is interesting that Minot, Van Hove and Somorjai[18] used extended Hückel cluster calculations similar to those of Muetterties and did not mention the presence of strong metal-β-hydrogen interactions.

We now turn to the metal-metal bonding changes upon chemisorption of the methyl group. We find that as the new M-C bond is formed the metal-metal bonds around the binding site are weakened. Thus, the overlap population between Co1 and Co2 drops from 0.185 in the bare metal to 0.170 in the covered surface (similarly for Cr and Ti the values are 0.462 and 0.411, 0.350 and 0.291, respectively). To some extent the new M-C bond is formed at the expense of weakening the bonds within the metal lattice. For a more detailed analysis of this general phenomenon the reader is referred to another contribution from our group.[21]

The overall effect of adsorption on the C-H bonds is small. The relevant overlap population is 0.779 in isolated CH_3, 0.787 in isolated CH_3^- and 0.791 (for the Co surface).

Further insight into the bonding mechanism is provided by analyzing the charge distributions. The methyl is calculated to be strongly negative with a charge of -0.585 (see Table 2). This is for Co. High negative values are observed for the other metal surfaces. Thus, if the metal and the CH_3 fragments are taken as neutral

when separated, then upon chemisorption strong electron transfer from the metal to the methyl takes place; the metal becomes positively, and the methyl negatively charged. This is true for Ti and Cr surfaces as well as Co, thought there are differences to which we will return later.

Table 2 here

Where does this electron transfer come from, and how can we reconcile it with the organometallic view of methyl as a donor? The electron transfer derives primarily from the large (80%) occupation of n on adsorption, and that in turn is a consequence of the $n+d_z2$,s bonding combinations, the large peak in the DOS at -12.6 eV, coming way below the Fermi level. To put it another way, and at the same time to answer the second question posed above, on the surface n is filled, and a better conceptual starting point might have been to think of it as an adsorbed CH_3^-, a carbanion. If one views the charge transfer as beginning from CH_3^- and $(slab)^+$ then the process of bonding is accompanied by a drift of 0.415 electrons from CH_3^- to the slab. The direction of this electron drift might make some organometallic chemists happier; we think what is important is that one perceives the equally valid dual viewpoints of the bonding process.

From which levels of the metal's "sea of electrons" do these transferred electrons come? We return here to a neutral CH_3 reference (i.e. the calculated transfer being to methyl). Examination of the electron distribution chart (for Co) 19 shows that most of the electrons (0.47 electrons) come from one metal atom--Co1, which is directly bonded to the organic fragment. The adjacent atoms in the surface layer, Co1, also participate by donating 0.12 electrons. The other atoms are merely spectators in the bonding process. The inner B' and the second-inner C' layers remain essentially unchanged. The only atom in the inner layers that "feels" the adsorbent is the Co atom located exactly below Co1, which gains 0.07 electrons. Interaction ④ in 10, which involves charge transfer within the metal slab, is small in this case.

Charges

	before	after adsorption	
A	−0.30	+0.17 CH₃ −0.58 −0.18	A'
B	+0.61	•CH₃ → +0.61	B'
A	−0.30	−0.37 −0.30	C'
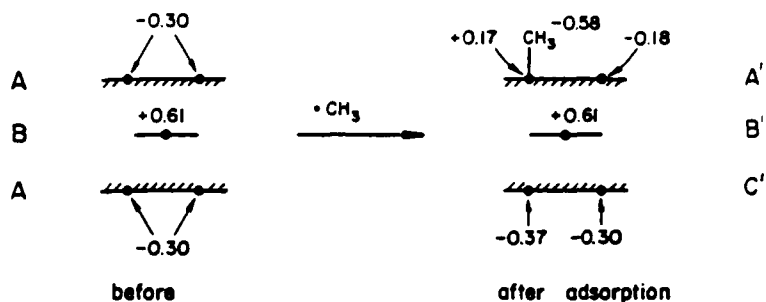
19

Thus the charge transfer is a localized phenomenon, occurring mainly between the two atoms (Co1 and C) that form the new bond. Furthermore, not all the orbitals on Co1 contribute. Most of the charge comes from the $d_z 2$ orbital (0.53 electrons), the d_{xz} and d_{yz} orbitals contribute only 0.002 electrons each. The small electron donation from the d_{xz} and d_{yz} orbitals is a strong indication that the p-type interactions with π^*-CH₃ are relatively weak and charge transfer occurs mainly in the σ-framework through the M-n interaction (see 17). Thus, based on the charge criteria, M-C bonding is due mainly to the σ M + n interaction. Similar conclusion can be drawn for the Ti and Cr surfaces.

To summarize: the overall picture that emerges from our analysis is that of localized bonding where essentially only one metal atom participates in the formation of the new metal-CH₃ bond. The orbitals that participate are also limited. In the metal slab these are mainly $d_z 2$ and s on M1 and on the methyl it is primarily the methyl lone pair, n. The other metal atoms as well as the other orbitals hardly feel the adsorbent. This bonding description is very similar to that in an isolated ML₅CH₃ complex, of which many are known. There is one difference in the surface case. In the molecular case the ML₅ acceptor orbital that interacts with the CH₃ n is an empty $d_z 2$-s-p_z hybrid, and that hybrid become populated upon interaction. In the case of the surface the orbital that interacts with CH₃ n is not one orbital, but the entire $d_z 2$ band. The metal actually loses electron density through this interaction, as some $d_z 2$-n antibonding combinations are pushed above the Fermi level.
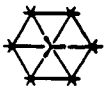
TABLE 2. Orbital Occupations of CH_3^-

Geometry		π	n	π^*	Total Charge
	Ti	3.98	1.74	0.01	-0.79
	Cr	3.99	1.64	0.02	-0.66
	Co	4.00	1.58	0.01	-0.59
	Ti	3.92	1.70	0.06	-0.77
	Cr	3.93	1.62	0.07	-0.63
	Co	3.95	1.54	0.03	-0.53
	Ti	3.92	1.70	0.06	-0.77
	Cr	3.84	1.60	0.11	-0.62
	Co	3.93	1.52	0.04	-0.52

TABLE 3. Bonding Information on the Surface as a Function of the Metal
          Electron Count.

	Overlap Population			Fermi Energy (eV)	Binding Energy	
	M-C	M-H	M-M		E_1(eV)	E_2(eV)
Co	0.415	-0.022	0.170	-8.48	3.73	0.47
Cr	0.418	-0.005	0.411	-7.51	4.29	0.09
Ti	0.374	-0.039	0.291	-6.47	5.42	0.16

a. $E_1 = [E(\text{slab}) + E(CH_3)] - E_{\text{total}}$;
$E_2 = [E(\text{slab}^+) + E(CH_3^-)] - E_{\text{total}}$. Thus the positive signs mean CH_3
or CH_3^- is bound. E_2 measures the covalent contribution to the total
binding energy E_1.

Let us examine now how the bonding between the methyl and the surface changes as the electron count of the metal is decreased. Relevant overlap population data for Co, Cr and Ti as well as the corresponding binding energies are presented in Table 3.

As one sweeps across the transition series from left to right the average energy of a d electron, the center of gravity of the d band, moves down. This variation may have certain consequence, for as the center of gravity of the band shifts different adsorbate levels may interact more or less strongly. A good illustration of this may be found in another reaction we have studied, CO chemisorption and dissociation.[19] As one moves to the left in the transition series, the CO π^* becomes increasingly occupied, with consequent dissociative chemisorption.

According to the COOP curve of Figure 6, the d band energy range above the n peak is mainly M-C nonbonding. Thus as the d-band is depopulated the M-C overlap population (which is summed up to the Fermi level) is expected to remain about the same. In the Ti case, however, the d band is higher in energy and should interact less effectively with n (by the energy criterion of eq. 2). This is reflected in the M-C overlap populations in Table 3.

Table 3 here

The metal-metal overlap population increases on going from Co to Cr, as expected from the fact that the top of the d-band is metal-metal antibonding. But from Cr to Ti some bonding states are emptied, so we expect the overlap population to decrease and the M-M bond to be weakened. Figure 8 shows a typical COOP curve for the M-M bond which is the basis of this reasoning.

Figure 8 here

The binding energies of the methyl fragment to the metal surface, which are also given in Table 3, are naturally of special interest. The binding energy is defined here as the energy of a covered unit cell minus the combined energies of the neutral methyl fragment and of a unit cell of the bare surface. Although the extended Hückel method is not expected to reproduce quantitatively the binding

energies we do believe that the relative binding energies have chemical significance. Unfortunately, there is no reliable experimental data which can be used to calibrate our calculation.

We have traced down above the origins of the bonding interactions between the metal and the methyl. The binding energy gives the total energetic consequences that occur as the methyl binds to the surface. These include the changes that occur in all bonds, specifically the M-C, M-M, M-H and C-H bonds. Why do the binding energies (E_1) that are defined as $E_1=[E(slab)+E(CH_3)]-E_{total}$ decrease on going from Ti to Co although the M-C bonds get stronger and the M-M bonds alternate in the way we described above (Table 3)? This apparent paradox is reminiscent of a similar situation which occurs in using frontier orbital arguments in analyzing the strength of simple two electron bonds.[23] Within this simplistic theoretical framework it seems that the strength of a bond should increase as the energy separation between the interacting orbitals decreases, i.e., as its covalent character increases. Highly ionic bonds, where the separation between the orbitals that form the bonds is very large, are therefore expected to be extremely weak, contrary to reality.[23] As we use here essentially frontier orbital logic (eq. 2) in analyzing the M-CH$_3$ bond, which on the basis of the charge distribution is substantially ionic, it is not surprising that similar problems arise. Picture 20 describes schematically the energetic consequences of the ionic character of the M-C bond. The M-C bond strength arises mainly from the fact that the approaching CH$_3$ radical brings along a "hole" at an energy of -11.75 eV, 3.26 eV below the Fermi level of cobalt. The M-C bond is formed by an electron transfer from the metal into this "hole" and a binding energy of 3.26 eV is gained in this process. Thus, the "ionic character" of the M-C bond can be described as responsible for 87% of the total binding energy (3.73 eV) of the methyl radical to the Co surface. The difference of 0.47 eV can be described as the "covalent contribution" to M-C bonding (E_2 value in Table 3, see also discussion below).
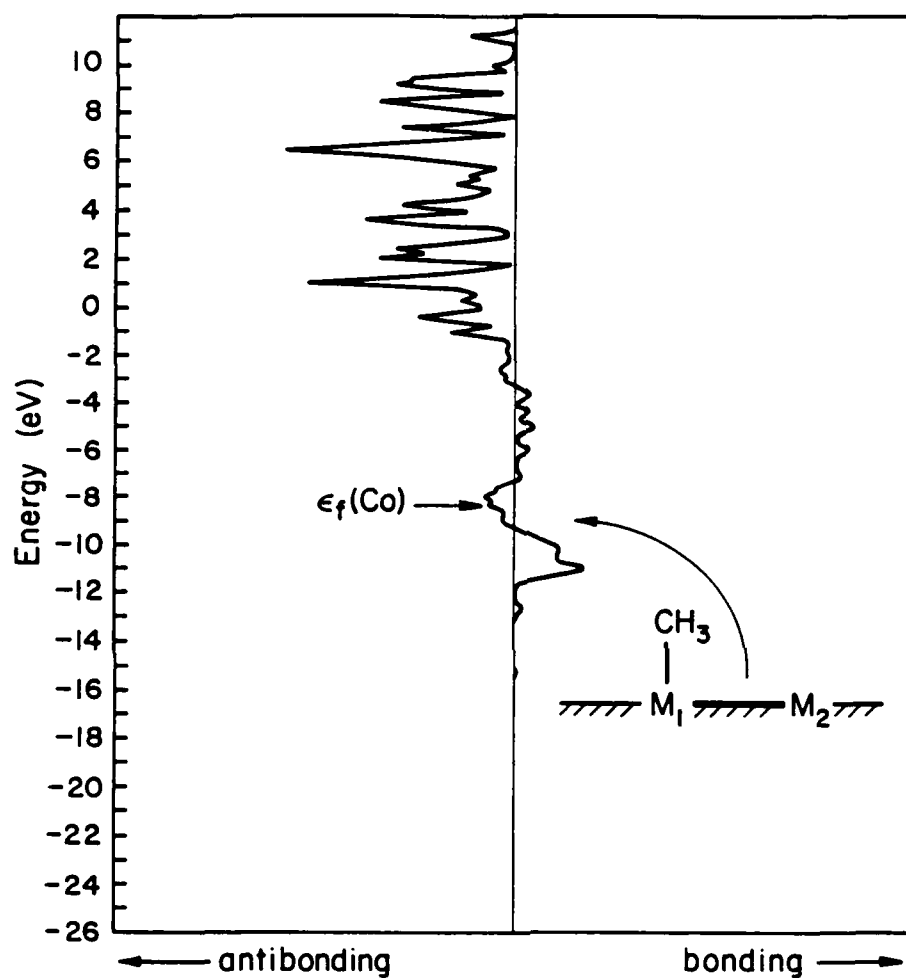
Figure 8: COOP curve for the surface M-M bond of the CH₃ on Co(0001) (on-top) system.

THE BRIDGING METHYL GEOMETRY, 8

Figure 9 displays the total DOS (dashed line) of the Co(0001) system upon chemisorption of CH_3 in a doubly bridging geometry. The darkened areas show the contributions of the organic fragment and the arrows indicate the location of these states in the isolated fragment. Figure 10 shows the COOP curves for the metal-carbon bonds. Comparison of Figures 9 and 5 and of 10 and 6 reveals immediately the similarity in the bonding mechanisms in the on-top and the bridged geometries. In both cases the interaction which is primarily responsible for the metal-carbon bonding is that with the n orbital. Nevertheless, there are important differences in the details of the bonding mechanisms in the two geometries and we concentrate our attention on these.

Figure 9 and 10 here

The major difference is obvious. In the "on-top" geometry only one surface atom contributes to M-CH_3 bonding, while in the bridging case two metal atoms are clearly involved. More interesting is the contribution of the various orbitals to M-C bonding. In contrast to $\underline{7}$, the carbon atom in $\underline{8}$ is located off the d_{xz} nodal plane and effective interaction with the n orbital can now occur, see $\underline{22}$ (contrast with $\underline{12}$).
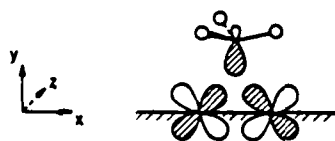
22

As seen in $\underline{22}$ these interactions take place with d_{xz} levels at or near the edge of the Brillouin zone, i.e. the top of the band. Projection of the d_{xz} levels (Figure 11) indeed shows considerable broadening of this band compared with $\underline{6}$

Figure 11 here

20
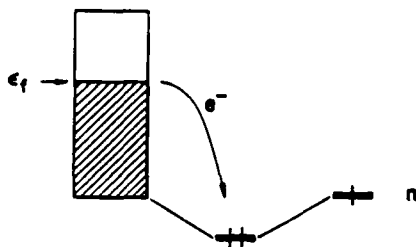
As we move from Co to Ti the Fermi level changes by ~2 eV to higher energy. The energy gain on filling the "hole" is now greater (see 20), and so is the binding energy and charge transfer to the methyl (-0.59 and -0.79 for Cr and Ti respectively). The smaller "ionic contribution" to the binding energy for Co compared to Ti is partially compensated by the increased "covalent character" of the Co-C bond which is reflected in the increased M-C overlap population (Table 3). The binding energy of methyl to Cr is therefore lower than that of Co-CH$_3$ by only 1.7 eV, not 2 eV as suggested in 20.

Once again it is useful to change perspective and think of the binding energy of a CH$_3^-$ anion to a positively charged slab. The "hole" is filled and ambiguities of charge transfer are avoided. Now the binding energy E$_2$, defined as E$_2$=[E(slab$^+$)+E(CH$_3^-$)]-E$_{total}$, is lower for Ti (0.16 eV) than for Co (0.47eV), paralleling the M-C overlap populations. Cr is intermediate between Ti and Co; due to its nonhexagonal lattice it might deviate from average behaviour.

A final point to be made about the on-top site is that the barrier for the rotation of the methyl group around its local C$_3$ axis of symmetry (see 21) is nearly zero. This is hardly surprising, for this is a sixfold barrier, and we know such to be very small in molecular cases.
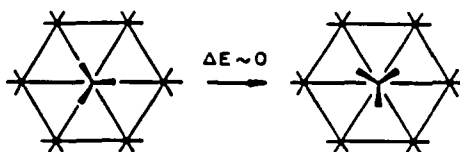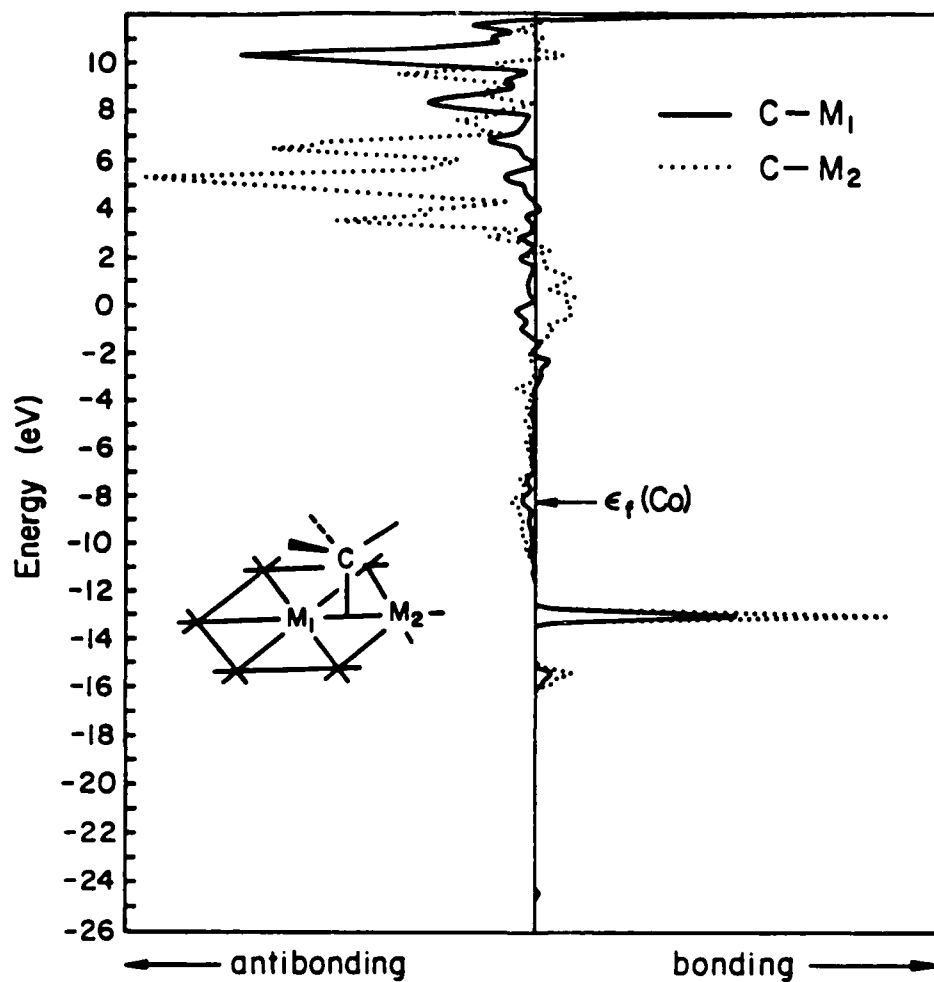
21

Figure 10: COOP curves of the two non-equivalent C-M bonds in the bridging CH_3 + Co(0001) system.
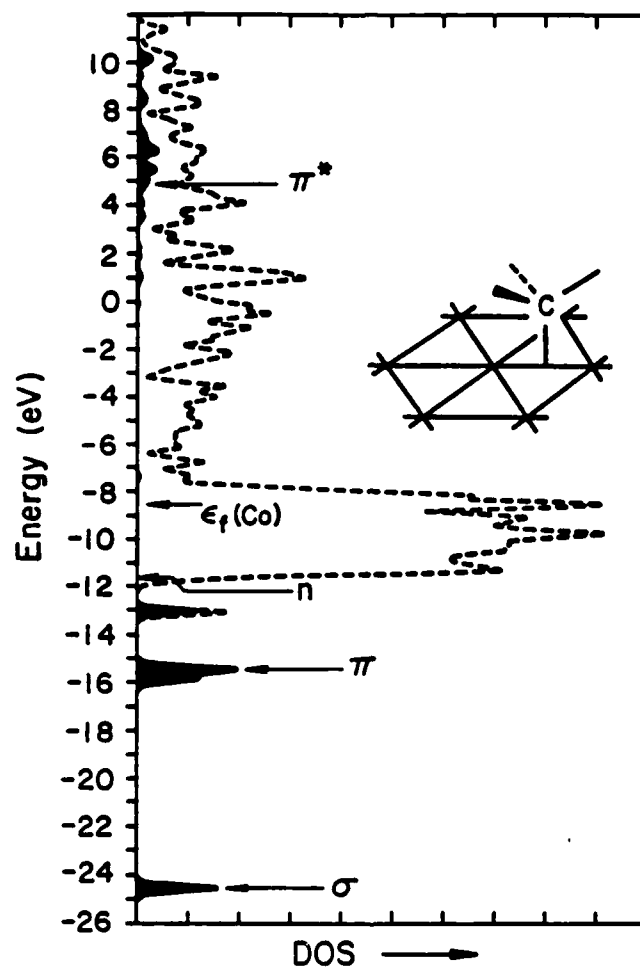
Figure 9: Total DOS (dashed line) and the CH_3 contribution (darkened area) of the bridging CH_3 + Co(0001) system. The arrows indicate where the free CH_3 MO levels were before the adsorption.

(Figure 5). In the bridging geometry the d_{xz} band contributes 12% (6% for each of the Co atoms) of the total number of states in the n band at -13ev. In 7 this contribution was close to zero. Another consequence of bridging is that n interacts effectively only with the bottom of the d_z2 band (23), and not with the top (24).

23   24
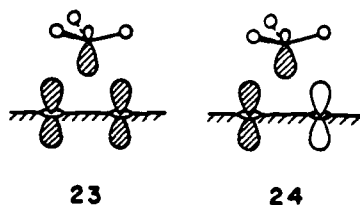
We thus expect that the contribution to M-C bonding from the d_z2 band will be smaller in the bridging mode than in the on-top. This is indeed observed. The contribution of the d_z2 band to M-C bonding (i.e. its portion of the n peak in the DOS) drops from 9% in 7 to less than 2% in 8 (compare Figures 11 and 6a). The participation of the s-band also diminishes from 16% in 7 to 12% in 8.

The contribution of the π-type interaction to M-C bonding is higher in the bridging than the on-top site. This is indicated in Figure 10 by the increased contribution of the π-CH_3 orbital at -15.3 eV to M-C bonding (compare with Figure 7). A major difference between 8 and 7 is that in the former the degeneracy of the methyl π-interactions is destroyed. These are two distinct components, one pointing along the M-M axis (i.e., x in 25) and the other in a direction perpendicular to it (y in 26). The π_x orbital interacts more strongly with the metal surface orbitals (see 25) than the π_y orbital (see 26). This is due primarily to the poorer orbital overlap in 26, but also to the energy of the piece of the d_{xz} or d_{yz} band with which overlap is effective. The representative d_{xz} orbital is near the top of its band (see the nodal relationship in 25) and so closer in energy to its π^*-CH_3 partner. The representative d_{yz} orbital is low in its band, 26.
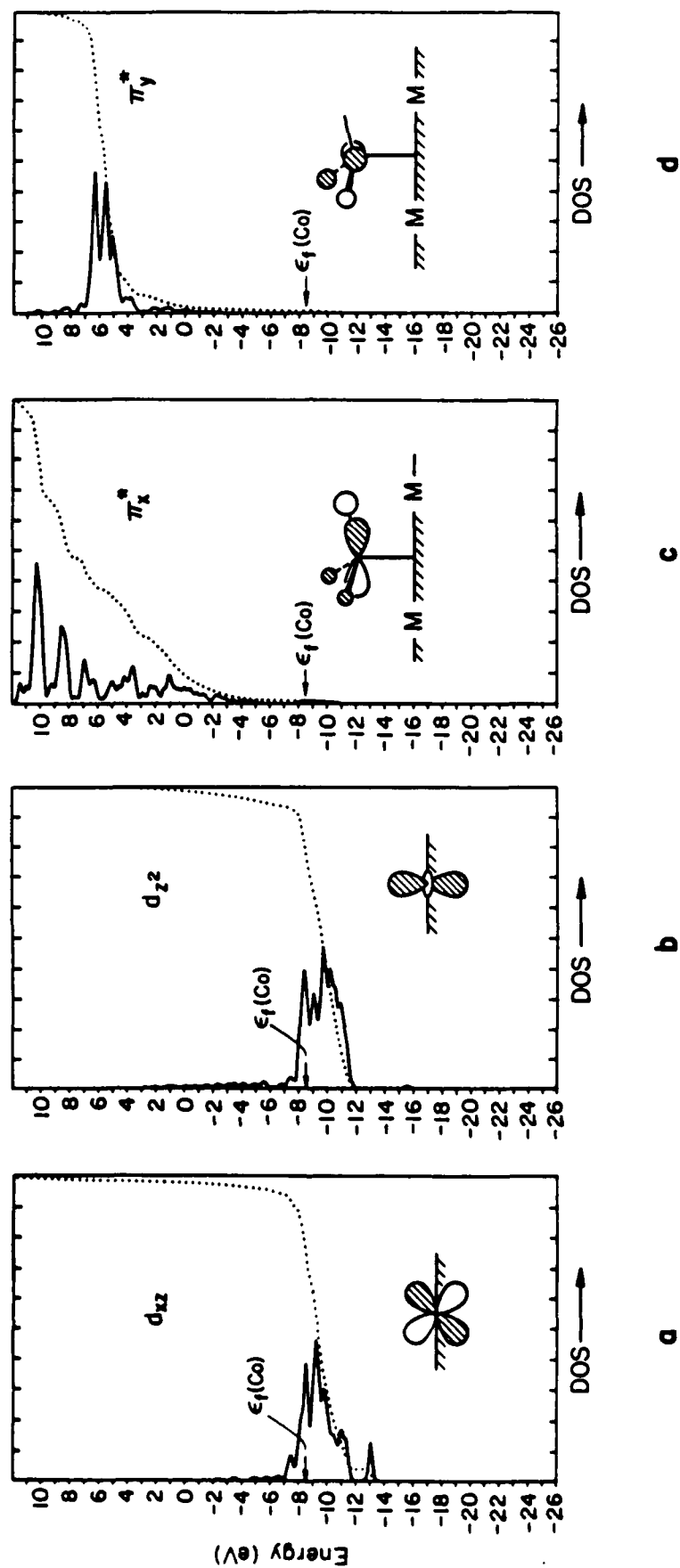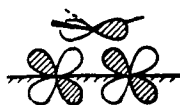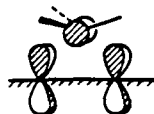
Figure 11: DOS of the bridging CH_3 + Co(0001) system. a. d_{xz}; b. d_{z^2}; c. π^*_x; d. π^*_y. The dotted lines are the integrations.

Energy (eV)

DOS →   DOS →   DOS →   DOS →

a   b   c   d

d_{xz} d_{z^2} π^*_x π^*_y

ϵ_f(Co) ϵ_f(Co) ϵ_f(Co) ϵ_f(Co)

25   **26**

This effect is beautifully exhibited by comparing Figures 11c and 11d which show the projected DOS curves of the methyls π^*_x and π^*_y orbitals respectively. While the π^*_x orbital is dispersed into a band of significant width indicating strong interaction with the metal, the π^*_y band remains relatively narrow.

The two bonded metal atoms contribute similarly, as expected, to the bonding of the CH_3 fragment. This is apparent from the total M-C overlap populations shown in 27, that indicate a slightly stronger Co1-C bond. Co1 is "staggered" with respect to the methyl hydrogens, Co2 "eclipsed".

			Total
Ti : 0.374	0.184	0.201	0.385
Cr : 0.418	0.227	0.209	0.436
Co : 0.414	0.224	0.208	0.432

27

Closer examination of the COOP curves in Figure 10 reveals an intriguing difference between Co1 and Co2. The COOP peak corresponding to the M+n interaction is almost twice as large for Co2 than for Co1. In the d-band region the contribution of Co2 to M-C antibonding is also larger than that of Co1. For cobalt, where the d-band is almost filled, the stronger contributions of Co2 to M-C bonding and antibonding nearly compensate and the Co1-C and Co2-C overlap populations are similar, the former being somewhat larger. As the d-band is depopulated the M2-C bond should gradually strengthen. The overlap populations calculated are in fact reversed for M - Ti, compared to Co (see 27).

The stronger M2-C interaction, in particular in the n band, must result from the different arrangement of the methyl hydrogens with respect to the two relevant metal atoms. There is a correlated differential in the direct M-H and C-H overlap

populations (see 28 and 29). But the effect is small and we are not certain
if it merits a detailed discussion.
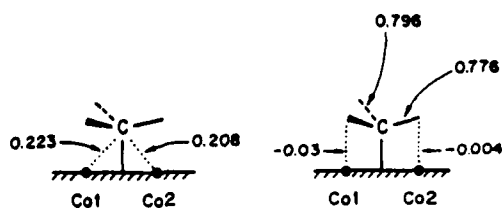

28   29

The total interaction between the methyl fragment and the metal surface seems
stronger in the bridged geometry than in the on-top geometry. Thus, in 8 the M+n
band that is the major contributor to M-C bonding is pushed to a lower energy by 0.2
eV (for Co) relative to its position in 7 - indicating a stronger bonding
interaction. Also, the M-C overlap population data indicates overall stronger M-C
bonding in 8.

Although the bonding between the metal atoms and the methyl is stronger in the
bridged geometry, the binding energy of the organic fragment to the surface is
lower in 8 compared to 7 see Table 4). Thus, for Co, Cr and Ti the binding
energies of methyl in the bridging geometry are by 1.1, 0.9 and 0.5 eV respectively
lower than in the on-top site. This apparent paradox of a stronger M-C bond that
results in a weaker binding of the CH_3 fragment to the surface becomes
comprehensible upon examining the M-M overlap populations in 30.

Ti	0.350	0.291	0.155
Cr	0.462	0.411	0.275
Co	0.184	0.170	0.110
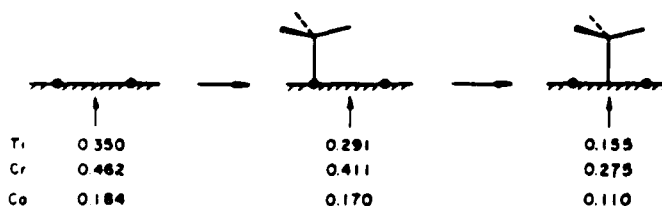
30

30 shows that the M1-M2 bond is considerably weakened on going from 7 to
8. This bond weakening is a direct consequence of the stronger metal-methyl
interactions that push many of the metal bands to higher energies. As the top of
the d-band is metal-metal antibonding (see Figure 8, the COOP for 7 is similar),

these bonds are weakened as the metal-fragment interactions become stronger. The

dominant n-d interaction pushes up above the Fermi level those metal states which

contribute to either M-M bonding or M-M antibonding in the on-top geometry. But

only M-M bonding states are lifted above the Fermi level by this interaction

at the bridging position, and the M-M bond is weakened more. Thus, the stronger M-C

bonding in 8 is gained in the expense of weakening the bonds within the metal

slab, therefore raising its energy. In the Co case (and to a smaller degree also

for Cr an Ti) the M-M bonding energy that is lost is greater than the M-C bonding

energy that is gained upon bridging and the binding energy of methyl is lower in 8

than 7. In addition, interaction 4 in 10 plays a role: as the M-M bonding

states are lifted up in energy, the electrons flow from these states into the top of

the d-band, which is M-M antibonding. Consequently, when the electron count on the

metal decreases and the M-M antibonding states are depopulated the difference in

binding energy between the on-top and the bridging geometry is reduced. In our

calculation the difference is 1.1 eV for Co and 0.9 eV for Cr, the on-top position

being more stable.

Only a few molecular complexes are known that have a methyl group bridging two

bonded metal atoms[24] (e.g. 31[24c] and 32[25]). In most such complexes the

methyl bridges two non-bonded metal atoms, as in 33.[26] Thus, it seems that in

analogy to our computations for the covered surface, in the molecular complexes the

bridging mode is accompanied by M-M bond weakening or by M-M bond cleavage.
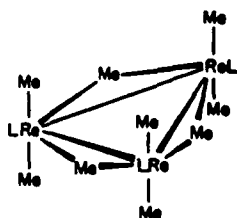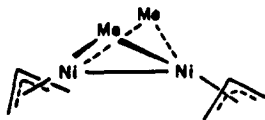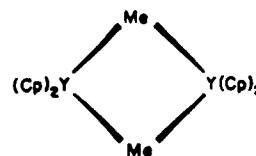
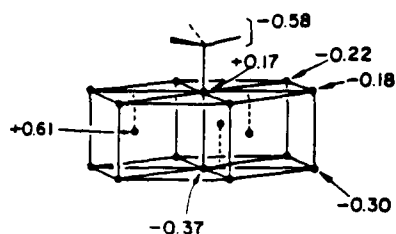31   32   33
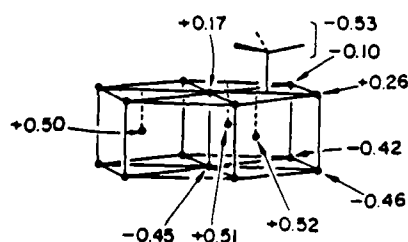
Finally, we comment on the charge transfer that occurs upon bridging. This is

shown in 34 and 35 for the cobalt surface.

34   35

As we can see the total transfer of charge from the metal to the methyl

fragment is nearly the same in 7 and 8 (0.585 and 0.531 electrons respectively).

However, there appear to be dramatic changes in the charge distributions within the

metal slab on going from 7 to 8. There is a substantial flow of charge from the

surface layer into the inner layers upon methyl bridging. The same is observed for

Cr and Ti surfaces. Thus for cobalt the calculations show that on going from 7 to

8 the surface A' layer loses 0.52 electrons while the B' and C' layers gain 0.30

and 0.36 electrons respectively. Thus, the Co surface layer which in the bare metal

is negatively charged becomes nearly neutral for on top bonding, and turns

positively charged in the bridging case. This substantial charge flow away from the

surface is easily understood in terms of the bonding picture that emerged from our

calculations. Bridging involves stronger interactions with the metal d-bands. The

surface bands that are involved in these interactions are pushed up to higher

energies and are therefore emptied. Charge flows to lower metal bands which are

concentrated in the inner slab layers. These charge flows provide a clear

determination of the importance of interaction④ in 10.

As in the on-top geometry, so also in the bridging site the methyl is

essentially freely rotating; there is no calculated rotational barrier.

THE THREE-FOLD BRIDGING OR CAPPING METHYL GEOMETRY, 9

Once we have analyzed in detail the on-top and the bridged geometries and have understood the bonding mechanism, then it is easy to predict what happens in the capping geometry 9. The trends that have been observed on going from 7 to 8 will hold also for moving from 8 to 9. In 9 the interactions between the methyl and the metal slab are the strongest, and the total M-C bonding increases, as expected, on going from 8 to 9. 36 and 37 show the overlap populations for the M-C and M-M bonds in both geometries. Concurrently on going from 8 to 9 the M-M bonds are weakened as reflected in the decreasing M-M total overlap populations (see 36 and 37). At high electron counts this results in a smaller binding energy for the capping geometry relative to the on-top mode (e.g., by 0.3 eV for Cr). For lower electron counts, many of the M-M bonding states, which are pushed up above the Fermi level by the CH_3-metal interaction, were originally empty. The gain in M-C bonding thus compensates more the loss in the M-M bonding in the lower electron count case. On the Cr surface our calculation shows no energetic difference between the bridging and capping sites and on Ti the capping geometry is more stable by 0.3eV. In all the cases under consideration, however, the on-top mode is the most stable one for CH_3.

|				
Ti:	0.229	0.155	0.261	0.191
Cr:	0.115	0.261	0.317	0.284, 0.100
Co:	0.144	0.110	0.155	0.113

36   **37**

The charge distributions also behave as expected. There is substantial electron flow from the surface layer into the inner metal layer. The charge on the methyl fragment decreases as its coordination number increases on the Co surface. Thus the CH_3 charge is -0.58 in 7, -0.53 in 8 and -0.49 in 9. This trend can also be rationalized within our bonding model using the following reasoning: If there is no interation between the metal and the CH_3 radical and the electrons are assigned to the lowest available levels, then the methyl's n orbital which is lower

in energy than the metal's d-band will be doubly occupied and the charge

distribution is: CH_3^- [metal slab]$^+$. When the $M-CH_3$ interactions are "turned on",

part of the methyl charge is transferred back to the metal. As the number and

efficiency of the interaction mechanisms increases, as is the case along the

progression 7 --> 8 --> 9, more charge is transferred back to the metal and

the organic fragment becomes less negative.

The capping or triply bridging geometry is the first where we find a

significant barrier of 6.3, 21.2 and 21.7 kcal/mol (for Co, Cr, Ti) for the rotation

of the methyl group. The most stable arrangement is such that the hydrogens point

towards three metal atoms. A side view is shown in 38. The less stable

arrangement in which the hydrogens point towards the center of three M-M bonds is

shown in 39. The M-H overlap populations which are given in 38 and 39

suggest that weak M-H attractive interactions favor 38 over 39, where these

interactions are repulsive. 38 is the only case where we find some indication

for the attractive M-H forces that Muetterties and co-workers found to be

significant.[22] The larger rotational barrier at lower electron count is

due to the following fact: At the eclipsed geometry 38 the hydrogens of the CH_3

group interact with both M-M bonding and antibonding states, whereas in the

staggered 39 they interact only with the M-M bonding states. Tnus 38 is

more stable. At lower band filling it is more so because the unfilled M-M

antibonding states act as acceptors. However, we are not sure whether the extended

Hückel method has overestimated the barrier. Better calculations are needed.

Ti	0.096
Cr	0.055
Co	0.014

|	
Ti	-0.012
Cr	-0.009
Co	-0.024
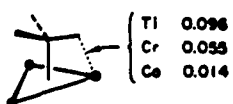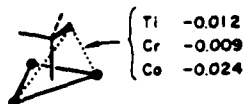
38   39

The computational results for all three sites of methyl binding are summarized

in Table 4.

Table 4 here

To conclude this section we summarize the main features of the bonding between a methyl fragment and the metal slab. The major interactions occur between the metal's surface bands and the CH_3 orbital. These interactions are σ type, involving surface d_{z^2} and s orbitals. The important difference from a molecular complex is that charge transfer in the σ system occurs from d_{z^2} (and s) to CH_3. But this is a consequence of the reference state as neutral CH_3, and if CH_3^- is chosen instead, the methyl group behaves in the way we would have expected. As one moves along the geometry series: on-top --> bridged --> triply bridging some additional M-C bonding is gained but this is generally achieved at the expense of considerable weakening of the metal-metal bonds in the surface layer. As a result the on-top geometry is the most stable geometry for all three metal surfaces.
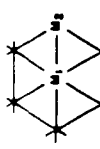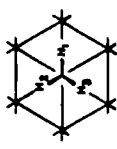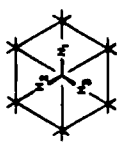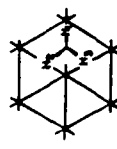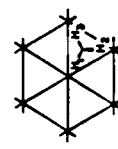
ADSORBED METHYLENE

We will follow the guidelines of our analysis for the methyl case. As in the methyl system three adsorption sites are studied: the 1-fold on-top geometry 40, the 2-fold bridging position 41 and the 3-fold bridging or capping position 42. For each of these geometries two conformers with respect to rotation around the C_{2v} axis of the methylene group were examined.

40   41   42
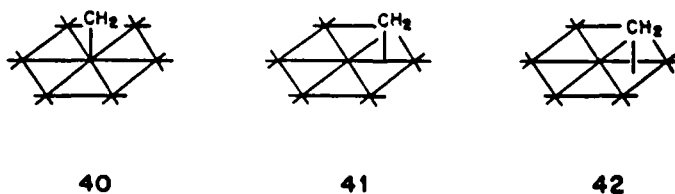
The major difference in the bonding of methyl and of methylene to the metal surface lies on the different set of orbitals that these two fragments bring to the bonding process. The relevant orbitals of methylene are displayed in 43 in increasing order of energy (in parenthesis, eV) from left to right. In the free

TABLE 4. Some Details of Energetics and Electron Distribution for Three Sites of Methyl Binding to Co(0001), Cr(110), and Ti(0001) surfaces.

		Fermi Level (eV)	Binding Energy (eV)		Overlap Population						
			E_1	E_2	$M_1\text{-}M_2$	$M_1\text{-}C$	$M_2\text{-}C$	$M_1\text{-}H_1$	$M_2\text{-}H_1$	$C\text{-}H_1$	$C\text{-}H_2$
	Ti	-6.48			0.350						
	Cr	-7.50			0.462						
	Co	-8.48			0.184						
	Ti	-6.47	5.42	0.16	0.291	0.374		-0.039	-0.000	0.805	0.805
	Cr	-7.51	4.29	0.09	0.411	0.418		-0.035	-0.005	0.800	0.800
	Co	-8.48	3.73	0.47	0.170	0.415		-0.022	-0.002	0.793	0.793
	Ti	-6.43	4.89	-0.36	0.155	0.184	0.201		0.011	0.791	0.794
	Cr	-7.40	3.36	-0.84	0.261	0.227	0.209		0.009	0.773	
	Co	-8.47	2.64	-0.62	0.110	0.224	0.208		-0.004	0.776	0.796
	Ti	-6.48	5.3	0.06	0.191	0.169	0.169	0.096		0.741	0.741
	Cr	-7.34	3.36	-0.85	0.284	0.174	0.160	0.055		0.759	
	Co	-8.45	2.36	-0.90	0.113	0.165	0.165	0.014		0.769	0.769

singlet methylene only π-CH$_2$ and σ are occupied. Note that for consistency with the

methyl case we should have called the lone pair orbital n, but it is customary to

designate it as σ in carbene chemistry.

π-CH$_2$ (-15.78) σ (-12.11)   p(-11.40) π^*-CH$_2$ (6.60)
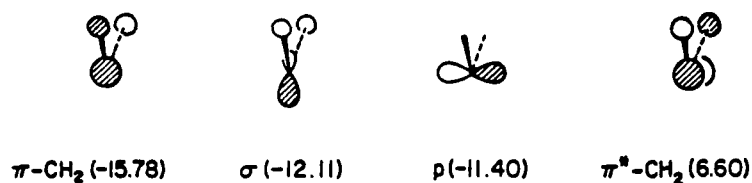
43

A schematic energy diagram of the methylene orbitals and the metal slab levels

is displayed in <u>44</u>. <u>44</u> also shows the position of the relevant orbitals of

the methyl radical.
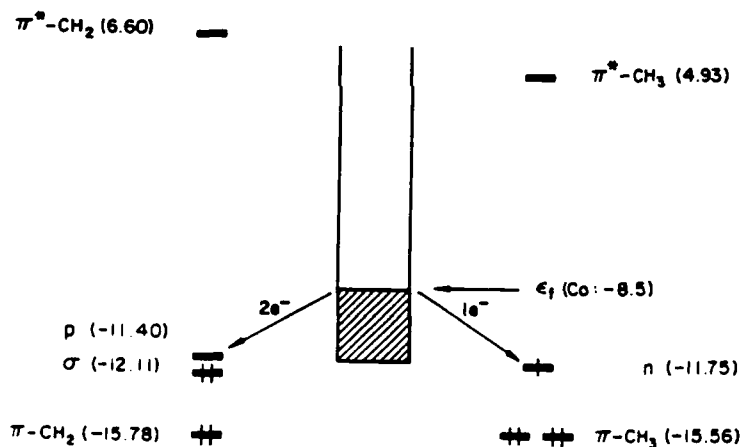
44

Let us examine first the most important features of the surface - carbene

bonding, those which hold for all the binding sites. Diagram <u>44</u> reveals at a

glance the important differences in the bonding of methyl and methylene to the

surface. The methyl fragment carries a singly occupied empty orbital at -11.75eV

while the methylene introduces an entirely vacant orbital at a similar energy. We

have seen above that most of the binding energy of the organic fragment to the metal

surface can be associated with the "ionic character" of the M-C bond, in other words with the energy gained upon filling the "hole" that the organic fragment is carrying. Using this naive picture we expect that methylene which carries 2 empty sites should be bound much more strongly to the surface than methyl, which provides only one vacancy. Note also that the empty orbital that methylene brings along is of p or π-type while that of methyl is of σ-type. The bonding of methylene to the metal surface is therefore expected to have a much more pronounced π-character than for methyl. We will see below that these qualitative expectations are indeed fulfilled.

Another important difference between methyl and methylene is that in CH_2 the n-orbital is doubly occupied while in CH_3 it is singly occupied. This orbital interacts mainly with filled metal levels (see $\underline{44}$). When two filled orbitals interact this results in a strong destabilization due to the occupation of antibonding orbitals. This would have indeed been the case for the interaction of the σ-orbital of CH_2 with a filled orbital of another molecular fragment. However, the situation in the metal slab is entirely different. The electrons which should enter the antibonding states can instead occupy empty metal levels which are lying near the Fermi level. These states, which we have shown above to be primarily bulk-like, serve as an empty reservoir for electrons that are pushed up by interactions between filled levels. These arguments are displayed schematically in $\underline{45}$.
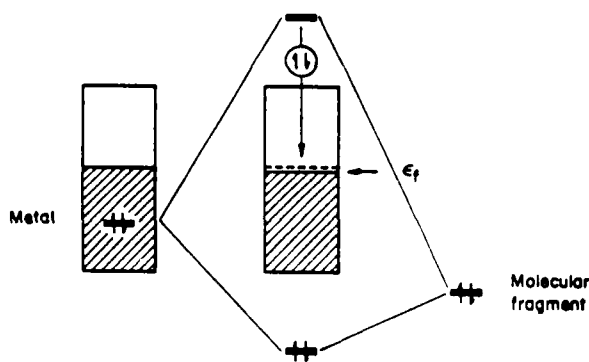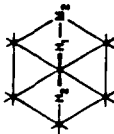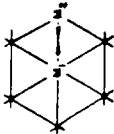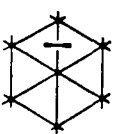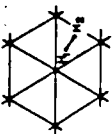

45

TABLE 5. Energetics and Electron Redistribution upon Methylene Bonding.

|		Fermi Level (eV)	Binding Energy (eV)		Overlap Populations								Charge on CH_2
			E_1	E_2	M_1-M_2	M_1-C	M_2-C	M_1-H_1	M_2-H_1	$C-H_1$	$C-H_2$	M_2-H_2	
	Ti	-6.49	10.38	0.64	0.287	0.551		-0.044	-0.003	0.805			-1.59
	Cr	-7.60	8.02	0.42	0.401	0.520		-0.035	-0.005	0.795			-1.53
	Co	-8.50	6.33	0.52	0.172	0.441		-0.021	-0.002	0.791			-1.54
	Ti	-6.44	9.94	0.20	0.149	0.283		-0.027		0.806			-1.46
	Cr	-7.45	7.15	-0.45	0.238	0.284		-0.029		0.791			-1.40
	Co	-8.47	5.31	-0.50	0.105	0.229		-0.030		0.790			-1.37
	Ti	-6.46	10.40	0.66	0.141	0.423		-0.038		0.807			-1.42
	Cr	-7.53	8.13	0.53	0.247	0.428		-0.031		0.803			-1.29
	Co	-8.48	6.35	0.54	0.101	0.396		-0.021		0.797			-1.17
	Ti	-6.46	10.05	0.30	0.151	0.177	0.346	-0.012		0.803	0.792	-0.025	-1.39
	Cr	-7.43	7.49	-0.11	0.272	0.160	0.365	-0.003		0.784			-1.22
	Co	-8.47	5.75	-0.06	0.106	0.169	0.329	-0.024		0.789	0.795	-0.027	-1.12

The strong destabilization that is associated with 4-electron interactions in molecules, and that controls much of their chemistry, has to a large extent diminished in metal-adsorbent systems. This is, we believe, one of the important characteristics of metals and metal surfaces, a factor that makes them behave so differently from the "analogous" isolated metal complexes.

We can proceed now to discuss in detail the different binding sites of methylene. Table 5 and 6 collects the computational data regarding the bonding characteristics of methylene in the different adsorption sites. Some of this data will be discussed in some detail in the text. We also refer the interested reader to a recent contribution from our group in which we studied the adsorption of vinylidene, H_2C-C: on metal surfaces.[21] In many aspects this system is similar to ours and we will refer to it when appropriate.

<u>Table 5 and 6 here</u>

ADSORBED METHYLENE IN THE 1-FOLD ON-TOP GEOMETRY, 40

We have studied two conformers shown in 46 and 47 differing by a 30° rotation around the metal-carbon bond. We find that the energy difference between these conformers is essentially zero. We will comment on the reasons for this tiny barrier later. We concentrate therefore on one geometry, 46, using the indicated coordinate system, but the analysis applies to 47 as well.
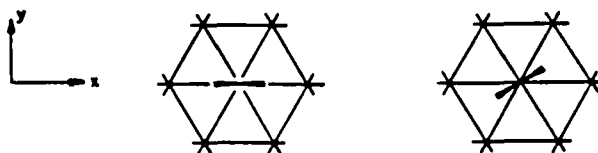
46   47

Figure 12a and 12b shows the total DOS curve (dashed line) of the Co system before and after the chemisorption of CH_2 in this geometry. The dark area in Figure 12b gives the states contributed by the methylene fragment and the straight lines in Figure 12a indicate the location of these states in the isolated organic fragment. Figure 12b can be compared with the analogous Figure 4 for the 1-fold chemisorbed methyl. The two orbitals of methylene that are most affected by the interaction with the metal are σ and p. These are pushed to lower energies by 1.2eV and 0.4eV respectively. The peak of the σ-band is located at a slightly lower energy in 46 than in 7. This is due primarily to the fact that σ-CH_2 is lower than n-CH_3 to start with (-12.1 vs. -11.8eV).
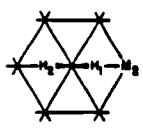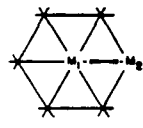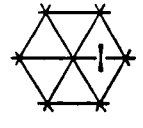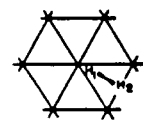
Figure 12 here

The fact that the σ orbital is affected more strongly than the p orbital by interaction with the metal indicates that the M-C bond is mainly of σ character. This interpretation is corroborated by Figure 13 which displays the COOP curve for the Co1-C bond. The strongest M-C bonding peak is at -13.0eV corresponding to the σ orbital of methylene. The p orbital also makes an important contribution to M-C bonding, as indicated by the peak at -11.2eV. But it does so to a smaller degree than the σ band.

Figure 13 here

Comparison of Figure 13 with the analogous COOP curve for methyl (Figure 6) is interesting. There are essential similarities, and small differences - the absence of a p bonding contribution in Figure 6, minor and understandable differences in the contribution of the π orbitals. Note also that around the Fermi levels of Co(d^9) indicated by the arrow in Figure 13, the M-C COOP curve is antibonding and it is more so for methylene than in the methyl system. Thus as the top of the d-band is depopulated the M-C bond is strengthened. The M-C overlap populations are in agreement: 0.441 for Co and 0.520 for Cr (Table 5). As in the methyl case, for methylene the M-M COOP curve (which is also shown in Figure 13) is also antibonding around the Fermi level of Co. Emptying the top of the metal band results therefore

TABLE 6. Orbital Occupations of CH_2 Group on Surfaces of Ti, Cr, Co.

Geometry		π	σ	p	π^*
	Ti	1.99	1.70	1.89	0.00
	Cr	2.00	1.64	1.90	0.01
	Co	2.00	1.59	1.96	0.01
	Ti	1.96	1.69	1.78	0.01
	Cr	1.96	1.62	1.81	0.01
	Co	1.97	1.55	1.86	0.01
	Ti	1.98	1.69	1.72	0.01
	Cr	1.99	1.60	1.69	0.02
	Co	2.00	1.53	1.64	0.01
	Ti	1.95	1.69	1.70	0.02
	Cr	1.96	1.60	1.64	0.02
	Co	1.97	1.53	1.62	0.02
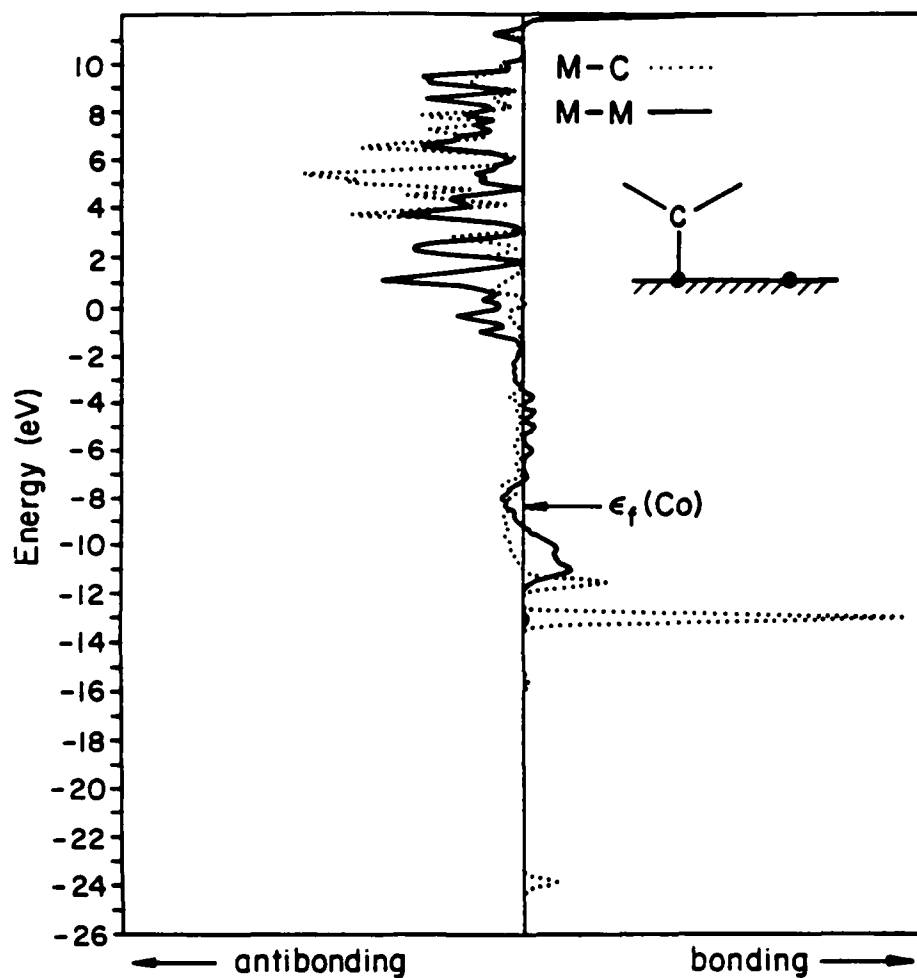
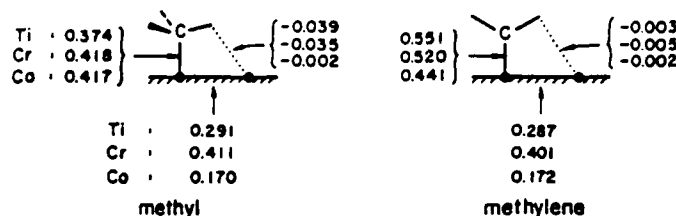Figure 13: COOP curves of the M-M (solid line) and the C-M (dotted line) bonds for the on-top CH$_2$ + Co(0001) system.
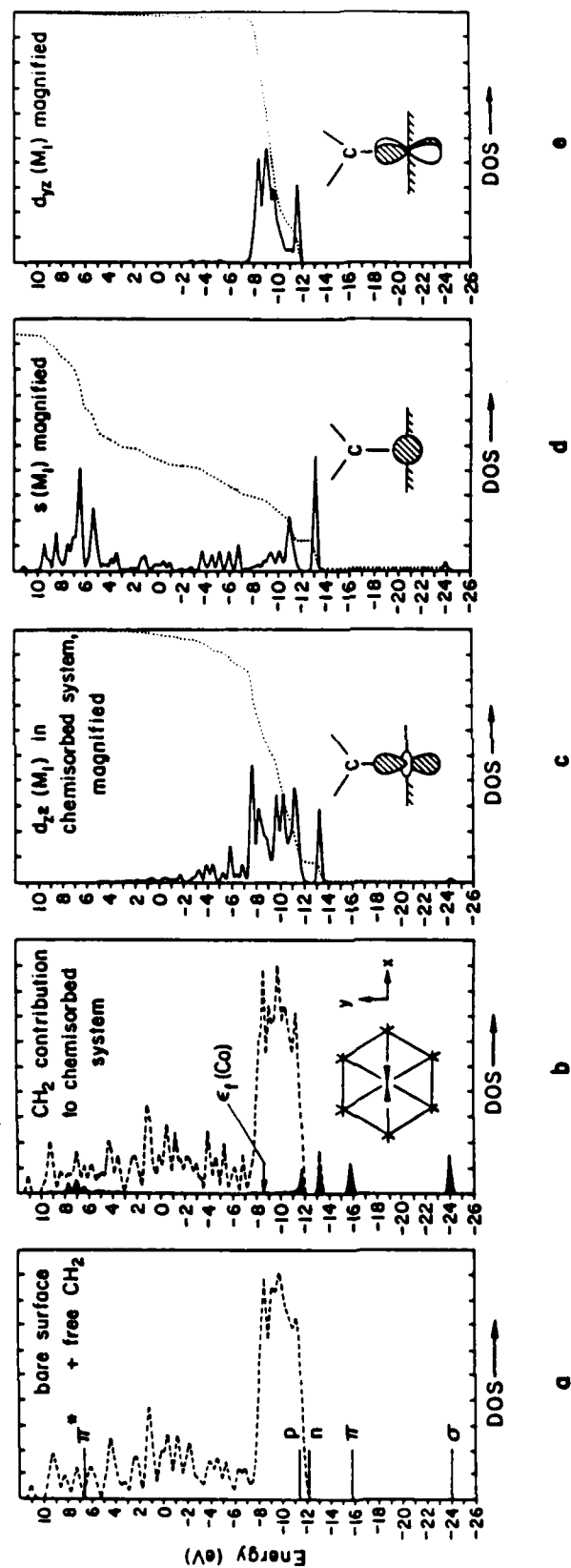
Figure 12: DOS of the on-top CH_2 + Co(0001) system. a. Bare metal surface (dashed line) plus free CH_2 (MO levels indicated by horizontal lines). b. Total DOS (dashed line) and the CH_2 contribution (darkened area) for the chemisorbed system. c. d_{z^2} states of the metal atom bonded to the CH_2 group (magnified). d. s states (magnified). e. d_{yz} states (magnified).

in a strengthening of the M-M bond, up to a certain point ($\sim d^5$), past which it is

weakened. The calculated overlap populations for the on-top methyl and methylene

geometries are shown in 48 (see also Table 5). Note that also for methylene the

M-H interactions are weakly antibonding.

Ti : 0.374 / Cr : 0.418 / Co : 0.417 | -0.039 / -0.035 / -0.002 | 0.551 / 0.520 / 0.441 | -0.003 / -0.005 / -0.002

Ti : 0.291 / Cr : 0.411 / Co : 0.170 | 0.287 / 0.401 / 0.172

methyl   methylene

48

The calculated total overlap populations in 48 indicate that the M-C bond

is stronger for methylene than for methyl. This comes from from the increased

contribution of π-bonding. The difference in the overlap populations between the

two cases is, however, too small to indicate the presence of a fully developed M-C

double bond character. Qualitatively, the M-CH$_2$ bond is best described as a partial

double bond.

The relatively modest increase in the M-C overlap population, and thus in the

M-C bond strength, upon substitution of methyl by methylene does not indicate, as we

have already emphasized earlier, that the binding energies of these fragments to the

metal surface are similar. This is because the overlap populations reflect only

what we have termed the "covalent" fraction of the bonding (E_2) while most of the

binding energy comes from an "ionic" transfer of electrons from the metal to the

organic fragment. For the adsorption of CH$_2$ on cobalt we calculate a binding energy

of 6.32eV compared with only 3.73eV for methyl. These values agree well with our

interpretation. The "ionic" binding energy is given by the energy difference

between the top of the bare cobalt band and the σ-orbital "hole", multiplied by 2

(for 2 electrons), i.e., 2x(11.40-8.48) = 5.84eV. The remaining fraction of the

binding energy: 6.32-5.84 = 0.48eV, can be associated with the "covalent" bonding.

For methyl, only one electron contributes to the "ionic" stabilization; i.e.,

11.75-8.48 = 3.27eV, and the total binding energy is only 3.73eV (leaving 0.46eV for "covalent" stabilization), roughly half than that of methylene.

On going from Co to Cr to Ti, the Fermi level becomes higher and the "ionic" energy gain is larger, increasing the total surface-adsorbent bonding interactions (see E_1 values in Table 5). The "covalent" bonding remains, as expected, roughly the same as the metal is altered (see E_2 values in Table 5).

Now that we have discussed the general features of the bonding of CH_2 to the metal surface let us analyze the bonding of CH_2 to the metal surface in some more detail. We have shown using Figures 12 and 13 that M-C bonding is associated mainly with the σ and p orbitals of CH_2. Which of the metal levels contribute more to the M-C bond?

Interactions with the n orbital of CH_2 involve mainly the metal's s and d_{z^2} bands as shown in 49 and 50 respectively. Interaction 49 and 50 are analogous to the σ interactions with the methyl fragment shown earlier in 13.
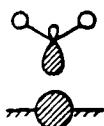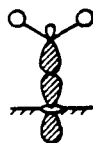

49   **50**

As for adsorbed CH_3, so also for CH_2 essentially the entire s and d_{z^2} bands are involved in the interaction. This is the reason that we don't show the orbital phases at the neighboring metal atom. Projection of the d_{z^2} states of Co1 shown in Figure 12c reveals that nearly 8% of these states contribute to the metal-σ band. For the s bands (Figure 12d) the contribution is slightly larger (12%). The strong interaction of the d_{z^2} band with the organic fragment is also evident from its large dispersion; nearly 40% of the d_{z^2}-states are above the Fermi level of cobalt.

The p orbital of CH_2 can interact with several metal bands. The major interaction is with the d_{yz} levels as shown in 51. According to Figure 12e, 17% of the d_{yz} states are involved in π-interactions with the p orbital. The neighboring metal atoms also contribute, as emphasized in 51 by the arrows. The

d_{xz} levels, being perpendicular to the p orbital, do not interact with the organic fragment (except for a minor interaction with the π^*-CH_2 orbital, which is of proper symmetry but lies 18eV above the p orbital). Some levels around the center of the d_z2 and s bands can also contribute to π bonding, as shown for d_z2 in 52. These interactions, however, do not in fact contribute much to the total π bonding, because of poor orbital overlap. Only 1-2% of the d_z2 levels contribute to the M-p band.
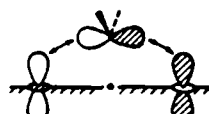
51   **52**

We can now understand why the barrier to the rotation of the CH_2 group is so small. The σ type interactions are invariant to rotation of the CH_2 group and are the same in 46 and 47. The important interactions for the rotation are the π type. As the CH_2 fragment is rotated towards geometry 47 the contribution of the d_{yz} bands to π bonding decreases due to smaller orbital overlaps. However, at the same time the contribution of the d_{xz} bands (which are zero in 46) increases and reaches its maximum in geometry 47. A nearly constant contribution of these levels to the M-C bonding is maintained as the CH_2 fragment rotates. The rotation barrier is six-fold and tiny. The different effectiveness of the σ and π interactions is manifested also in the appropriate metal DOS.

In 55, we look at the charge distribution in the adsorbed methylene. We find two comparisons to be useful, one with the bare metal 54 and the other with the analogous 1-fold on-top methyl system 53. The data in 53-55 is for the Co surface and data for other electron counts can be found in Table 5. As the CH_2 fragment provides 2 vacancies for the metal electrons while the methyl provides only one, the charge transfer to the organic fragment is much higher in the

Charges

53   **54**   **55**
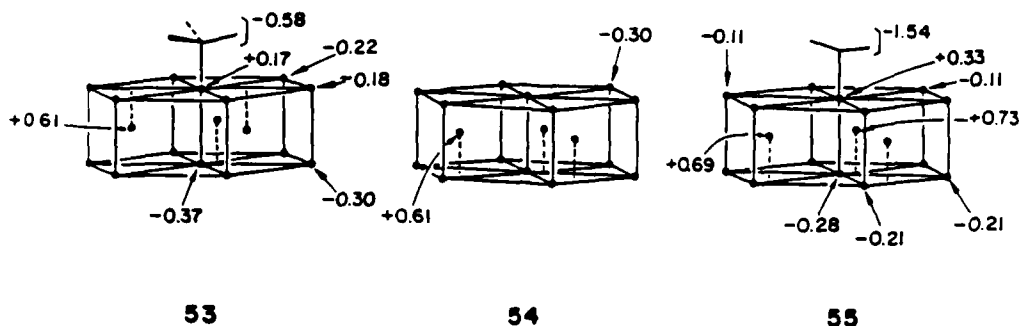
methylene system. The CH_2 charge is -1.54 compared with -0.58 for CH_3. Using the adsorbed methyl system as the reference point we calculate that abstraction of a hydrogen atom causes 0.90 electrons to flow from the metal to the organic fragment. The charge is donated roughly equally from all three metal layers. Comparison with the bare surface shows that as in the methyl system, the charge that is donated to the methylene comes mainly from the Co atom that is directly bonded to it. This cobalt atom contributes 0.64 electrons. However, the electron demand placed by the methylene fragment is so large that the neighboring atoms in the surface layer as well as metal atoms in the bulk also contribute. The metal atoms adjacent to the adsorption site contribute 0.19 electrons each and those in the B' and C' layers 0.32 and 0.20 electrons respectively. In the methyl case charge transfer from the inner metal layers is very small (see 21).

Numerous examples of carbene complexes of type 40 either substituted or unsubstituted are known.[1a,11] Their bonding was analyzed in detail by our group[27a-d] as well as by others[27e] and we will not dwell on this point here. The reader is also referred to a recent relevant paper which reports the preparation and the characterization of the first simple unligated carbene complex $FeCH_2$.[28] Note, however, that to our best knowledge there is not a single known structure of a bimetallic carbene complex of type 40. These complexes exist commonly in a bridged geometry but 1-fold structures have been suggested as intermediates in their reactions.[29-31]

ADSORBED METHYLENE: THE 2-FOLD BRIDGED GEOMETRY 41

We have studied two bridged geometries, perpendicular 56 and parallel 57. It is advantageous to analyze these geometries together although they differ substantially in energy, 56 being lower in energy. We will come back to this point later.

As in the 1-fold geometry it is useful to discuss the metal - methylene bonding in terms of σ and π contributions. The σ interactions are expected to be similar in the two geometries, as those interactions remain reasonably invariant to rotation around the z-axis. Futhermore, in comparison to the on-top geometry 40, the changes in the σ bonding are expected to be similar to those that occur in the methyl systems, i.e., 7 --> 8. For the σ framework we indeed find strong similarities between the methyl and the methylene systems. In both systems σ interactions are stronger in the bridged geometry.

Perpendicular   Parallel
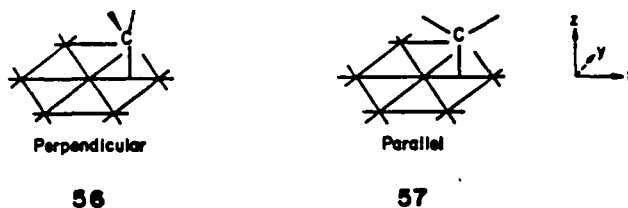
56   **57**

The total density of states for methylene on Co(0001), bringing in the perpendicular conformation 56, is shown in Figure 14. The total DOS for the parallel conformation is similar, though it differ in critical aspects to be discussed below. Decompositions of the DOS identify methylene levels. Note that both σ and p bands are stablized in the adsorbate - surface complex.

Figure 14 here

The dramatic difference between perpendicular and parallel geometries, 56 and 57 is revealed the metal-carbon COOP curves which are displayed in Figures 15a and 15b for 56 and 57 respectively. Note that in contrast to 8, here symmetry dictates identical COOP curves for Co1-C and Co2-C, of which only one is shown. The contribution of states descending from the methylene p state to M-C bonding are approximately twice as great in 56 than in 57. In the
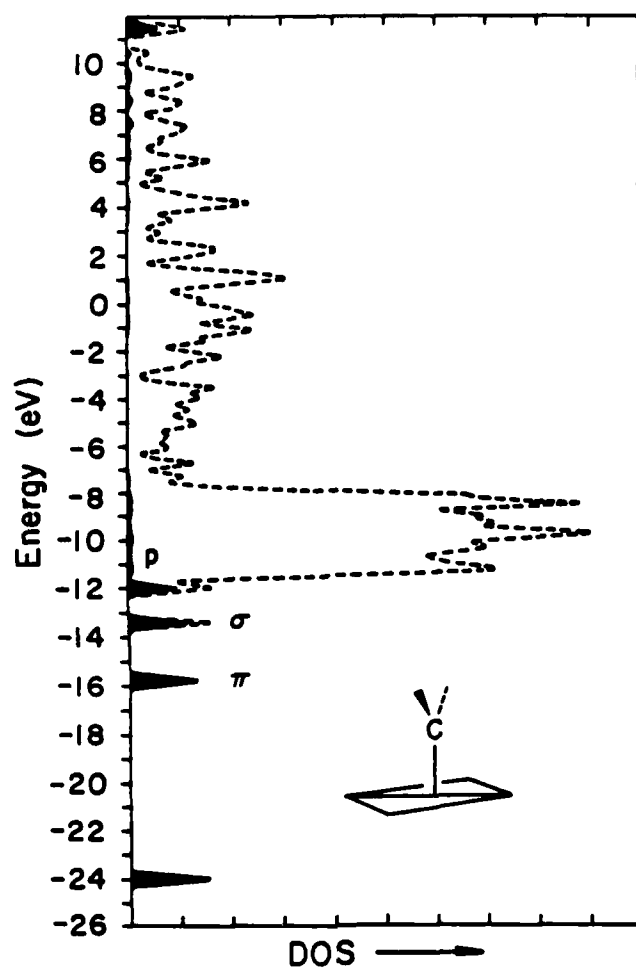
Figure 14: Total DOS (dashed line) and the CH_2 contribution (darkened area) for the bridging CH_2 + Co(0001) system (CH_2 perpendicular to the Co-Co bond).

perpendicular geometry the M-C bonding is roughly half π and half σ in character while in the parallel σ bonding is dominating.

Figure 15 here

The stronger π bonding in 56 compared with 57 results from a more efficient overlap in the perpendicular geometry between the p orbital and the appropriate metal states. In the parallel conformation the overlap between the carbene's p orbital and the top of the d_z2, for example, is poor (see 58) so that there is practically no contribution of d_z2 to the p band. In the perpendicular geometry, on the other hand, overlap is excellent (see 59) and 6% of the d_z2 states contribute to the M-p bonding band. Other metal states that contribute significantly to π-bonding are the top of the s-band (~5%, see 60) and the top of the d_x2-_y2 band (~1%). d_{xz} also contributes, although its share is very small (~2%, see 61). The stronger π interraction in the perpendicular geometry are reflected in the greater M-C overlap populations. Accompanying this is a weakening of the bridged M-M bond, but the magnitude of that effect is small (see Table 5).

58   59   60   61
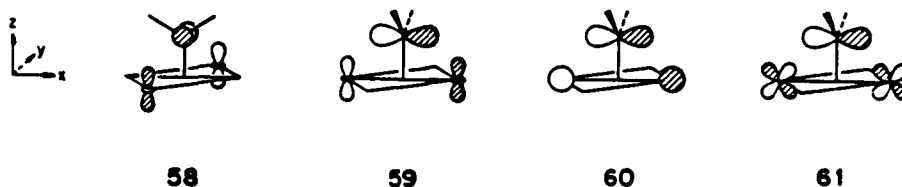
The stronger M-C bonds in 56 suggest that this conformation should be more stable than 57, as observed. For all metal surface we calculate substantial energy differences between the two conformations (ca. 1.0eV for Co and Cr ca. 0.5eV for Ti). Note that these energy differences also give the barriers for rotation of the CH_2 group around the z-axis. It is interesting to note that these barriers are similar in magnitude to those found in molecular carbene complexes of the 1-fold type.[27,29,30] This similarity is not surprising because the key orbital interaction that dictates the magnitude of these barriers is similar in the molecular and the surface systems.
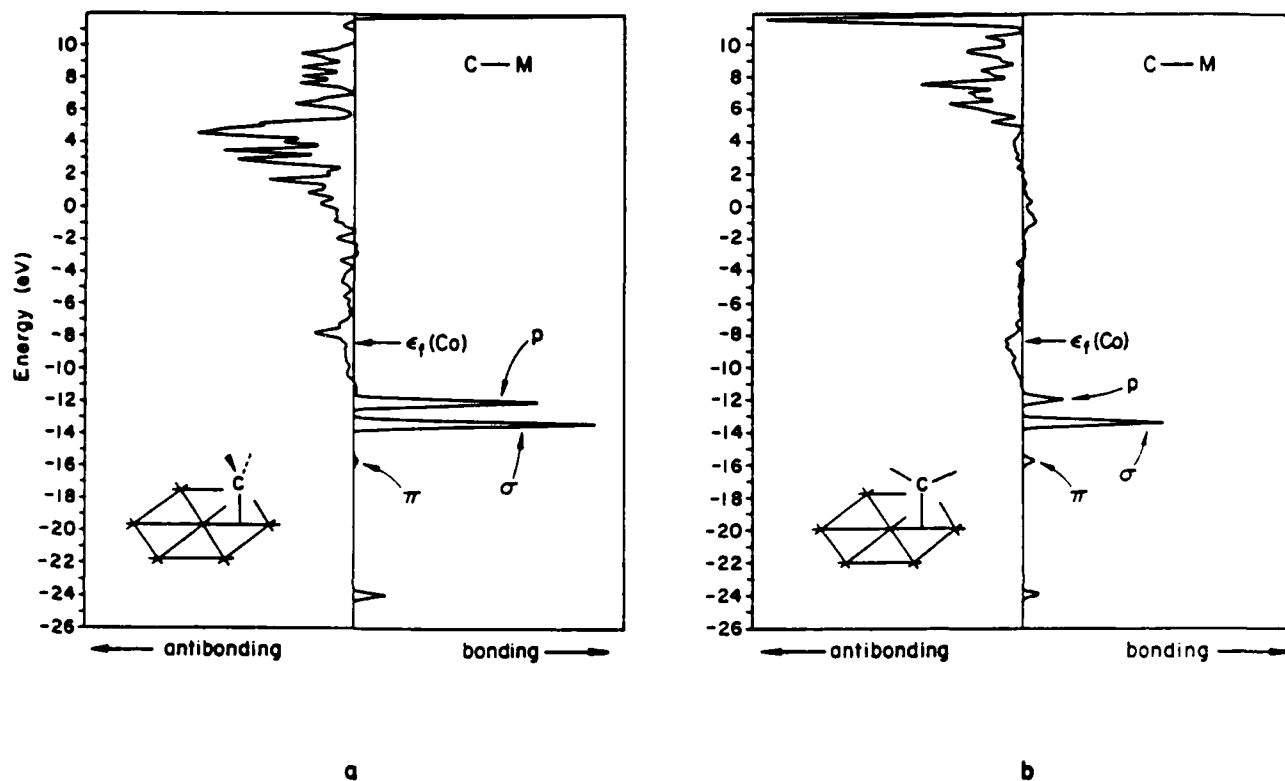
Figure 15: COOP curves for the M-C bond. a. Perpendicular; b. Parallel CH$_2$ on Co(0001).

Our result that the perpendicular geometry is substantially more stable than the parallel geometry agrees with that of Minot et al[18] but is in contrast to the conclusions reached by Muetterties et al,[22] who suggested that the parallel geometry is favored by strong metal-hydrogen interactions. As in the previously discussed systems, we find small antibonding interactions between the metal and the hydrogens in either 56 or 57 and for all electron counts (Table 5). Note that our results are in line with the known structures of analogous bridged molecular complexes, which invariably have a perpendicular geometry with respect to the bridged M-M vector. Relevant molecules can be found in references 1a and 11. It is interesting to compare our results with those of Silvestre and Hoffmann who have found that the related vinylidene $(CH_2=C:)$ binds to a Pt surface most strongly in the parallel geometry 62.[21] The corresponding perpendicular conformation is substantially higher in energy.
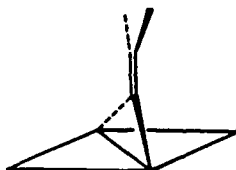
62

Although at first glance this result may seem to be in conflict with that of for methylene, in fact it is not. Examination of both systems reveals that exactly the same orbitals and interactions dictate the higher stabilities of 56 and 62 relative to the corresponding $90°$-rotated structures. The reversed final geometrical outcome results from the different topologies of the orbitals of the two carbenes at hand. In CH_2 the carbene acceptor p orbital is perpendicular to the HCH plane while in vinylidene it lies in the molecular plane. Thus, interactions with the carbene's p orbital dictate a planar geometry 62 for the vinylidene and a perpendicular geometry 56 for methylene. Note that essentially the same reasons

lead us to construct the planar ethylene molecule from vinylidene and hydrogen but a
tetrahedral (i.e., "perpendicular") molecule (methane) from methylene and H_2.

An important result of the calculations is that the adsorption of methylene
fragment on all metal surfaces examined has essentially the same energy in the
2-fold perpendicular geometry 56 and in the 1-fold on-top geometry 40. This
result is to be contrasted with methyl adsorption where the 1-fold site (6) of Co,
Cr and Ti is preferred over the 2-fold bridged site (7) by 1.1eV, 0.9eV and 0.5eV
respectively. Why do methyl and methylene choose different adsorption sites? The
answer lies again in the presence of the empty p orbital of methylene. We have
emphasized above for methyl that as the organic fragment moves to a more highly
coordinated site its interaction with the surface strengthens, pushing many d-states
to higher energies. The overall effect is that the total energy rises and the
bridged sites become less stable than the 1-fold site. The same effects are
operating in the methylene system but here the additional π-stabilization which is
gained in the bridged geometry is so large that it overrides the destabilization
which results from the higher energy of the metal
centered bands, and the total energy drops. Indeed, a comparison of the 1-fold site
with the bridged parallel position where the π-stabilization is weak reveals the
"normal" stability order, with the 1-fold site having the lower energy.

Changing the metal surface has a small effect on the relative energies of the
1-fold and the perpendicular bridged, sites. For Co, Cr and Ti, the energy
differences are 0.002, 0.11 and 0.02 eV, respectively, favoring 56. Similarly,
on a Pt surface, vinylidene favors the 2-fold bridged site.[21] These results are
also in agreement with those of Minot and co-workers.[18]

Finally, we comment on the charge distribution. We remind the reader that in
analyzing the charges it is useful to look at the separated molecules as [metal]$^+$
and [organic fragment]$^-$. In the case of methylene the charge-transferred extreme is
actually CH_2^{2-}, p orbital completely filled. As the metal-adsorbent interactions
become more efficient electrons are transferred from the adsorbent to the metal.
The calculational results for methylene (see Table 5) are very similar to those

obtained in the methyl system (see 34). In both systems bridging increases the interactions between the metal and the organic fragment and consequently charge is transferred from the adsorbent back to the metal. For example, the charge on the methylene drops from -1.54 to -1.37 when the geometry is changed from the on-top to the 2-fold parallel on the Co surface. More interestingly, the migration of the organic fragment from a 1-fold to a 2-fold site is accompanied by a massive reorganization of charge within the metal slab; electrons flow from the surface layer into the inner layers, avoiding the high lying bands which are centered around the adsorbing metal atoms. It is instructive that quantitatively these inner metal charge reorganizations are practically identical for the geometry changes 40 -->
57 (Table 5) and

7 --> 8 (see 34). This emphasizes that similar basic changes occur in the metal-adsorbent interactions when the organic fragment migrates from a 1-fold to a 2-fold site, regardless of whether it is methyl or methylene. On top of these basic changes additional interactions, specific to the organic molecule at hand, may alter somewhat the final picture. Thus when the methylene is rotated to geometry 56 and strong π-interactions are put into play, additional charge (relative to 57) flows from the methylene, which becomes less negative, into the metal slab. There it is partitioned mainly between the surface and the B' layers.

THE 3-FOLD BRIDGING OR CAPPING GEOMETRY, 42

The analysis of the bonding at this site is straightforward, using the experience gained in the study of the methyl system and of the various adsorption sites of methylene. The COOP curves of the Co-C bonds are displayed in Figure 16.

Figure 16 here

The numbering of the metal atoms and the precise orientation of the methylene group is shown in 63. The solid line in Figure 16 gives the COOP curve for the Co1-C bond and the dotted line shows the corresponding curve for the two identical Co2-C
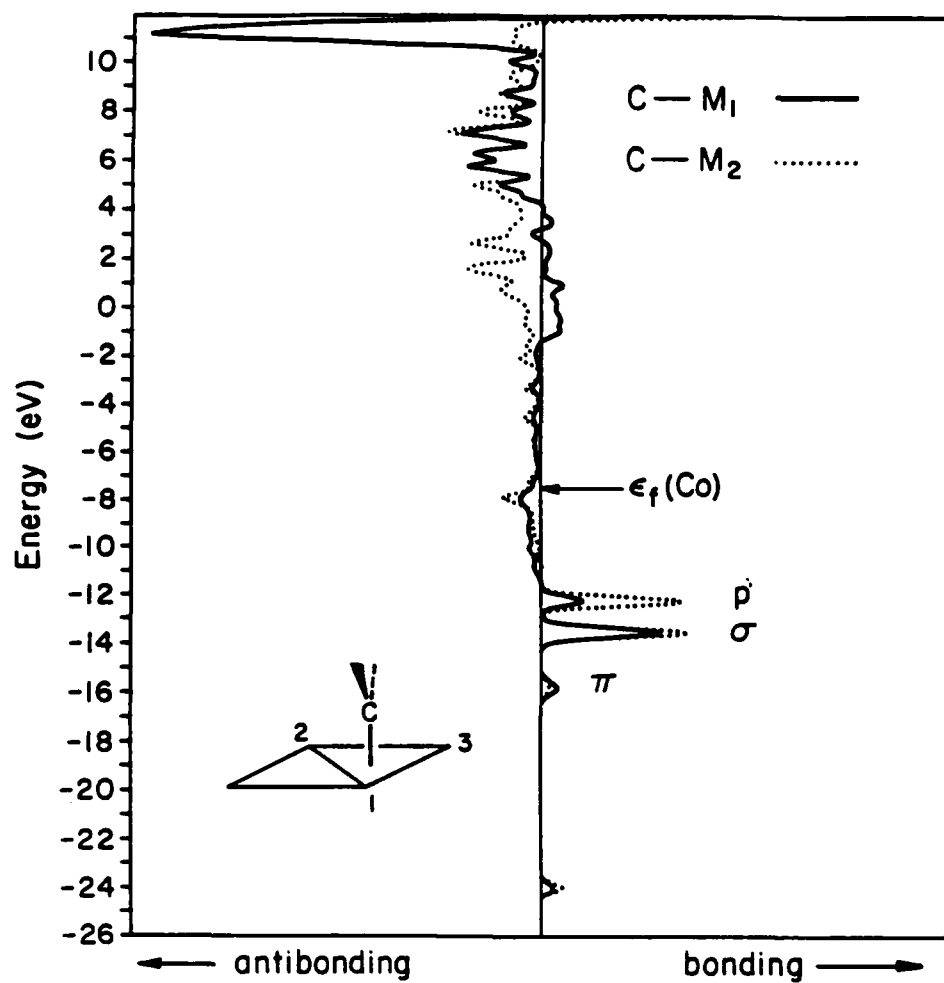
Figure 16: COOP curves for the M1-C and M2-C Bonds. CH_2 group is above the triangular hollow of the Co(0001) surface.

and Co3-C bonds. The COOP curve shows that, similarly to the 2-fold $\underline{56}$ system, also in $\underline{63}$ both σ (band at -13.6eV) and π interactions (band at -12.2eV) contribute effectively to Co-C bonding. Typical σ and π-interactions with the metal's d_z2 band are depicted in $\underline{64}$ and $\underline{65}$ respectively. Similar interactions with other metal bands in particular s and to some extent d_{xz} and d_{yz}, also contribute to bonding.

63   64   65
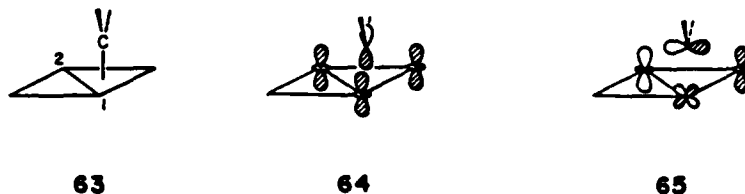
Figure 16 reveals an interesting aspect of the bonding at the 3-fold site and provides a nice demonstration of the analytical power of COOP curves in general. σ-bonding (peak at -13.6eV) is contributed equally (except for a small perturbation induced by the non-symmetrical arrangement of the methylene hydrogens) by all three metal atoms. In contrast Co2 and Co3 contribute to π-bonding (peak at -12.2eV) much more than Co1. This result can be interpreted quite easily. In $\underline{64}$ the p orbital of methylene is aligned parallel to the Co2-Co3 vector allowing strong overlap with the bands centered around these metal atoms. The topology of the interacting orbitals is similar to that in the perpendicular 2-fold geometry. The interaction of Co1 with the p orbital is much smaller, the situation resembles that of Co1 in the parallel 2-fold geometry. Upon rotation of the methylene group by $30°$ in a clockwise direction Co1 and Co3 change roles; now Co1 and Co2 contribute to π-bonding more than Co3. At intermediate rotation angles metal bands combine effectively to maintain the level of π-bonding, so that at the triangular hollow site the adsorbed methylene fragment is essentially freely rotating.

We have already indicated in various places along the discussion that when the organic fragment migrates to a more highly bridged site its interactions with the metal strengthen. Geometry $\underline{42}$ is no exception. For all three metal surfaces the total M-C overlap population (Table 5) is higher in the 3-fold geometry (e.g.

0.827 for Co) than in the 2-fold perpendicular geometry (0.792 for Co). Other trends that we have observed for the _8_ --> _9_ migration of methyl hold also for methylene (Table 4). As most of the energy which is associated with π bonding was already gained in the 2-fold geometry further bridging leads to the "normal" increase in the total energy, or equivalently to a decrease in the binding energy of the organic molecule to the metal. Binding of methylene at the 3-fold site of cobalt is consequently by 0.6eV less favorable than binding at the 2-fold or at the on-top sites. Similar trend holds for the Cr and the Ti surfaces.

Finally, we note that we are not aware of molecular trinuclear transition metal carbene complexes that are stable in the 3-fold capping geometry. Polymetallic carbene complexes usually adopt the 2-fold perpendicular geometry.[1a,11]

We can now proceed to analyze the adsorption of the last fragment - methyne (CH).

ADSORBED METHYNE, CH
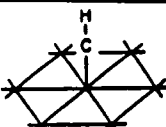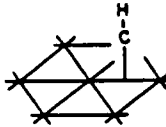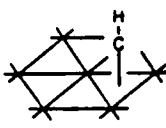
We will compare three different adsorption sites _66_, _67_ and _68_.
Again, the calculations are performed for an "unbiased" C-M distance of 2.1Å for all three geometries. The binding energies, overlap populations and charges are tabulated in Table 7. We will analyze the bonding based on DOS and COOP curves.

Table 7 here

66   67   68
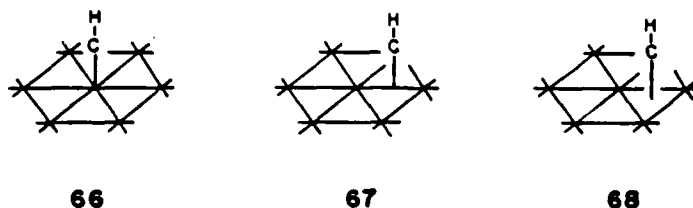
The MO's of the methyne group before and after the adsorption on the hexagonal metal surface in a capping mode are shown in Figure 17. The reason we look at the capping geometry is that this site is the preferred one for high metal electron

TABLE 7. Binding Energies and Mulliken Populations of CH Chemisorbed on Various Metal Surfaces.

Geometry		Fermi Level	Binding Energy (eV)		Overlap Population			
			E_1	E_2	M_1–M_2	M_1–C	M–H	C–H
	Ti	−6.50	15.51	0.95	0.268	0.702		0.788
	Cr	−7.64	11.56	0.30	0.380	0.593		0.775
	Co	−8.53	8.84	0.15	0.173	0.419		0.772
	Ti	−6.49	15.97	1.41	0.129	0.522		0.799
	Cr	−7.58	11.99	0.74	0.218	0.494	−0.024	0.781
	Co	−8.51	9.05	0.36	0.091	0.397	−0.014	0.776
	Ti	−6.47	16.11	1.55	0.142	0.449	−0.035	0.804
	Cr		12.43	1.17	0.260	0.432	−0.024	0.786
	Co	−8.50	9.36	0.68	0.092	0.391	−0.014	0.779

counts. At the left side are the surface states plus the CH levels before the chemisorption takes place, the right side is what happens after CH is chemisorbed on

Figure 17 here

the metal surface. CH has five MO's: one of the two carbon sp hybrids pointing toward the hydrogen forms C-H σ and σ^* orbitals. The other hybrid, directed away from the hydrogen, is mainly non-bonding, and so are the degenerate p_x, p_y orbitals. The σ orbital is low in energy and we expect it interacts poorly with the metal d band. σ^* is high up in energy (off-scale in Figure 17), also out of effective interaction range. What is left for bonding with the surface are the n and p_x, p_y orbitals.

Let us focus on Figure 17b. We see that n is pushed down by ~1eV; at higher energy p is smeared out over the region of -12.3 ~ -8eV. Both CH orbitals interact with the metal surface. Which metal orbitals are effective in this interaction? Figure 18 shows projections of metal d_z2 and d_{xz}, d_{yz}. The d_z2 orbital picks up a

Figure 18 here

resonance with the CH p orbital at -12eV: interactions of type 69a are involved. The small peak in the p projection in Figure 17 at -8eV is also a consequence of this mixing. The d_{xz}, d_{yz} set has resonances with both CH p and n in Figure 18. Combinations of type 69b and 69c are effective.
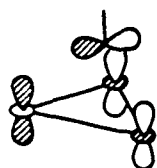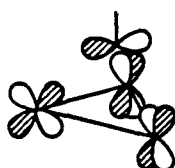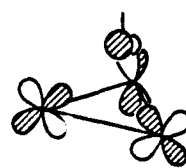
69a   69b   69c

What happens as CH moves to other adsorption sites, on-top or bridging? We do not show the DOS plots here, but the n level is pushed down a little less than in the capping site. More of a difference is observed in the fate of the p level. It is at ~ -12.5eV for 68, -12.1eV for 67 and -11.7eV for the on-top geometry.

Motivated by Muetterties and co-worker's speculation that CH group might not be perpendicular to the surface due to M-H interaction , we compared two geometries
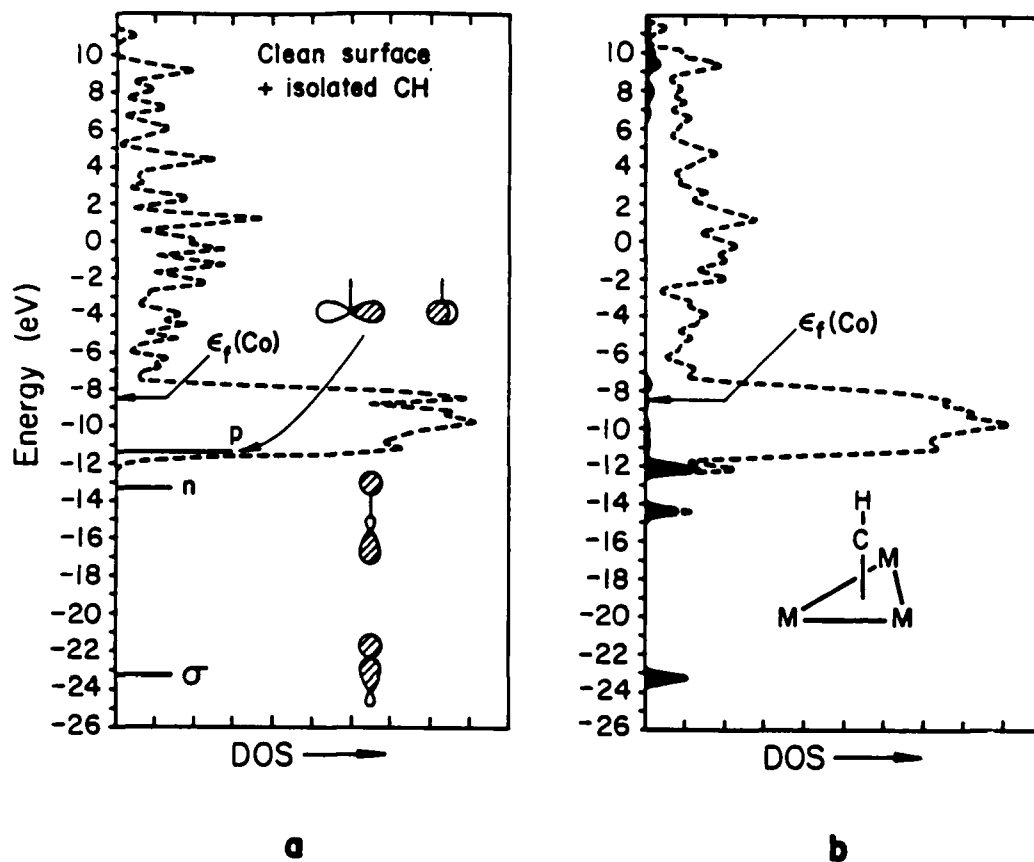
Figure 17: DOS of the CH + Co(0001) slab system before (a) and after (b) CH chemisorbs on the metal surface (capping geometry). CH states are shown by horizontal bars (a) or darkened area (b).
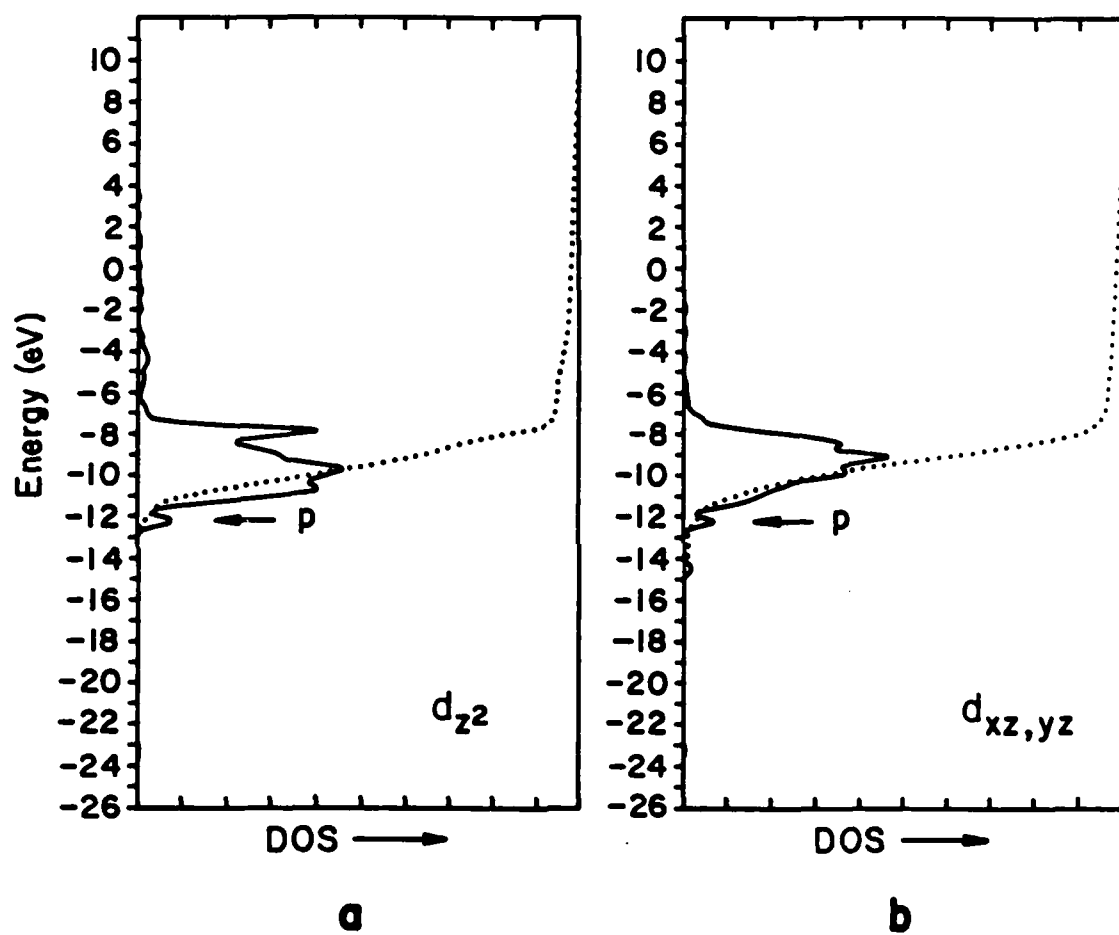
Figure 18: DOS of the capping CH + Co(0001) systems. a. d_{z^2}; b. $d_{xz,yz}$. Notice both d_{z^2} and $d_{xz,yz}$ resonate with CH p around -11.2eV.

70a - 67 and 70b. Our calculation shows no significant energetic difference, 70b being slightly higher in energy. Nearly all the organometallic analogues have CH or CR in a symmetrical, μ_3 or capping geometry, 71.[32] Binuclear complex with a bridging CR are well-known,[37a] as are mononuclear $L_nM \equiv CR$ acetylene analogues.[37b]
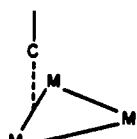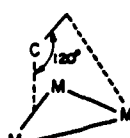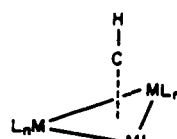

a   70   b   71

To summarize our results concerning various CH_x groups on the surface, we can simply state that for equal C-M distances, for all adsorption sites, the CH_x group would prefer to adopt a geometry which can restore it's missing C-H bond(s). Thus, CH_3 on-top, CH_2 bridging, and CH capping are energetically the most stable geometries. This agrees with previous theoretical studies and the available experimental information.

So far we have said nothing of reactivity. But most of the experimental studies of CH_x groups cannot avoid the dynamic aspect. Reactions occur. For example, CH_2 on Fe(100) is believed to dissociate into CH + H_2, beginning at the bridging position, with one of the C-H bonds parallel to the surface.[33] On a Co surface the dehydrogenation of CH_2 occurs at a relatively low temperature, 180K, indicating a small barrier for the process $CH_{2ads} \longrightarrow CH_{ads} + H_{ads}$.[34] In the next section we are going to analyze the migration of CH_x groups on a surface and how the electronic factor affects various reaction processes.

Migration on the Surface

Migration of species adsorbed on a surface is a phenomenon of substantial significance in many areas of surface science (e.g., adhesion, lubrication, etc.). For catalysis, the case of interest here, knowledge of the barriers for the migration of the adsorbed fragments is fundamental to the understanding of the mechanism of surface reactions. In the FT synthesis, for example, it is important to know if in the coupling step (step 3, scheme 1) the rate determining process is the migration of the two (or more) fragments towards each other, or if it is the chemical barrier associated with the coupling reaction itself. Unfortunately, the experimental characterization of surface migration (or diffusion) is difficult,[35] and for the CH_x fragments little such information is available.

Recently, Muetterties, Shustorovich and Baetzold developed a remarkably useful and versatile theoretical model for surface migration of atoms and diatomic molecules. This is based on a Morse potential for the metal-adsorbent interactions and on the assumption that the M-X (M = metal, X = adsorbent) bond order is conserved along the migration path.[36] Our approach is different and is based on the actual calculation of several selected points on the potential energy surface. All the necessary data for analyzing the migration of the CH_x fragments on the metal surface have been already presented above. A disadvantage of our approach has already been mentioned above - we rely on a molecular orbital method which is very approximate, especially when it deals with the energetics of bond formation. The conclusions we reach gain a little strength when they are supported by overlap population analysis, which together with the energies and other bonding arguments form a self-consistent conceptual picture.
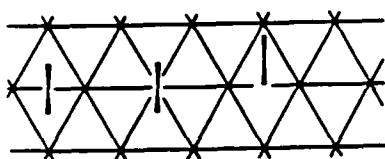
In drawings 72, 73 and 74 we have collected what the computations give for the relative binding energies (in eV) at the three symmetry distinguished adsorption sites, of methyl, methylene and methyne, respectively. In each drawing we present the calculated values for Co, Cr and Ti surfaces.
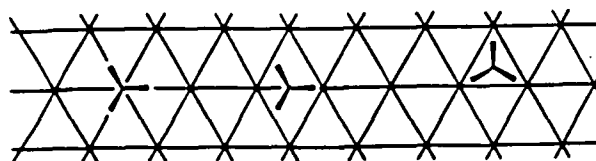
Relative E (eV) :

Co :	0.0	1.1	1.4
Cr :	0.0	0.9	0.9
Ti :	0.0	0.5	0.5

72

Relative E (eV) :

Co :	0.0	0.0	0.6
Cr :	0.0	0.1	0.5
Ti :	0.0	0.0	0.3

73
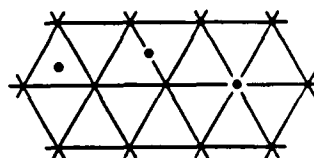
Relative E (eV) :

Co	0.0	0.3	0.5
Cr	0.0	0.4	0.9
Ti	0.0	0.1	0.6

74

A low migration barrier can be observed only if there are at least two sites connected or nearby on the metal surface for which the binding energies of the organic fragment are similar. Let us call these sites A and B. In this case the lowest energy path for the migration of the fragment is simply along the A --> B --> A ... path. The energy barrier for the migration is then determined by the energy differences between points A and B. The relative energies of the other binding sites (C, D, etc.) are of no significance to the migration process because

even if these points are very high in energy they can be circumvented by migration

along the A --> B --> A path.

Let us look first at the migration of a methyl fragment that is shown in

72. For a cobalt surface the site with the highest binding energy (i.e., the

lowest point on the potential energy surface) is the 1-fold "on-top" site. The two

other sites are considerably higher in energy. The lower energy one of these is the

2-fold, 1.1eV higher in energy than the 1-fold site. The theoretical prediction is

that the migration of methyl on a cobalt surface will require relatively high

temperatures and should proceed mainly via the path shown by the dotted line in

75. Migration occurs along the (formal) metal-metal bonds. When the electron

count on the metal is lowered the bridged positions are differentially stabilized

and the barriers to migration should be considerably lower. For the Ti surface the

barrier to migration along the path shown in 76 (which is the lowest in energy)

is only 0.1eV. For the Cr surface the barrier is calculated to be the same (0.9eV)

along either path 75 or 76.
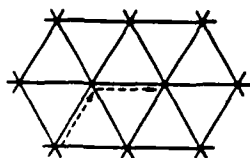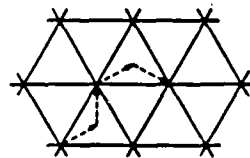

75   **76**

Why does the migration barrier decrease as the metal d band is depopulated?

Remember the main interaction is between the methyl lone pair n and the metal d

band, 77. The metal d band region is weakly C-M antibonding (c.f. Figure 6).

The strength of the antibonding character depends on the overlap between n and the

metal d band. The higher the coordination number of the CH_3 group, the stronger the

C-M antibonding character in the metal d band. Thus at high d band filling the

capping geometry is less stable, because of its stronger C-M antibonding

contribution within the increasingly occupied d band. At lower band filling the C-M

antibonding feature is reduced, and the higher coordination sites of CH_3 stabilize n

more. So the barrier is reduced.
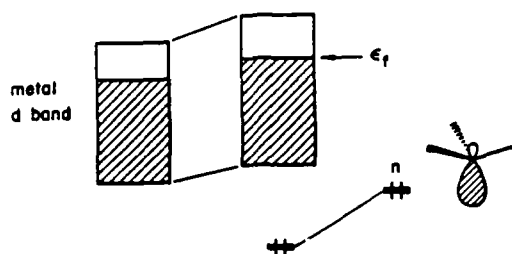
77

For methylene the situation is different. Migration on a cobalt surface occurs with no barrier along a path (with no rotation of the CH_2 group) shown by the dashed line in $\underline{78}$. The same lowest energy migration path is calculated for CH_2 on the Cr and Ti surfaces (see also the more detailed discussion above).
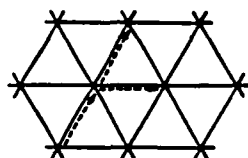

78

The migration of a CH fragment is relatively facile; the barriers along path $\underline{79}$ are only 0.3eV, 0.4eV and 0.1eV for Co, Cr and Ti respectively. This migration path remains the lowest in energy for all metals, and for those with lower electron counts the binding preference for the 2- and 3-fold sites even increases.
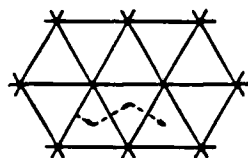
79

The reason that the migration barriers for CH_2 and CH do not change much at low metal band filling derives from the fact that in addition to orbital n (σ) some other orbitals (p) also play a decisive role in the bonding. Details of the analysis have been given above. One can say that the p orbital, being very close to the d band in energy, mixes very strongly with the metal orbitals (c.f. Figures 13b,

15,19 and 21). This mixing, shown in 80, may contribute to C-M bonding even at high d band filling. Thus two types of interaction 77, 80 compete to determine the migration barrier.
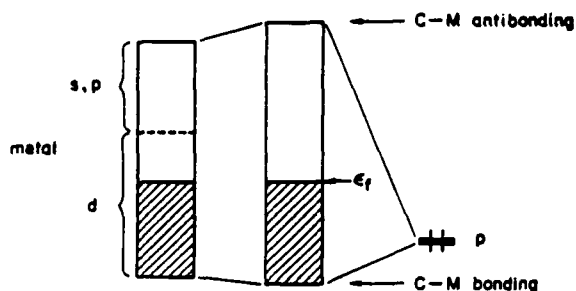

80

Knowledge of the barriers to migration has, of course, interesting implications regarding the coupling steps in the FT synthesis. For example, the calculations suggest that on a cobalt surface, the coupling of methyl and methylene may occur preferably by migration of CH_2 towards the adsorbed methyl rather than by migration of methyl. Furthermore, the coupling of two methyl fragments may involve a substantial barrier for migration, while the coupling of two methylenes should require no such barrier. To demonstrate the implications of these results let us assume that the barriers to the coupling processes themselves are small so that the migration processes determine the rate of the FT reaction. The above results suggest that in such a case the rate of coupling of two methyls, but not that of two methylenes, should be reduced at lower temperatures. Thus, the coupling of two methylenes (or of a methylene and a methyl) would be favored at lower temperatures and higher yields of ethylene expected. Similar analysis can lead to interesting conclusions regarding the Cr and Ti metal surfaces and the other coupling reactions.

THE COUPLING REACTIONS

The coupling reactions in Scheme 3 determine length and olefin proportion of the FT product. Do electronic factors control these reaction? Why does the Schult-Flory distribution change when a different metal catalyst is used?[1c] Such information could certainly help chemists design new catalysts with specified selectivities.[52] We do not intend and certainly cannot answer all those questions, but we hope to extract some useful information from our calculations. In this treatment we assume that methyl and methylene are reasonaly good models for other adsorbed alkyl (C_nH_{2n-1}) or alkylidene (C_nH_{2n}) fragments.
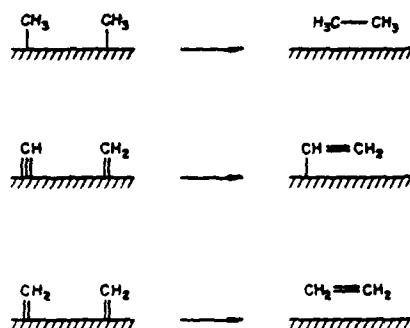

Scheme 3

$\underline{CH_3 + CH_3}$
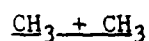
All the previous calculations were performed assuming a 1/3 coverage for reasons of computational economy. If we bring another CH_3 group into the unit cell, the high 2/3 coverage will certainly lead to great crowding. A geometry such as $\underline{81}$ is forced. In our calculation for this and all other reactions we delete the interaction of the C_1 groups between unit cells, so that there is no crowding whose cause is inter-cell interaction. In other words, we are modeling a reaction at very low coverage.
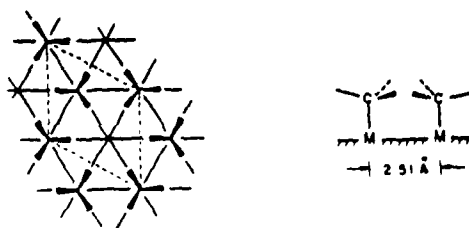
The DOS curves for CH_3 on Co in such a coverage (not shown here) show a splitting of all CH_3 states. Such a splitting in the occupied states, shown in 82 for a lowlying σ orbital, is highly destabilizing. This is a typical four-electron two-center repulsion. The COOP curves also indicate regions of C-C

$$\sigma_1 + \sigma_2 \qquad \sigma_1 - \sigma_2$$
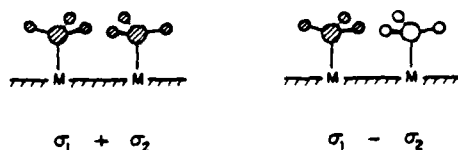
82

antibonding. 83 gives computed binding energies per CH_3, down considerably from the low coverage case (Table 4). The differences in the binding energies E_1 in 83 and Table 4, which we call the proximity barrier, are 0.77eV, 0.53eV, and -0.05eV for Co, Cr and Ti.


Binding E per CH_3 (eV):

	E_1	E_2
Co	1.3	-1.9
Cr	3.8	-0.4
Ti	5.5	0.25

83

What happens when two CH_3 groups couple? The reaction begins withe both CH_3 lone pairs nearly filled, i.e. near a CH_3^- representation. A new C-C σ bond forms, and as usual we must consider σ and σ^* combinations, $n_1 \pm n_2$. Both are filled initially, but as the C-C bond is more completely formed the σ^* combination will be pushed up and eventually will dump its electrons into the metal d-band.

Let us sample such a reaction on the surface by using a transit along a single reaction coordinate θ 84. The "umbrella handle" of the CH_3 group is moved along

$$\theta = 0° \qquad\qquad \theta = 90°$$
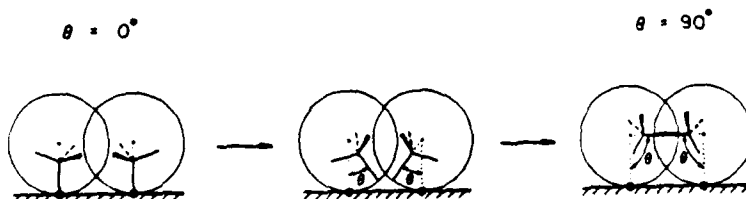
and perpendicular to an arc of a circle. The circle is defined as "standing" on the metal atom, such that when the rotation angle $\theta = 90^\circ$ the C-C distance is 1.54 Å (C to surface separation is 2.59Å). $\theta = 0^\circ$ corresponds to the initial geometry with the "umbrella handle" perpendicular to the surface and bonded to the metal atom. This transit may not be optimal, a true reaction path, but it can give us some information concerning the controlling electronic factors. Full exploration of the potential surface is not realistic with our computational capabilities.

Figures 19 and 20 show the methyl lone pair contribution to the total DOS and C-C COOP curve along the reaction coordinate θ. Before the coupling starts ($\theta = 0^\circ$) n-CH_3 already has split into two peaks around -13eV. The higher one is n_1-n_2 (c.f. 82) and the lower one n_1+n_2. But at a C-C separation of 2.51Å n_1-n_2 is still hardly antibonding. At $\theta = 30^\circ$ the antibonding portion (-12 --> 7eV, of Figure 19) separates from the bonding part (~ -14eV) and at $\theta = 60^\circ$ is well above the Fermi level.

Figures 19, 20 here

What if the position of the Fermi level changes? From the above discussion the total energy of the system increases along the path as n_1-n_2 becomes more antibonding. When n_1-n_2 is pushed above the Fermi level it becomes empty. After this turning point in the reaction path the total energy should go down again as n_1+n_2 becomes more bonding. The position of the Fermi level determines the turning point and the barrier height. The higher the Fermi level, the further away that turning point from the starting geometry, and the higher the barrier. Figure 21, showing the computed energy profile along the idealized reaction path, confirms this line of reasoning. The coupling barrier on Co is lower than that on Cr, which in turn is lower than that on Ti.

Figure 21 here

$CH_3 + CH_2$

This is the chain propagating step in the FT process. The binding energies E_1 in 85 tell us that some 55 kcal/mol per CH_3 + CH_2 (the proximity barrier) is
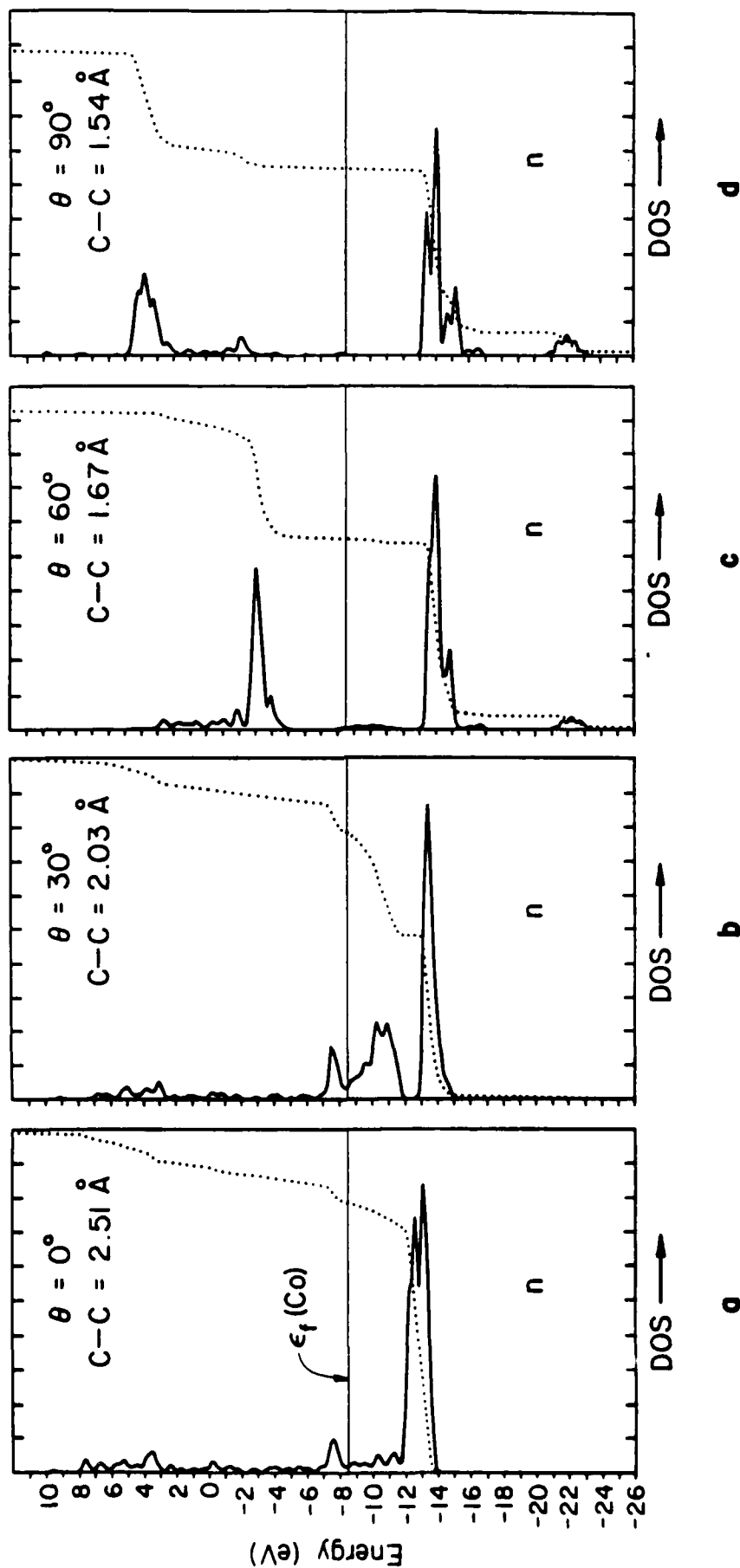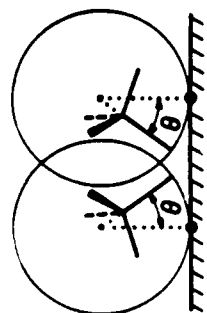
Figure 19: n-CH₃ DOS evolution along a coupling reaction coordination θ on Co(0001).
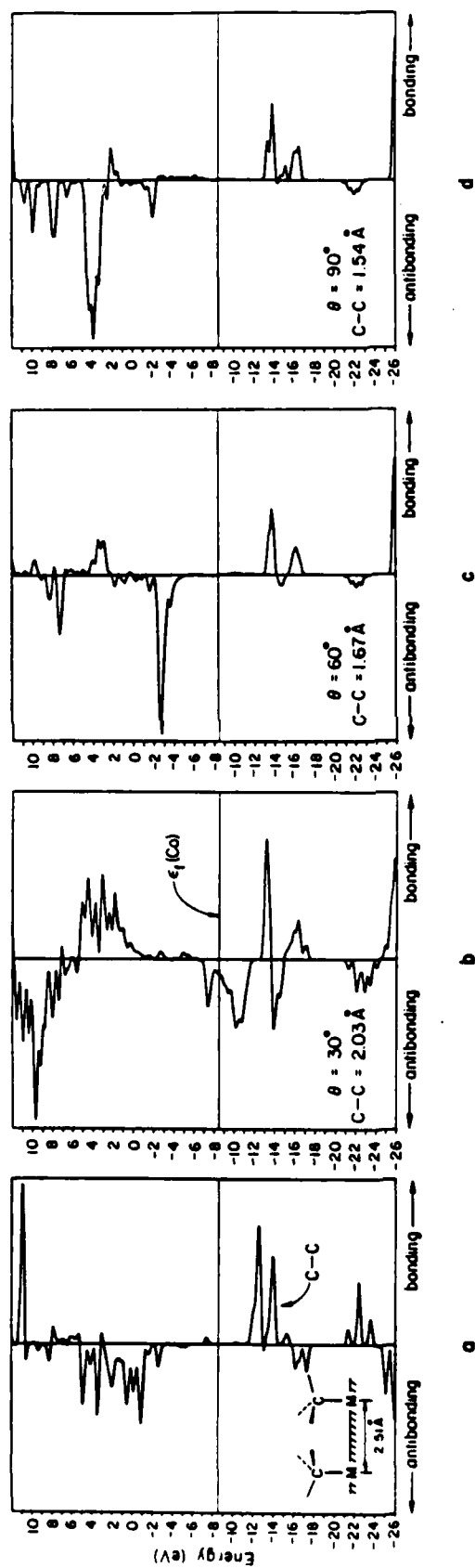
Figure 20: C-C COOP evolution along the reaction path θ on Co(0001).
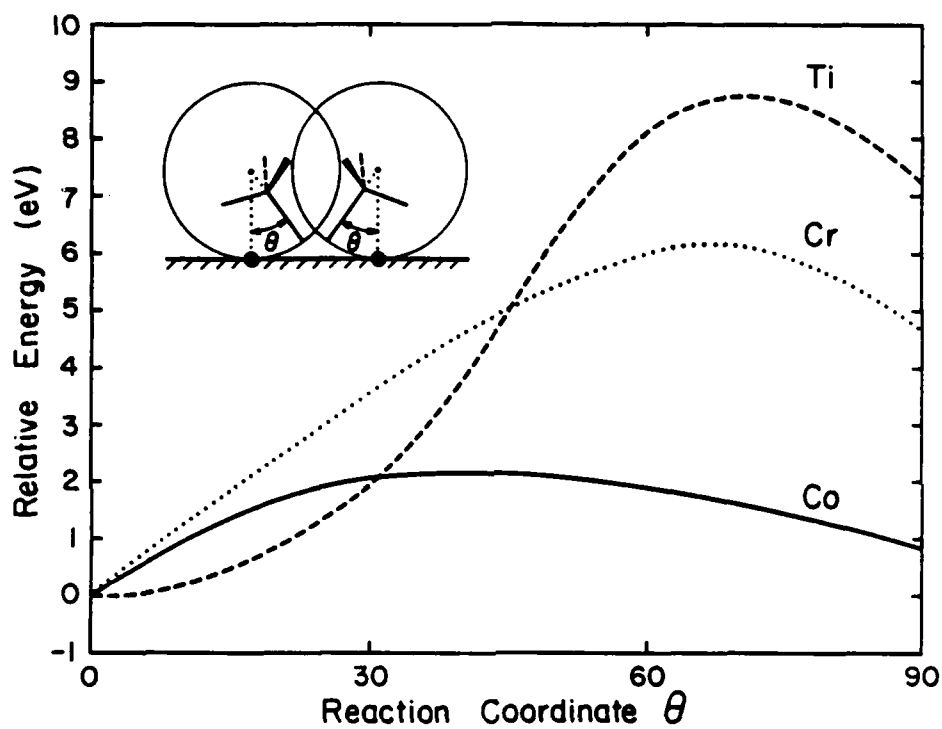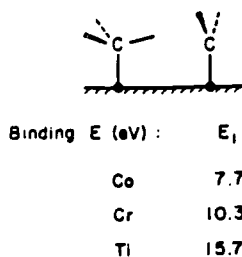
Figure 21: Relative energy of the $CH_3 + CH_3$ system along the coupling reaction path θ. The three curves correspond to different metal surfaces (Co, Cr and Ti).

:eeded to bring the C_1 group to the geometry $\underline{85}$, compared to 36 Kcal/mol (0.77eV per CH_3) for $\underline{83}$.

Binding E (eV) :		E_1
	Co	7.7
	Cr	10.3
	Ti	15.7

85

The reaction coordinate is chosen again to be a single parameter θ, $\underline{86}$. The C-C distance (decreasing from 2.51 to 1.54Å), the angle α between the C-C bond and the CH_3 "umbrella handle" (also decreasing, from $90°$ to $0°$) and the HCM2 angle β (from $120°$ to $109.5°$) on the CH_2 group are chosen to vary linearly with θ. θ itself changes from $90°$ to $109.5°$.
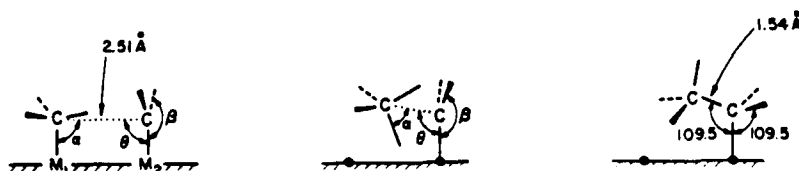
86

Along this transit we expect that one C-M bond (from CH_3 to a metal atom) is broken and C-C bond formed. The CH_3 group, formally bonded to the surface by a double bond, loses some of its C-M bonding when the hydrogens are bent downwards. This is because the CH_2 orbitals rehybridize and in the final geometry there is a hybrid pointing away from the metal atom, shown in $\underline{87}$. That hybrid is gradually pushed up by an approaching methyl n orbital, $\underline{88}$. Thus the potential energy curve should rise due to the four-electron repulsion $\underline{88}$, and then drop down after the antibonding level is pushed above the Fermi level and transfers its electrons to the metal.
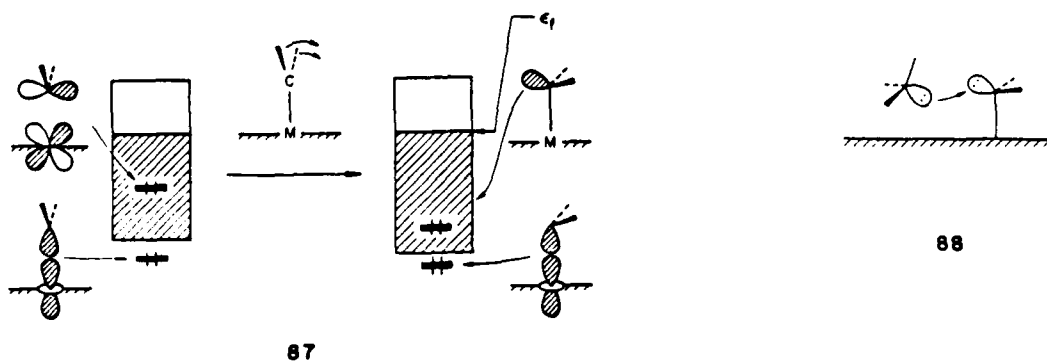
87

88

Figure 22 shows the contribution of the methylene p orbital (in local coordinates) to the total DOS along the reaction coordinate. A portion of the total contribution, corresponding to the C-C σ^* level, gradually climbs from below the Fermi level. Figure 23 is the computed potential energy curve along the reaction path. Again as the metal Fermi level is lowered the barrier height is reduced and the peak shifted to the left side, for reasons similar to those discussed for the $CH_3 + CH_3$ case. The $n\text{-}CH_3$ and $n\text{-}CH_2$ states also have a portion corresponding to the C-C σ^* level rising up along the reaction path as expected, but these graphs are not shown here.

<u>Figures 22, 23 here</u>

$CH_2 + CH_2$

The surface precursor could start in either a parallel, <u>89</u>, or a perpendicular geometry, <u>90</u>. The possibility of the perpendicular mode is anticipated from our earlier discussion that the capping geometry for a CH_2 group on the hexagonal surface may have lower energy for low d band filling (see <u>78</u>). Let us see how the calculations check out our expectations.
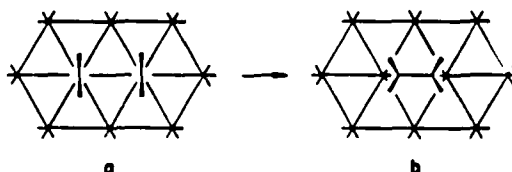
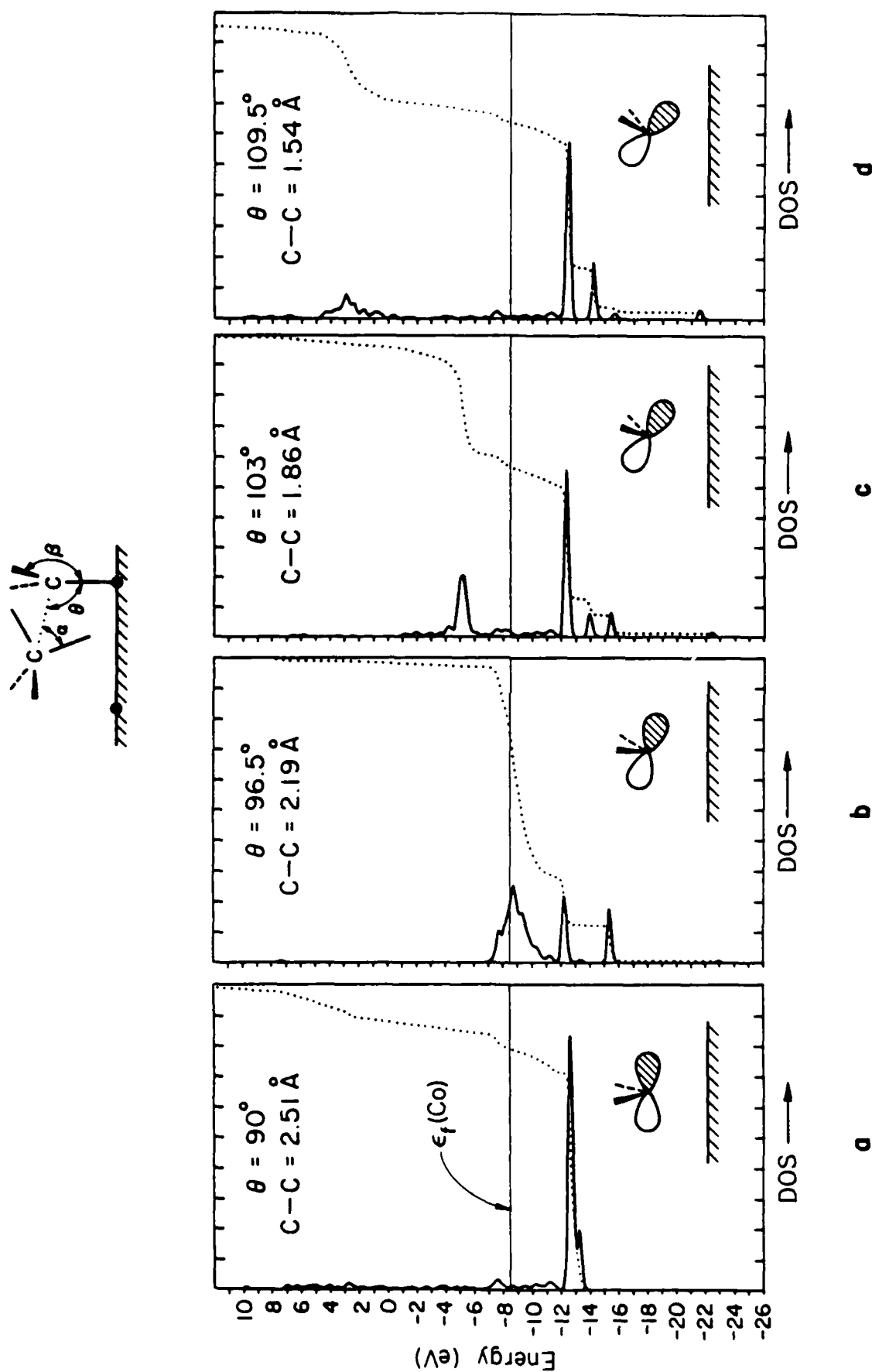
a   b

89

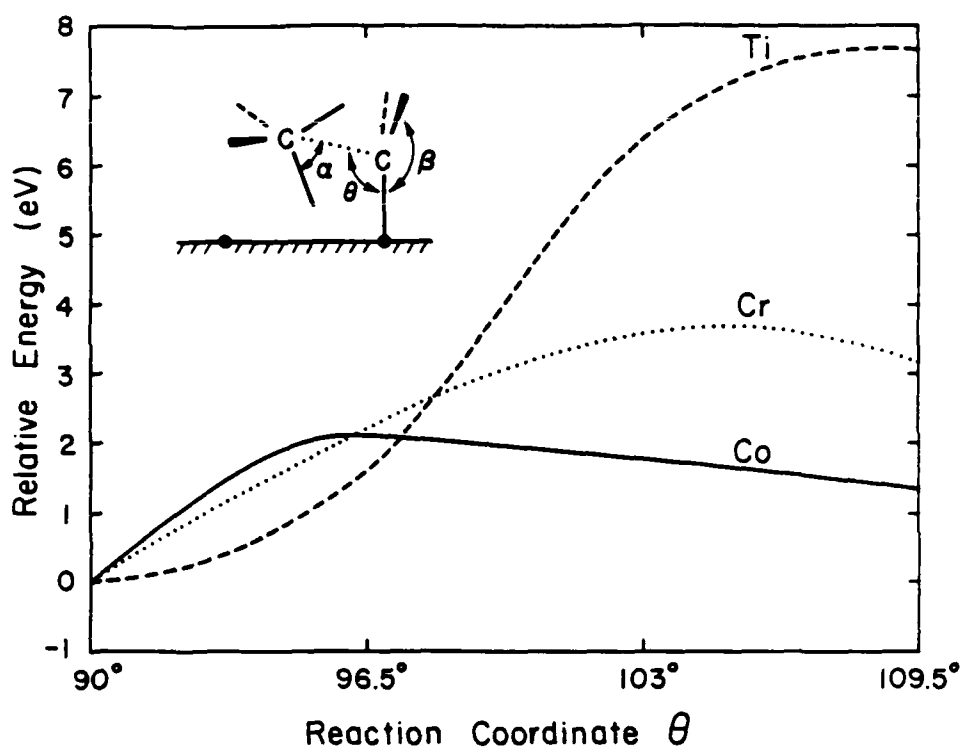Figure 22: Methylene p state evolution along a reaction path on Co(0001).

Figure 23: Relative energy of the $CH_3 + CH_2$ system along the reaction coordinate. Three curves correspond to three metal sufaces (Co, Cr and Ti).
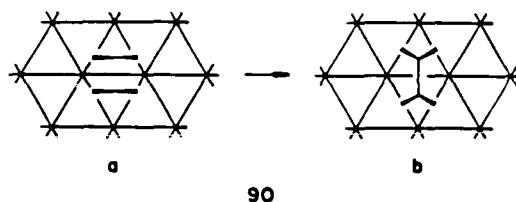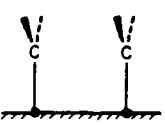
90

Figure 24 shows the CH_2 contribution to the total DOS for geometry 89a. The calculation is performed assuming a low coverage, i.e., interaction between CH_2 groups other than those two under consideration is deleted. The two CH_2 groups at a C-C separation of 2.51Å interact with each other weakly, so each MO level is split into two, as we can see from Figure 24. The "four-electron repulsion" reduces somewhat the stability of the system. 91 shows the binding energies for each CH_2. The numerical values tell us that it costs some 12 kcal/mol energy (proximity barrier) to bring two CH_2 groups together at a separation of 2.51Å.

Binding E per CH_2 (eV) :

	E_1	E_2
Co	5 8	0.04
Cr	7.7	0.3
Ti	10.5	0.8

91

Figure 24 here

The other geometry, 90a, with each CH_2 group sitting directly above the metal triangular hollow, requires a C-C separation of 1.45Å. This is obviously not a realistic starting geometry and our calculation indeed gives a large
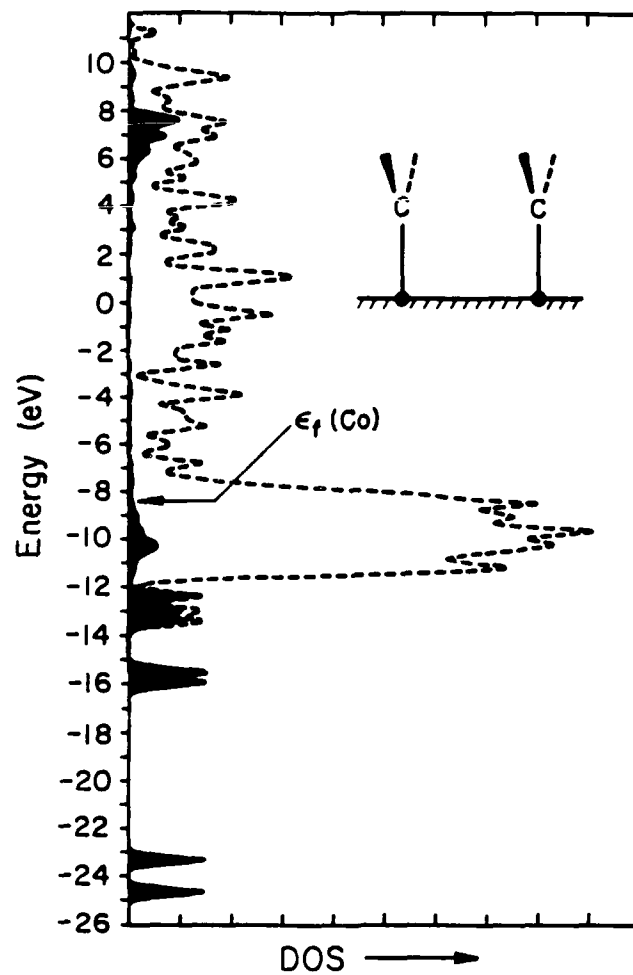
Figure 24: Total DOS (dashed line) and the CH_2 contribution (darkened area) of the CH_2 + CH_2 on Co(0001) system.

repulsion. To find the appropriate reaction path for that geometry is beyond our means. Instead we will explore some limited parts of the potential surface, in particular those very close to the final product in the coupling reaction.

But what is the final geometry? As we have said before the molecular complex 92 has a "parallel" geometry. The C-C distance is ~ 1.52Å, characteristic of a single bond. The C-M distance is ~ 2.0Å (M-Fe)[38a], suggesting a single C-M bond. And the hydrogens bend away from the metal.
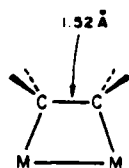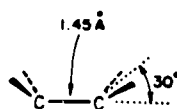
92   93

Some information is available concerning the geometry of chemisorbed ethylene. Ibach and Lehwald have compared the vibrational frequencies of C_2H_4 on Pt(111) with those of Zeise's salt {K[PtCl$_3$(C$_2$H$_4$)·H$_2$O} and concluded that the carbon atoms have sp^3-hybridization.[39] Comparison of experimental photoemission data with an SCF-LCAO calculation on ethylene in different geometries by Demuth suggested that the C-C distance is 1.34 - 1.49Å and the C-C-H angle is 106° - 109.5° for ethylene on Cu(111), Ni(111), Pd(111), and Pt(111).[40] A recent HREELS study by Stroscio, Bare and Ho also suggests that adsorbed ethylene is characterized by sp^3 hybridization.[41a] Comparison of NEXAFS of gaseous and chemisorbed (on Pt(111)) ethylene led to a proposal of a single C-C distance of 1.53Å.[41b]

Interestingly, on Pt(111) precovered with oxygen there is a mixture of both di-σ bonded (sp^3) and π bonded (sp^2) ethylene.[42a] On NiO(100) evidence exists for two adsorption states of ethylene.[42b] At high temperature ethylene also transforms into ethylidyne H$_3$C-C≡.[42,43] Other possibilities include hydrogenolysis[44] or dehydrogenation[43c] of ethylene on the surface. Since the pioneering work of Rösch and Rhodin,[45d] Anderson,[45e] and Demuth,[40] there have been many theoretical studies of ethylene interacting with metallic clusters of finite size.[45] A recent paper by Baetzold[45f] studies ethylene on (111) layers.

From the available experimental information we choose the following geometry
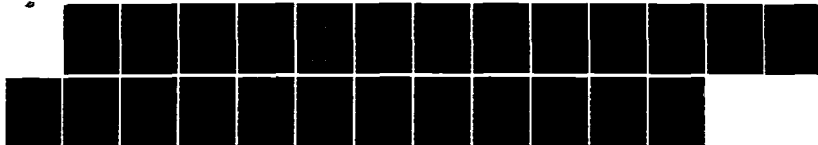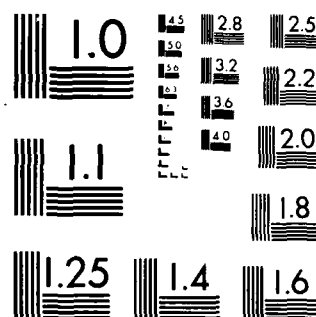
MICROCOPY RESOLUTION TEST CHART

NATIONAL BUREAU OF STANDARDS 1963 A

93: C-C = 1.45Å, the HCH plane bends upward by 30° but the HCH angle remains 120°. We are going to compare three different adsorption sites 94, 95, and 96, assuming a C-M distance 2.1Å for all. Since most experimental studies are on late transition metals[43r], we will perform the calculation only for Co(0001). The choice of these geometries is based on our knowledge of organometallic compounds, in particular those in ref. 38 and the structure of Zeise's salt.[47]

94   95   96
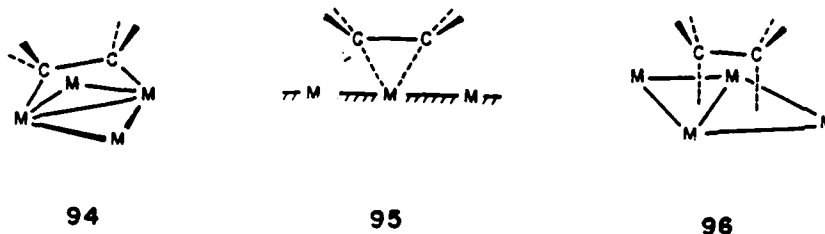
Figure 25 here

For the small degree of bending or puckering assumed, the ethylene orbitals will change little on going from the planar molecule to the puckered 93. Figure 25 confirms this and also serves to remind us of the orbitals of ethylene, easily related to those of two interacting CH_2 groups.[48] π and π^*, responsible for the important forward and back-donation in the Dewar-Chatt-Duncanson Model,[46] acquire a little σ character. Another σ orbital, with its lobes directed inward, may also play an important role in the bonding, especially in geometry 95. 97 might be an effective overlap in that geometry.

97
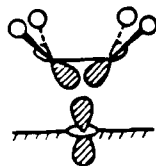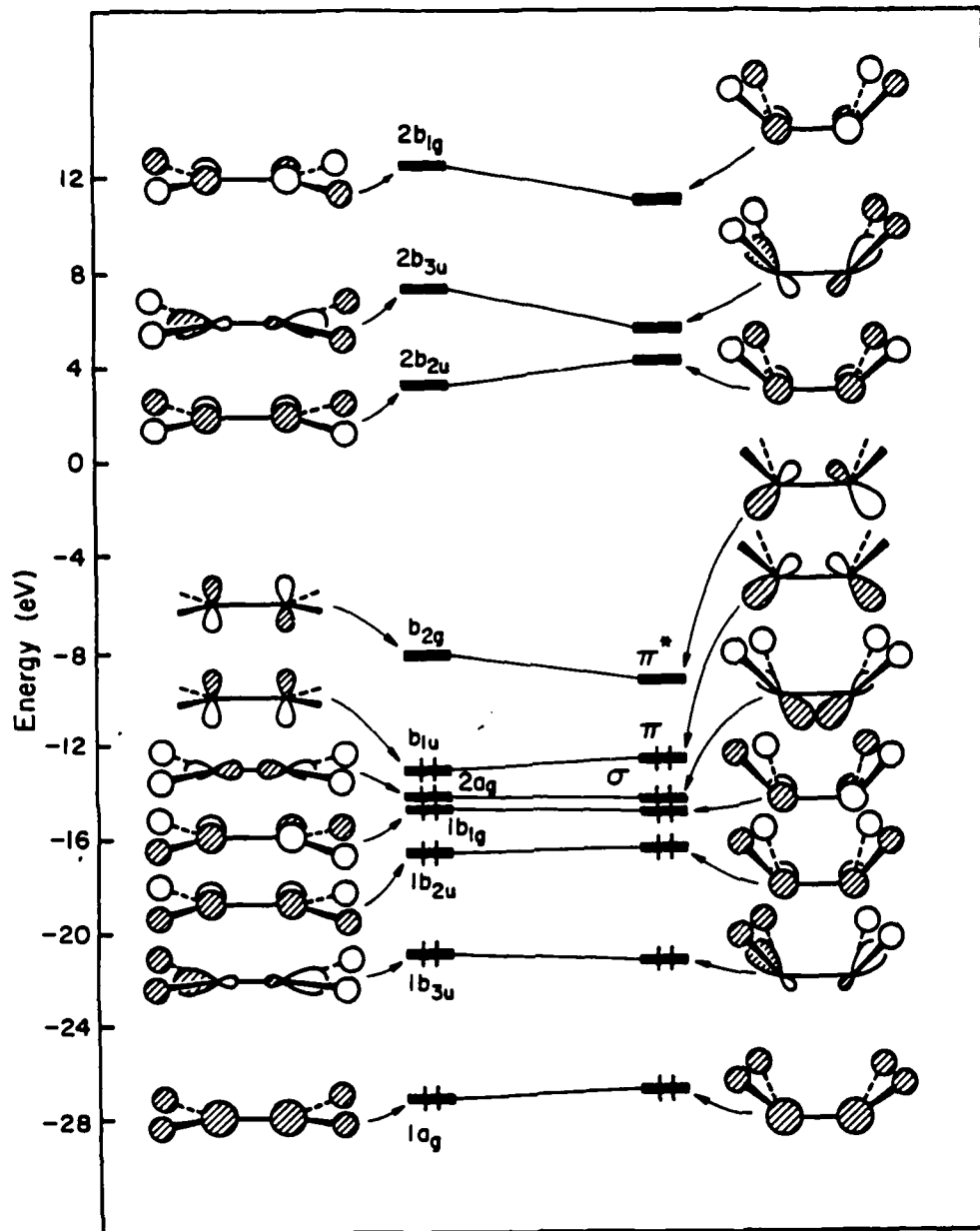
Figure 25: A Walsh diagram for ethylene from the planar to the bent (30°) geometry.

We compare the ethylene orbital contribution to the total DOS for those three

absorption sites, 94, 95 and 96 in Figure 26. As we can see upon

adsorption all occupied orbitals (up to π) remain approximately where they were

before adsorption. The unoccupied orbitals (above π^*) are all smeared out, more so

for geometry 96.

Figure 26 here

Let us zoom in at those three orbitals σ, π and π^* whose lobes point toward the

metal surface and thus should have the greatest potential for metal-ethylene

interaction. The calculations (summarized in part in Table 8) show that σ interacts

little, most in the capping geometry 96. Even there it donates no more than 4%

of its electron density to the surface. A typical interaction involved is

Table 8 here

98. A similar conclusion holds for π; in the capping geometry π donates more

electrons and is pushed down more. But in the butterfly geometry 95 there is no

indication that the interaction is stronger than in the sawhorse geometry, mostly

due to the fact that π has its lobes pointing outward, away from the metal atom,

99. Table 8 shows that π has donated substantial density to the surface.
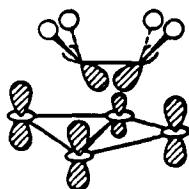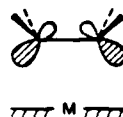
98   99

The biggest difference occurs in the π^* orbital, and for this one we offer a

decomposition of the DOS in Figure 27. π^* is smeared out more along the energy

scale as the geometry goes from 94 (sawhorse) to 95 (butterfly) to 96

(capping). In the sawhorse geometry π^* interacts only with the top of the d band

(M-M antibonding). A characteristic interaction (d_{z^2}) is shown in 100. In

the butterfly modes it interacts with the entire d_{xz} band 101, especially

those portions that match the energy of π^*. So we expect the interaction to be

Figure 27 here

Figure 26: A comparison of total DOS for ethylene (bent) chemisorbed systems of different adsorption geometries on Co(0001). a) The sawhorse geometry. b) The butterfly geometry. c) The capping geometry. The darkened area shows the ethylene contribution.

Figure 27: A comparison of the distribution of ethylene π^* states in three adsorption geometries: a. sawhorse; b. butterfly; c. capping.
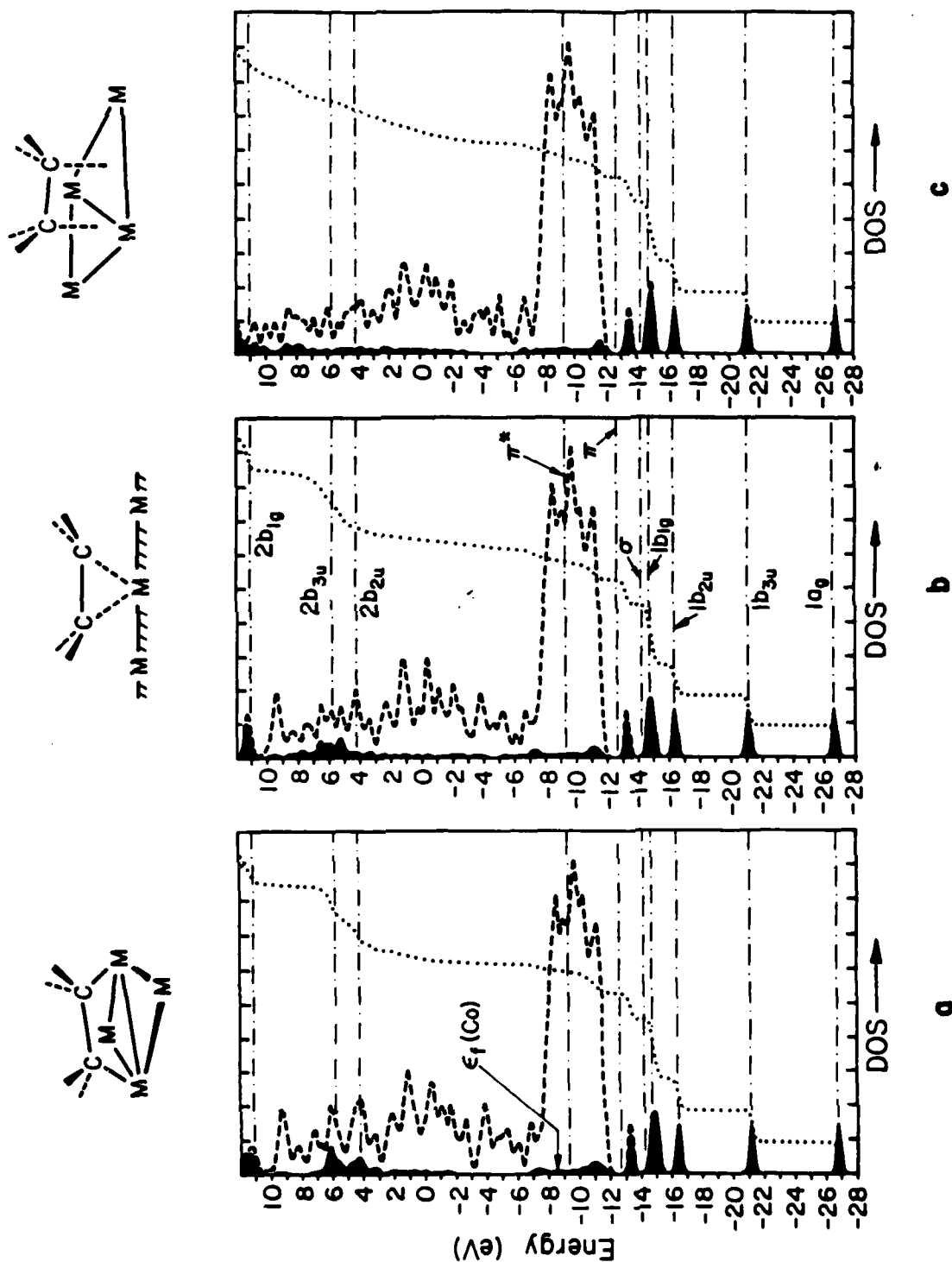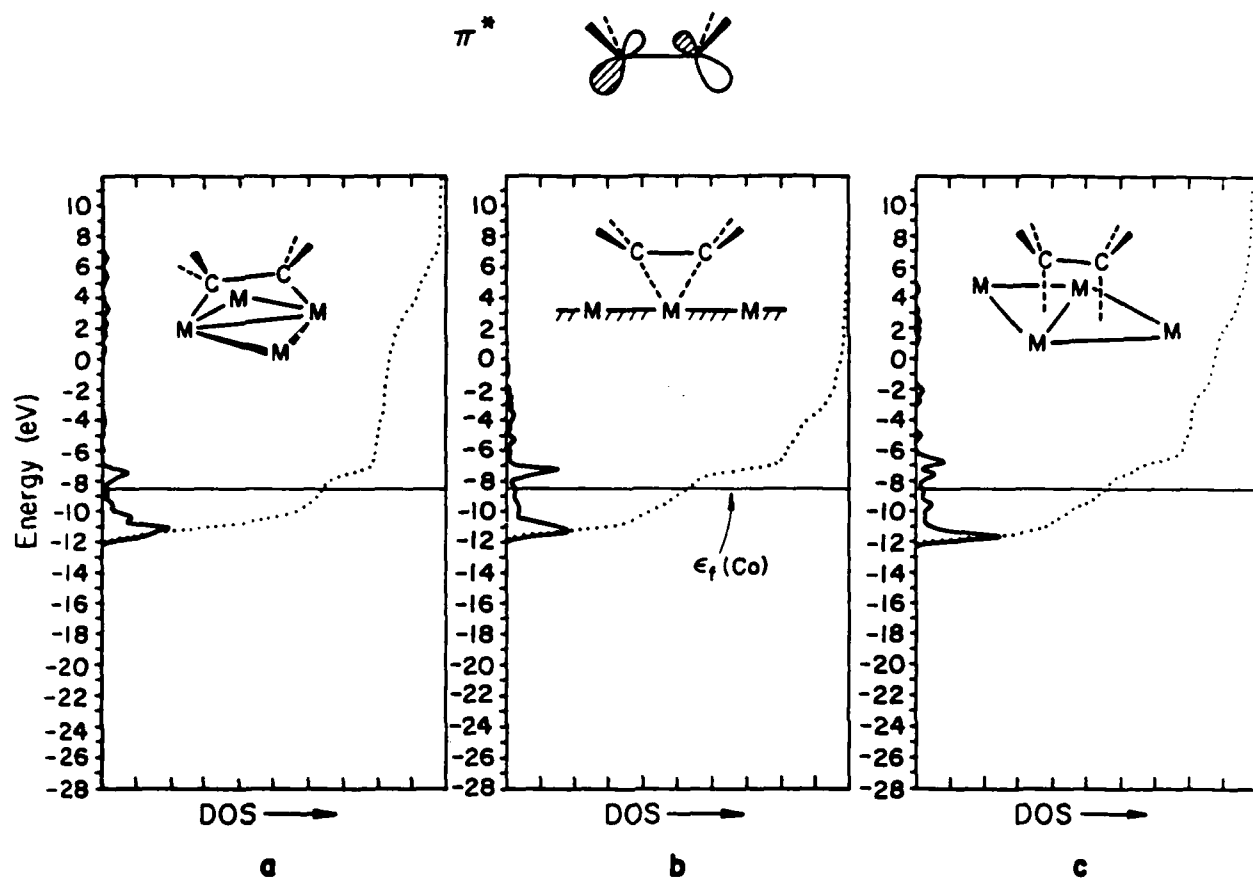
stronger and π^* spread out more. The capping geometry 96, still remains the most effective for interaction and we see π^* dispersed most. Again this is due to the fact that more metal atoms and orbital combinations are available to interact with π^*. From its band width and proximity to the Fermi level we can conclude that π^* has the strongest interaction with the metal and is primarily responsible for the binding.

100   101
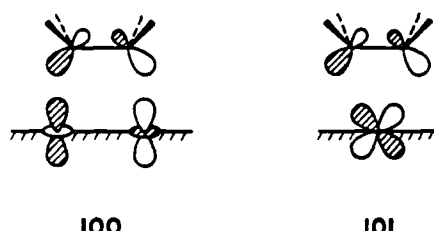
The top of the wide π^* band is C-M antibonding and the bottom C-M bonding. The stronger the interaction between π^* and metal the more profound the antibonding or bonding character. Thus at low band filling that geometry which allows stronger interaction has more bonding, but at high band filling more antibonding. This kind of reasoning can extend our considerations to surfaces other than the one considered here.

Table 8 collects the bonding information for all three geometries. As we have said before, the π^* interaction with the metal strengthens on going from sawhorse (94) to butterfly (95) to capping (96) geometries. The stronger interaction for the capping geometry is supported also by the fact that ethylene donates more changes to the metal (see last column in Table 8). Our calculation also suggests that on the sawhorse geometry π^* is filled more and ethylene dissociation into CH_2's should be more facile.

The sawhorse mode is categorized as the di-σ-bonding and the butterfly as the π-bonding mode in surface science literature. Experimental studies[43p] as well as theoretical calculations[45d] tell us that π is pushed down more in the π-bonding than in the di-σ-bonding geometry. Our calculation is no exception, but in addition

indicates the driving force behind the stronger interaction in the butterfly
geometry.

CONCLUSIONS

Let us summarize several important results and discuss the possible
consequences. In the C_1 fragment part we concluded that n-CH_3 or σ-CH_2
(= n-CH_2) is responsible to the binding of the corresponding species to the
surface. n-CH_3 or σ-CH_2 is pushed down in energy and its bonding partner, the metal
d band region, is characterized by weak M-C antibonding. This is shown
schematically in 103.
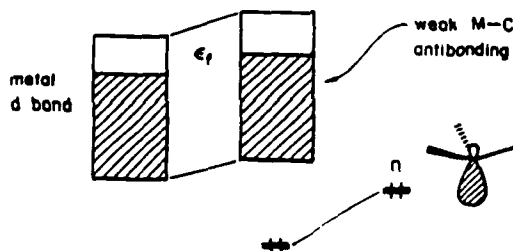
102

We saw what happens as the methyl group is moved from the on-top site 103
to the 2-fold bridging site 104 to the 3-fold bridging site 105. For
symmetry and overlap reasons the antibonding feature in the d band region becomes
stronger and the total energy of the system goes up along with this migration.
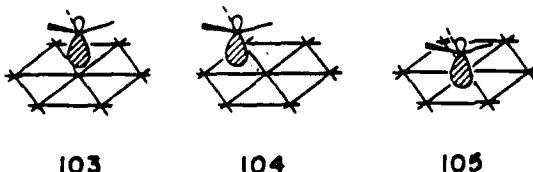
103   104   105

Also the methyl to metal antibonding character grows with the metal d band filling. The binding energy decreases for most of the binding sites and at the same time the difference between the binding energies for these absorption sites is enhanced (cf. Table 4 and 79). Therefore the methyl group should become less mobile on the surface as d bands are more occupied. For the same reason the "covalent" contribution E_2 to the binding energy of CH_2 and CH on a metal surface also decreases as the metal d band is more populated. The reduced mobility as the metal d band is more occupied contributes to a smaller reaction rate, but the decrease in binding energy means an increased desorption rate, 106.

percentage d-band occupancy
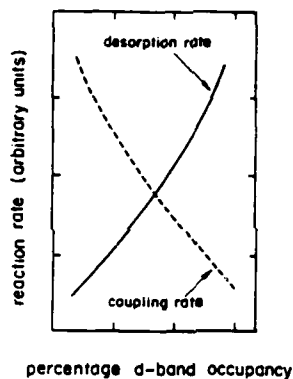
106

What will be the consequence of 106? First of all fact that the C_1 groups are less mobile on the surface of higher d band filling may contribute to the experimental fact that the average hydrocarbon chain length in the FT product catalyzed by a metal at the right side of the transition series in the Periodic Table is smaller than that produced by a catalyst at the left side.[50] Secondly it is experimentally known that the reactivity of an FT metal catalyst has a maximum as one moves across the transition series.[49-51] Norskov attributed the trend to the decrease in binding energy and the adsorption rate of the adsorbate along the

Table 8. Binding Characteristics of Ethylene on the Co(0001) Surface

Geometry	Binding E(eV)[a]	Overlap Population[b]		Orbital Occupation			Total Charge on Ethylene
		C-C	C-M	σ	π	π^*	
	2.0	0.83	0.38	1.94	1.75	1.28	-1.0
	1.0	0.86	0.23	1.95	1.79	1.08	-0.4
	-0.7	0.85	0.10	1.92	1.73	0.90	-0.9

a. The binding energy is defined as E(slab) + E(planar ethylene) - E(system).
    A positive sign means ethylene is bound.

b. For a comparison the C-C overlap population for the planar molecule is
    1.30 and for the bent one 1.16.

transition series.[51] The decrease in binding energy, he argued, is due to an increase in the antibonding between the adsorbate and the metal. This is exactly what we have in 102. So at the left side of the transition series the binding is so strong that it inhibits the coupling reaction and subsequent desorption. At the right side he concluded the adsorption rate is small and the reactivity low. Our study shows that the decrease in the mobility may also contribute to the low reactivity at the right side of the transition series.

At this point we conclude our first look at FT system in its later stages. So much more remains to be done, and with better calculations than ours. But we believe that we have gained some insight into the essence of the bonding of CH_3, CH_2, CH and C_2H_4 to metal surfaces, and the migration propensity and coupling capabilities of these important surface species. One useful conceptual decomposition of the barriers, often small, sometimes large, that are found on the way to products, is the following: there are preferred sites of chemisorption, differential barriers to migration on the surface, a proximity or crowding effect for the nearing of fragments prior to reaction, and, finally, an activation energy for actual coupling and desorption.

ACKNOWLEDGEMENT

APPENDIX

All calculations are of the extended Hückel tight binding type,[14] with the parameters given in Table 9. The M-C distance is chosen to be a fixed 2.1Å throughout the calculations although experimental data indicate different M-C distances for various adsorption sites and different C_1 fragments.[22] The choice of a constant M-C distance comes from our experience that overlap populations

for bonds of "unbiased" or equal length will be indicators of the relative bond strengths. The Co-Co distance in the hcp slab is 2.51Å,[20a] C-H 1.09Å. The total energies, DOS, COOP are calculated on a 10-k-point set from ref. 53, but wherever symmetry permits the 10-k-point set is reduced to a 7- or 5- special k point set.

Table 9 here

Table 9. Extended Hückel Parameters

Orbital		H_{ii}, eV	$\zeta_1{}^d$	ζ_2	$c_1{}^a$	c_2
Co	3d	− 9.7	5.55	1.9	0.5448	0.6556
	4s	− 7.8	2.0			
	4p	− 3.8	2.0			
Cr	3d	− 7.9	4.95	1.6	0.4876	0.7205
	4s	− 7.3	1.7			
	4p	− 3.6	1.7			
Ti	3d	− 5.9	4.55	1.4	0.4206	0.7839
	4s	− 6.3	1.5			
	4p	− 3.2	1.5			
C	2s	−21.4	1.625			
	2p	−11.4	1.625			
H	1s	−13.6	1.3			

a. Exponents and coefficients in a double ζ expansion of the 3d orbital.

REFERENCES

1.　　For recent reviews see:

　　(a) Herrmann, W.A. _Angew.Chem.Int.Ed.Engl._, 1982 , 21, 117;

　　(b) Biloen, P.; Sachtler, W.M.H. _Adv.in Cat._, 1981, 30, 165;

　　(c) Keim, W. Ed., "Catalysis in C_1 Chemistry", D. Reidel: Dordrecht, 1983;

　　(d) Goodman,D.W. _Acc. Chem. Res._, 1984, 17, 194;

　　(e) Anderson, R.B. "The Fischer-Tropsch Synthesis"; Academic Press: New York,
　　　　1984;

　　(f) Anderson, J.R.; Boudart, M. "Catalysis"; Springer-Verlag: Berlin, 1981.

2.　　Fischer, F.; Tropsch, H. _Brennst Chem._, 1926, 7, 97; _Chem.Ber._,
　　　　1926, 59, 830.

3.　　Craxford, S.R.; Rideal, E.K. _J. Chem. Soc._, 1939, 1604.

4.　　For a recent criticism of this mechanism see:

　　　　Henrici-Olive, G.; Olive, S. _J.Mol Catal._, 1982, 16, 111;

　　　　and for a counter-argument see:

　　　　Smutek, M. _ibid._, 1984, 24, 257.

5.　(a) Biloen, P.; Helle, J.N., Sachtler, W.M.H. _J.Catal._ 1979, 58, 95;

　　(b) Biloen, P. _Rec. Trav. Chim. Pays-Bas_ 1980, 99, 33.

6.　　Brady, R.C. III; Petit, R. _J. Am. Chem. Soc._, 1980, 102, 6181;
　　　　1981, 103, 287;

7.　(a) Low, G.G.; Bell, A.T. _J. Catal._, 1979, 57, 397;

　　(b) Joyner, R.W.; Roberts, M.W. _Chem. Phys. Lett._, 1974, 29, 447;

　　(c) Roberts, M.W.; _Chem. Soc. Rev._, 1977, 6, 373;

　　(d) Broden, G.; Rhodin, T.N.; Brucker, C.; Benbow, R.; Hurych, Z. _Surf. Sci._,
　　　　1976, 59, 593.

8.　　Frohning, C.D.; Kölbel, H.; Ralek, M.; Rottig, W.; Schnur, F.; Schulz, H. in
　　　　Balbe, J.; "Chemierohstoffe aus Kohle, Thieme, Stuttgart, 1977, Chap. 8,
　　　　pp. 219-299.

9.　　Wang, C.J.; Ekerdt, J.G. _J. Catal._, 1984, 86, 239.

10.   Ekstrom, A.; Lapszewicz, J. J. Phys. Chem., 1984, 88, 4577.

11. (a) Hahn, J.E. Prog. Inorg. Chem., 1984, 31, 205;

     (b) Holton, J.; Lappert, M.F.; Pearce, R.; Yarrow, P.I.W. Chem. Rev., 1983, 83, 135;

     (c) Nutton, A.; de Miguel, A.V.; Isobe, K.; Maitlis, P. J.Chem.Soc., Chem.Commun., 1983, 166.

12.   Kaminsky, M.P.; Winograd, N.; Geoffroy, G.L.; Vannice, M.A. J. Am. Chem. Soc., 1986, 108, 1315. For other related studies see references therein.

13. (a) For an excellent review see: Somorjai, G.A. Chem. Soc.Rev., 1984, 13, 321;

     (b) Koestner, R.J.; Van Hove, M.A.; Somorjai, G.A. J. Phys. Chem., 1983, 87, 203.

14. (a) Hoffmann, R., J. Chem. Phys., 1963, 39, 1397;

     (b) Hoffmann, R.; Lipscomb, W.N. ibid., 1962, 36, 2179;

     (c) for the implementation of the E.H. formalism to generate band structures, see: Whangbo, M.-H.; Hoffmann, R.; Woodward, R.B. Proc.Roy. Soc.(London), 1979, A-366, 23.

15.   Saillard, J.-Y.; Hoffmann, R. J. Am. Chem. Soc., 1984, 106, 2006.

16.   Shustorovich, E.; Baetzold, R.C.; Muetterties, E.L. J. Phys.Chem., 1983, 87, 1100.

17. (a) Baetzold, R.C. J. Phys. Chem., 1984, 88, 5583;

     (b) Baetzold, R.C.; Monnier, J.R. J. Phys. Chem., accepted.

18. (a) Minot, C.; Van Hove, M.A.; Somorjai, G.A. Surf.Sci. 1982, 127, 441;

     (b) Anderson, A.B.; Onwood, D.D. Surf. Sci., 1985, 154, L261;

     (c) Ray, N.K.; Anderson, A.B. Surf. Sci., 1983, 125, 803; 119, 35;

     (d) Anderson, A.B. Surf. Sci., 1977, 62, 119.

19. (a) Sung, S.-S.; Hoffmann, R. J. Am. Chem. Soc., 1985, 107, 578;

     (b) Blyholder, G. J.Phys.Chem., 1964, 68, 2772;

(c) Anderson, A.B. _J.Chem.Phys._, 1976, 64, 4046;

(d) van Santen, R.A. _Proc.Int.Cong.Catal._, 8th,1984;

(e) Andreoni, W.; Varma, C.M. _Phys.Rev.B_, 1981, 23, 437;

(f) Allison, J.N.; Goddard, W.A.III _Surf.Sci._, 1981, 110, L615;

(g) Doyen, G.; Ertl, G. _Surf.Sci._, 1977, B5, 641; 1977, 69, 157;

(h) Bagus, P.S.; Hermann, K. _Phys.Rev.B_, 1977, 16, 4195;

(i) Davenport, J.W. _Phys.Rev.Lett._, 1976, 36,945;

(j) Bullett, D.W.; Cohen, M.L. _J.Phys._, 1977, C10, 2101;

(k) Andzelm, J.; Salahub, D.R. _Intl.J.Quantum Chem._, 1986, 29, 1091;

20. (a) Ashcroft, N.W.; Mermin, N.D. "Solid State Physics"; Saunders College:
Philadelphia, 1976;

(b) Kittel C. "Introduction to to Solid State Physics";
J. Wiley: New York, 1976;

(c) Harrison, W.A. "Solid State Theory", Dover Publications
Inc.: New York, 1980;

(d) Shustorovich, E.; Baetzold, R.C.; Muetterties, E.L. _J. Phys. Chem._,
1983, 87, 1100; Baetzold, R.C. _Solid State Comm._, 1982, 44,
781; Varma, C.M.; Wilson, A.J. _Phys. Rev. B_, 1980, 22, 3795;
Varma, C.M. _ibid._, 1981, 23, 437.
The difference in work function between Mn and Cu is ~1ev, see:
"Handbook of Thermionic Properties," G.V. Samsanov, ed., Plenum Press Data
Division, New York, 1966; Michaelson, H.B. _J. Appl. Phys._, 1977, 48,
4729.

21. Silvestre, J.; Hoffmann, R. _Langmuir_, 1985, 1, 621.

22. (a) Gavin, R.M.Jr; Reutt, J.; Muetterties, E.L. _Proc. Natl. Acad.Sci. U.S.A._,
1981, 78, 3981;

(b) Muetterties, E.L. _J.Organomet.Chem._, 1980, 200, 177.

23. Fleming, I. "Frontier Orbitals and Organic Chemical Reactions";
John Wiley & Sons: New York, 1976.

24. (a) Hursthouse, M.B.; Malik, K.M.A.; Sales, K.D. _J. Chem. Soc. Dalton Trans._,

<u>1978</u>, 1314.

(b) Mertis, K.; Edwards, P.G.; Wilkinson, G.; Malik, K.M.A.; Hursthouse, M.B. <u>J. Chem. Soc. Dalton Trans.</u>, <u>1981</u>, 705.

(c) Masters, A.F.; Mertis, K.; Gibson, J.F.; Wilkinson, G. <u>Nouv. J. Chim.</u>, <u>1977</u>, <u>1</u>, 389.

(d) Edwards, P.G.; Mertis, K.; Wilkinson, G.; Hursthouse, M.B.; Malik, K.M.A. <u>J. Chem. Soc. Dalton Trans.</u>, <u>1980</u>, 334.

25. Krüger, C.; Sekutowski, J.C.; Berke, H.; Hoffman, D. <u>Z. Naturforsch.</u>, <u>1978</u>, <u>33b</u>, 1110.

26. Holton, J.; Lappert, M.F.; Ballard, D.G.H.; Pearce, R.; Atwood, J.L.; Hunter, W.E. <u>J. Chem. Soc. Dalton Trans.</u>, <u>1979</u>, <u>54</u>.

27. (a) Lauher, J.W.; Hoffmann, R. <u>J. Am. Chem. Soc.</u>, <u>1976</u>, <u>98</u>, 1729.

(b) Goddard, R.J.; Hoffmann, R.; Jemmis, E.D. <u>J. Am. Chem. Soc.</u>, <u>1980</u>, <u>102</u>, 7667.

(c) Hoffmann, R.; Wilker, C.N.; Eisenstein, D. <u>ibid.</u>, <u>1982</u>, <u>104</u>, 632.

(d) Eisenstein, O.; Hoffmann, R. <u>ibid.</u>, <u>1981</u>, <u>103</u>, 5582.

(e) Rappe, A.K.; Goddard, W.A. III <u>ibid.</u>, <u>1980</u>, <u>102</u>, 5114; <u>1982</u>, <u>104</u>, 448;

(f) Kostić, N.M.; Fenske, R.F. <u>J.Am.Chem.Soc.</u>, <u>1982</u>, <u>104</u>, 3879.

28. Chang, S.-C.; Kafafi, Z.H.; Hauge, R.H.; Billups, W.E.; Margrave, J.L. <u>J. Am. Chem. Soc.</u>, <u>1985</u>, <u>107</u>, 1447.

29. Dyke, A.F.; Knox, A.R.; Mead, K.A.; Woodward P. <u>J. Chem. Soc. Chem. Comm.</u>, <u>1981</u>, 861.

30. Laws, W.J.; Puddephatt, R.J. <u>ibid.</u>, <u>1983</u>, 1020.

31. For the structure of surface-bonded CH_2 see for example:

(a) Demuth, J.E.; Ibach, H. <u>Surf. Sci.</u>, <u>1978</u>, <u>78</u>, L238;

(b) McBreen,P.H.; Erley, W.; Ibach, H. <u>Surf.Sci.</u>, <u>1984</u>, <u>148</u>, 292.

32. See for example:

(a) Herrmann, W.A.; Plank, J.; Guggolz, E.; Ziegler, M.L. <u>Angew. Chem.</u>, <u>1980</u>, <u>92</u>, 660; <u>Angew. Chem. Int. Ed. Engl.</u>, <u>1980</u>, <u>19</u>, 651;

74

Herrmann, W.A.; Plank, J.; Riedel, D.; Ziegler, M.L.; Weidenhammer, K.;

Guggole, E.; Balbach, B. J. Am. Chem. Soc., 1981, 103, 63.

(b) Dimas, P.A.; Duesler, E.N.; Lawson, R.J.; Shapley, J.R.

J. Am. Chem. Soc., 1980, 102, 7787.

(c) Howard, M.W.; Kettle, S.F.; Oxton, J.A.; Powell, D.B.; Sheppard, N.;

Skinner, P. J. Chem. Soc. Faraday Trans. II, 1981, 77, 397.

33.   Rhodin, T.N.; Brucker, C.F.; Anderson, A.B. J. Phys. Chem., 1978,

82, 894.

34.   Steinbach, F.; Kiss, J.; Krall, R. Surf. Sci., 1985, 157, 401.

35. (a) Ertl, G. In "The Nature of the Surface Chemical Bond"; Rhodin, T.N.; Ertl,

G. eds.; North Holland: Amsterdm, 1979; Chapter 5;

(b) Schmidt, L.D. In "Interactions on Metal Surfaces"; Gomer, R.; ed.; Springer:

Berlin, 1975;

(c) Muetterties, E.L.; Rhodin, T.N.; Band, E.; Brucker, C.F.; Pretzer, W.R.

Chem.Rev., 1979, 79, 91.

36. (a) Baetzold, R. Surf. Sci., 1985, 150, 193.

(b) Muetterties, E.L.; Shustorovich, E.; Baetzold, R.C. Preprint.

37. (a) Holton, J.; Lappert, M.F.; Pearce, R.; Yarrow, P.I.W. Chem.Rev.,

1983, 83, 135;

(b) Fischer, E.O.; Schubert, U. J.Organomet.Chem, 1975, 100, 59.

38. (a) Bonnet, J.J.; Mathieu, R.; Poilblanc, R.; Ibers, J.A.

J. Amer. Chem. Soc., 1979, 101, 7487-7496;

(b) Green, M.; Laguna, A.; Spencer, J.L.; Stone, F.G.A.

J. Chem. Soc., Dalton Trans., 1977, 1010-1016;

(c) Motyl, K.; Norton, J.R.; Schauer, C.K.; Anderson, O.P.

J. Amer. Chem. Soc., 1982, 104, 7325-7327;

(d) Burke, M.R.; Takats, J.; Grevels, F.-W.; Reuvers, J.G.A.

J. Am. Chem. Soc., 1983, 105, 4092-4093;

(e) Theopold, K.M.; Bergman, R.G. Organometallics, 1982, 1, 1571-1579;

(f) Dedieu, A.; Hoffmann, R. J. Amer. Chem. Soc., 1978, 100, 2074-2079;

(g) Wilker, C.N.; Hoffmann, R. Nouveau J. Chim., 1983, 7, 535.

39.   Ibach, H.; Lehwald, S. J. Vac. Sci. Technol., 1978, 15, 407.

40.   Demuth, J.E. IBM J. Res. Develop., 1978, 22, 265.

41. (a) Stroscio, J.A.; Bare, S.R.; Ho, W. Surf. Sci., 1984, 148, 499;

    (b) Stöhr, J.; Sette, F.; Johnson, A.L. Phys. Rev. Lett., 1985, 53, 1684;

    (c) Horsley, J.A.; Stöhr, J.; Koestner, R.J. J. Chem. Phys., 1985, 83, 3146;

42. (a) Steininger, H.; Ibach, H.; Lehwald, S. ibid., 1982, 117, 685;

    (b) Furstenau, R.P.; Langell, M.A. Surf. Sci., 1985, 159, 108.

43. (a) Koestner, R.J.; van Hove, M.A.; Somorjai, G.A. Surf. Sci., 1982, 121, 321;

    (b) Lloyd, D.R.; Netzer, F.P. ibid., 1983, 129, L249;

    (c) Creighton, J.R.; White, J.M. ibid., 1983, 129, 327;

    (d) Demuth, J.E. ibid., 1979, 80, 315, 367;

    (e) Albert, M.R.; Snedden, L.G.; Eberhardt, W.; Greuter, F.; Gustafsson, T.; Plummer, E.W. ibid., 1982, 120, 19;

    (f) Baro, A.M.; Ibach, H. J. Chem. Phys., 1981, 74, 4194;

    (g) Ibach, H.; Hopster, H.; Sexton, B. Appl. Phys., 1977, 14, 21;

    (h) Felter, T.E.; Weinberg, W.H. Surf. Sci., 1981, 103, 265;

    (i) Gates, J.A.; Kesmodel, L.L. ibid., 1983, 124, 68; 1982, 120, L461;

    (j) Kesmodel, L.L.; Gates, J.A. Surf. Sci., 1981, 111, L747;

    (k) Lehwald, S.; Ibach, H. Surf. Sci., 1979, 89, 425;

    (l) Dubois, L.H.; Caster, D.G.; Somorjai, G.A. J. Chem. Phys., 1980, 72, 5234;

    (m) Kesmodel, L.L.; Dubois, L.H.; Somorjai, G.A. ibid., 1979, 70, 2180;

    (n) Stair, P.C.; Somorjai, G.A. ibid., 1977, 66, 2036;

    (o) Lo, W.J.; Chung, Y.W.; Kesmodel, L.L.; Stair, P.C.; Somorjai, G.A. Solid State Comm., 1977, 22, 335;

(p) Demuth, J.E.; Eastman, D.E. Phys. Rev. Lett., 1974, 32, 1123;

(q) Skinner, P.; Howard, M.W.; Oxton, I.A.; Kettle, S.F.A.; Powell, D.B.;
Sheppard, N. J. Chem. Soc. Faraday Trans. II, 1981, 77, 1203;

(r) Stuve, E.M.; Madix, R.J. J.Phys.Chem., 1985, 89, 3183; Surf.Sci.,
1985, 160, 293;

(s) Hills, M.M.; Parmeter, J.E.; Mullins, C.B.; Weinberg, W.H.
J.Am.Chem.Soc., 1986, 108, 3554.

44.   Goodman, D.W. Surf. Sci., 1982, 123, L679.

45.   See for example:

(a) Anderson, A.B.; Hoffmann, R. J. Chem. Phys., 1974, 61, 4545;

(b) Anderson, A.B. J. Am. Chem. Soc., 1977, 99, 696;

(c) Howard, I.A.; Dresselhaus, G. Surf. Sci., 1984, 136, 229;

(d) Rösch, N.; Rhodin, T.N. Phys. Rev. Lett., 1974, 32, 1189;

(e) Anderson, A.B. J.Chem.Phys., 1976, 65, 1729.

(f) Baetzold, R. C., in press

46. (a) Dewar, M.J.S. Bull. Soc. Chim. Fr., 1951, 18, C79;

(b) Chatt, J.; Duncanson, L.A. J. Chem. Soc., 1953, 2939.

47.   Love, R.A.; Koetzle, T.F.; Williams, G.J.B.; Andrews, L.C.; Bau, R.
Inorg. Chem., 1975, 14, 2653.

48.   Jorgensen, W.L.; Salem, L. "The Organic Chemist's Book of Orbitals";
Academic Press: New York, 1973; pp. 11-17.

49.   Vannice, M.A. J. Catalysis, 1975, 37, 449, 462.

50. (a) Bond, G.C.; "Catalysis by Metals"; Academic Press: New York, 1962;

(b) Boudart, M. "Kinetics of Chemical Processes"; Prentice-Hall: Englewood
Cliffs, N.J., 1968;

(c) See also Chapter 4 in Ref. 1e; Sinfelt, J.H. in Ref. 1f,
Vol. 1, Chapter 5; Schwab, G.-M. in Ref. 1f, Vol. 2, Chapter 1.

51.   Norskov, J.K. Physica, 1984, 127B, 193.

52.   Sinfelt, J.H. Ref. 1f, Vol. 1, p. 282; J. Catalysis, 1973, 29, 308;
Acc. Chem. Res., 1977, 10, 15; Scientific American, 1985,
253, No. 3, 90.

53.   Pack, J.D.; Monkhorst, H.J. <u>Phys. Rev. B</u>, <u>1977</u>, <u>16</u>, 1748.

FIGURE CAPTIONS

Figure 1: Total DOS (dashed lines) of the Co(0001), Cr(110) and Ti(0001)

three-layer slabs. The solid lines show the contribution from s and p states in a

and b respectively for the Co case. ϵ_f indicates the Fermi level. Cr and Ti total

state densities are shown in c and d. The d band center of gravity and the Fermi

level shifts to higher energy on going from Co to Ti.

Figure 2: A schematic picture showing the relative charge on surface and bulk atoms

(b) caused by different effective band width for each kind of atom (a).

Figure 3: Molecular orbitals of a CH_3 group.

Figure 4: Total DOS (dashed line) and the CH_3 contribution (darkened area) when a

CH_3 group is chemisorbed in an on-top geometry on Co(0001) (a) and Ti(0001) (b)

surfaces. The arrows indicate the CH_3 MO levels before the adsorption occurs.

Figure 5: DOS of the chemisorbed Co(0001) (CH_3 on-top). a. DOS before the

adsorption, the dashed line indicates the metal DOS, the horizontal lines show the

free CH_3 MO levels. b. Total DOS after the chemisorption occurs. c. n-CH_3

(magnified) states in the chemisorbed system. d and e show the d_z2 and s states

(magnified) of the metal atom below the CH_3 group.

Figure 6: COOP curve of the M-C bond of a CH_3 group on Co(0001) in the on-top

geometry.

Figure 7: A comparison of the d_z2 states. a corresponds to the metal below the CH_3

group and b the adjacent metal atom (the one not capped by a CH_3).

Figure 8: COOP curve for the surface M-M bond of the CH_3 on Co(0001) (on-top)

system.

Figure 9: Total DOS (dashed line) and the CH_3 contribution (darkened area) of the

bridging CH_3 + Co(0001) system. The arrows indicate where the free CH_3 MO levels

were before the adsorption.

Figure 10: COOP curves of the two non-equivalent C-M bonds in the bridging CH_3 +

Co(0001) system.

Figure 11: DOS of the bridging CH_3 + Co(0001) system. a. d_{xz}; b. d_z2; c. π^*_x; d. π^*_y. The dotted lines are the integrations.

Figure 12: DOS of the on-top CH_2 + Co(0001) system. a. Bare metal surface (dashed line) plus free CH_2 (MO levels indicated by horizontal lines). b. Total DOS (dashed line) and the CH_2 contribution (darkened area) for the chemisorbed system. c. d_z2 states of the metal atom bonded to the CH_2 group (magnified). d. s states (magnified). e. d_{yz} states (magnified).

Figure 13: COOP curves of the M-M (solid line) and the C-M (dotted line) bonds for the on-top CH_2 + Co(0001) system.

Figure 14: Total DOS (dashed line) and the CH_2 contribution (darkened area) for the bridging CH_2 + Co(0001) system (CH_2 perpendicular to the Co-Co bond).

Figure 15: COOP curves for the M-C bond. a. Perpendicular; b. Parallel CH_2 on Co(0001).

Figure 16: COOP curves for the M1-C and M2-C Bonds. CH_2 group is above the triangular hollow of the Co(0001) surface.

Figure 17: DOS of the CH + Co(0001) slab system before (a) and after (b) CH chemisorbs on the metal surface (capping geometry). CH states are shown by horizontal bars (a) or darkened area (b).

Figure 18: DOS of the capping CH + Co(0001) systems. a. d_z2; b. $d_{xz,yz}$. Notice both d_z2 and $d_{xz,yz}$ resonate with CH p around -11.2eV.

Figure 19: n-CH_3 DOS evolution along a coupling reaction coordination θ on Co(0001).

Figure 20: C-C COOP evolution along the reaction path θ on Co(0001).

Figure 21: Relative energy of the CH_3+CH_3 system along the coupling reaction path θ. The three curves correspond to different metal surfaces (Co, Cr and Ti).

Figure 22: Methylene p state evolution along a reaction path on Co(0001).

Figure 23: Relative energy of the CH_3 + CH_2 system along the reaction coordinate. Three curves correspond to three metal sufaces (Co, Cr and Ti).

Figure 24: Total DOS (dashed line) and the CH_2 contribution (darkened area) of the CH_2 + CH_2 on Co(0001) system.

Figure 25: A Walsh diagram for ethylene from the planar to the bent (30°) geometry.

Figure 26: A comparison of total DOS for ethylene (bent) chemisorbed systems of different adsorption geometries on Co(0001). a) The sawhorse geometry. b) The butterfly geometry. c) The capping geometry. The darkened area shows the ethylene contribution.

Figure 27: A comparison of the distribution of ethylene π^* states in three adsorption geometries: a. sawhorse; b. butterfly; c. capping.

EMD

12 - 86

DTIC